

Austrian Journal of Technical and Natural Sciences

**Nº 3–4 2022
March– April**

Austrian Journal of Technical and Natural Sciences

Scientific journal

№ 3 – 4 2022 (March– April)

ISSN 2310-5607

Editor-in-chief Hong Han, China, Doctor of Engineering Sciences

International editorial board

Andronov Vladimir Anatolyevitch, Ukraine, Doctor of Engineering Sciences
Bestugin Alexander Roaldovich, Russia, Doctor of Engineering Sciences
S.R.Boselin Prabhu, India, Doctor of Engineering Sciences
Frolova Tatiana Vladimirovna, Ukraine, Doctor of Medicine
Inoyatova Flora Ilyasovna, Uzbekistan, Doctor of Medicine
Kambur Maria Dmitrievna, Ukraine, Doctor of Veterinary Medicine
Kurdzeka Aliaksandr, Russia, Doctor of Veterinary Medicine
Khentov Viktor Yakovlevich, Russia, Doctor of Chemistry
Kushaliyev Kaisar Zhalitovich, Kazakhstan, Doctor of Veterinary Medicine
Mambetullaeva Svetlana Mirzamuratovna, Uzbekistan, Doctor of Biological Sciences
Manasaryan Grigoriy Genrihovich, Armenia, Doctor of Engineering Sciences
Martirosyan Vilena Akopovna, Armenia, Doctor of Engineering Sciences
Miryuk Olga Alexandrovna, Kazakhstan, Doctor of Engineering Sciences
Nagiyev Polad Yusif, Azerbaijan, Ph.D. of Agricultural Sciences
Nemikin Alexey Andreevich, Russia, Ph.D. of Agricultural Sciences
Nenko Nataliya Ivanovna, Russia, Doctor of Agricultural Sciences

Ogirko Igor Vasilievich, Ukraine, Doctor of Engineering Sciences
Platov Sergey Iosifovich, Russia, Doctor of Engineering Sciences
Rayiha Amenzade, Azerbaijan, Doctor of architecture
Shakhova Irina Aleksandrovna, Uzbekistan, Doctor of Medicine
Skopin Pavel Igorevich, Russia, Doctor of Medicine
Suleymanov Suleyman Fayzullaevich, Uzbekistan, Ph.D. of Medicine
Tegza Alexandra Alexeevna, Kazakhstan, Doctor of Veterinary Medicine
Zamazay Andrey Anatolievich, Ukraine, Doctor of Veterinary Medicine
Zhanadilov Shaizinda, Uzbekistan, Doctor of Medicine

Proofreading Kristin Theissen
Cover design Andreas Vogel
Additional design Stephan Friedman
Editorial office Premier Publishing s.r.o.
Praha 8 – Karlín, Lyčkovovo nám. 508/7, PSČ 18600
E-mail: pub@ppublishing.org
Homepage: ppublishing.org

Austrian Journal of Technical and Natural Sciences is an international, German/English/Russian language, peer-reviewed journal. It is published bi-monthly with circulation of 1000 copies.

The decisive criterion for accepting a manuscript for publication is scientific quality. All research articles published in this journal have undergone a rigorous peer review. Based on initial screening by the editors, each paper is anonymized and reviewed by at least two anonymous referees. Recommending the articles for publishing, the reviewers confirm that in their opinion the submitted article contains important or new scientific results.

Premier Publishing s.r.o. is not responsible for the stylistic content of the article. The responsibility for the stylistic content lies on an author of an article.

Instructions for authors

Full instructions for manuscript preparation and submission can be found through the Premier Publishing s.r.o. home page at:
<http://ppublishing.org>.

Material disclaimer

The opinions expressed in the conference proceedings do not necessarily reflect those of the Premier Publishing s.r.o., the editor, the editorial board, or the organization to which the authors are affiliated.

Premier Publishing s.r.o. is not responsible for the stylistic content of the article. The responsibility for the stylistic content lies on an author of an article.

Included to the open access repositories:



© Premier Publishing s.r.o.

All rights reserved; no part of this publication may be reproduced, stored in a retrieval system, or transmitted in any form or by any means, electronic, mechanical, photocopying, recording, or otherwise, without prior written permission of the Publisher.

Typeset in Berling by Ziegler Buchdruckerei, Linz, Austria.

Printed by Premier Publishing s.r.o., Vienna, Austria on acid-free paper.

Section 1. Mathematics

<https://doi.org/10.29013/AJT-22-3.4-3-10>

*Javadov Khaladdin,
Engineer of oil and gas industry
Baku, Azerbaijan*

DISTRIBUTION OF PRIME NUMBERS. INVOLUTE NATURE OF PRIME NUMBERS. RIEMANN HYPOTHESIS

Abstract

This manuscript is related to Prime numbers distribution, and I am not going to give an additional information about Riemann Hypothesis and history behind of it. I will try to keep simple.

And yet, her main idea is that there is a certain pattern in the distribution of simple (i.e., divisible only by 1 and by itself) numbers among natural (i.e. integers in general). This allows us to represent any natural number in the form of a product of several factors, regardless of the value of this number. In practice, this is used, for example, in computer data encryption, when the selection of factors that make up some large natural number takes such a huge amount of time that it becomes, in fact, impossible to solve the cipher.

Keywords: prime numbers, Riemann Hypothesis, pattern in the distribution of simple, computer data encryption

Riemann Hypothesis from Wikipedia.

We all know what the Prime Numbers are:

2, 3, 5, 7, 11, 13, 17, 19and so

I have just put the Prime numbers on the parallel line with Natural Numbers, and we know what the Natural numbers are:

1, 2, 3, 4, 5, 6, 7, 8, 9... and so and we can compare the natural and prime numbers.

Table 1.

1	2	0.5	2
2	3	0.666667	1.5
3	5	0.6	1.666667
4	7	0.571429	1.75
5	11	0.454545	2.2
6	13	0.461538	2.166667

7	17	0.411765	2.428571
8	19	0.421053	2.375
9	23	0.391304	2.555556
10	29	0.344828	2.9
11	31	0.354839	2.818182
12	37	0.324324	3.083333
13	41	0.317073	3.153846
14	43	0.325581	3.071429
15	47	0.319149	3.133333
16	53	0.301887	3.3125
17	59	0.288136	3.470588
18	61	0.295082	3.388889
19	67	0.283582	3.526316
20	71	0.28169	3.55
21	73	0.287671	3.47619

22	79	0.278481	3.590909
23	83	0.277108	3.608696
24	89	0.269663	3.708333
25	97	0.257732	3.88

The first column is the natural numbers, the second column is the prime numbers, I just pulled 25 rows.

The 3rd column is P_n/N_n , and 4th column is N_n/P_n .

So we can see from the table that P_n/N_n starts with 0.5, 0.66, 0.51, and goes down to 0.25, and N_n/P_n goes up starting from 2 to 3.88 accordingly for 25 rows.

If we take the P_n 10000 (real P_n is 9973), so related N_n will be 1273

For P_n 100000 (real P_n number 99991), and there 4459 N_n (between 50000 and 100000) accordingly.

For P_n 1000000 (real number 999983), and there 3591 N_n (between 950000 and 1000000) accordingly.

Table 2.

Number of Prime numbers	Number of natural numbers
1000	168
1000 000	78498
1000 000000	50847 534
1000 000000 000	37607 912018
1000 000000 000000	29844 570422 669
1000 0000000000000000	24739954287740860

If I continue dividing P_n to N_n , so P_n/N_n will be following

$$168/1000=0.16 \text{ for } 1000$$

$$\text{For } 1000000 \text{ } P_n/N_n \text{ will be } 0.078$$

$$\text{For } 1000000 \text{ } 000 \text{ } P_n/N_n \text{ will be } 0.05$$

$$\text{For } 1000000 \text{ } 000000 \text{ } P_n/N_n \text{ will be equal to } 0.037$$

$$\text{For } 1000 \text{ } 000000 \text{ } 000000 \text{ will be equal to } 0.029$$

For 1000 000000 000000 000 P_n/N_n will be equal 0.024 and then I used my own calculations (some error and deviation is possible) and made the following results:

$$\text{For } 10^{*21} \text{ } P_n/N_n \text{ will be equal}$$

$$2.1088148460552 \times$$

$$\times 10^{*16}/1000000000000000 \text{ } 000000=0.021$$

$$\text{For } 10^{*33} \text{ } P_n/N_n \text{ will be equal } 0.012$$

$$\text{For } 10^{*42} \text{ } P_n/N_n \text{ will be equal } 0.010$$

$$\text{For } 10^{*51} \text{ } P_n/N_n \text{ will be equal to } 0.008$$

$$\text{For } 10^{*90} \text{ } P_n/N_n \text{ will be equal to } 0.007$$

$$\text{For } 10^{*120} \text{ } P_n/N_n \text{ will be equal to } 0.002$$

$$\text{For } 10^{*180} \text{ } P_n/N_n \text{ will be equal to } 0.001$$

And for last my calculations $10^{*270} \text{ } P_n/N_n$ will be equal 0.0009

And for $10^{*1000} \text{ } P_n/N_n$ will be equal P_n/N_n will be equal to 0.0001.

As we see from calculations, when we increase P_n and N_n , the relationship P_n/N_n seeks to zero (0)

We found the following statements here:

Every Prime Number is higher/bigger than the Natural Number in his(it's) row.

Prime number can be found from the table above:

P_n/N_n decreases during all axis, and seeks to zero, which may mean the following:

P_n will get ahead the number of natural numbers, so any $N_n/P_n=0$ for big natural and prime numbers.

This one doesn't prove any relationship between Prime and Natural Numbers.

Also, the following relationship is found during calculations:

Table 3.

Prime number	(Prime number divided by number of natural numbers against)
1000/168	5.9524
1000 000/78498	12.7392
1000 000000/50847534	19.6665
10000000000000/37607912018	26.5901
1000 000000 000000/29844570422669	33.5069
10000000000000000000/24739954287740860	40.4204

We here that, difference in all cases is equal to 6.92, appr to 7.

$$\text{And for } 10^{*21} \text{ it will be } 47.34$$

$$\text{For } 10^{*24} \text{ it will be equal to } 54.26$$

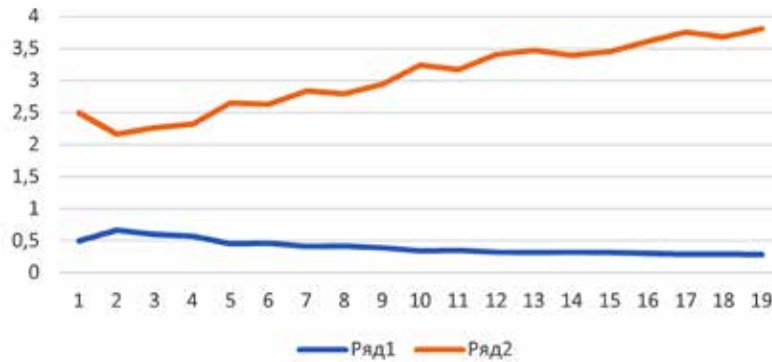
For 10^{*27} it will be equal to 61.18 etc, this will be helpful during finding the Prime Number against the Natural Number:

Let's make some graphics of this dependence:

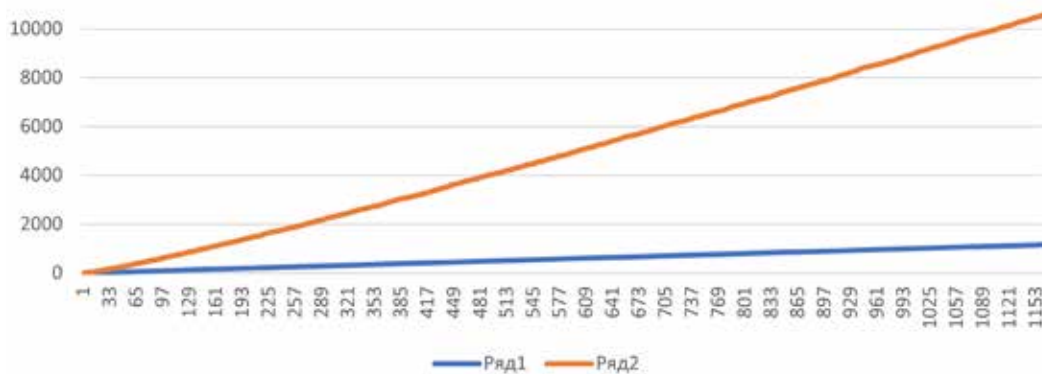
Just for information, I used only first 50000 of Prime Numbers, i.e. till 49999, and the Natural

number for this 5133. I tried to do calculations and with the numbers around 100000 or higher, I experienced problem with excel and my PC.

On the pi.1 we see behavior of 2 lines -series 1 is Natural Numbers, and series 2 prime numbers. We see that lines are being retired from each other.



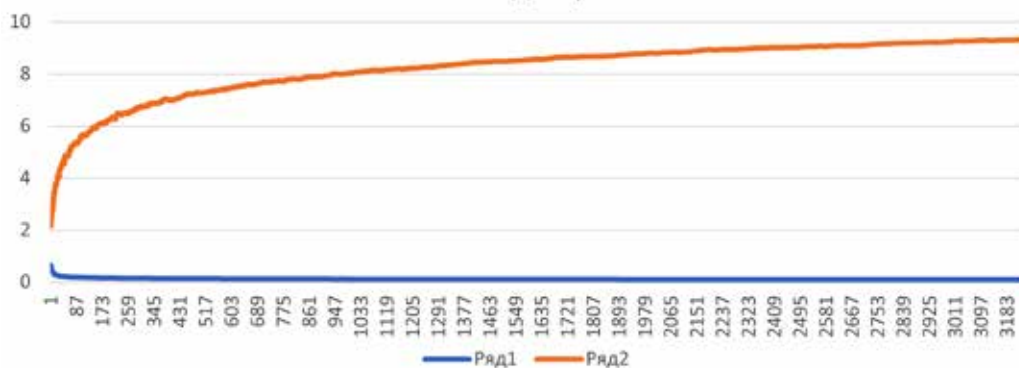
Picture 1. Prime number till 19/67



Picture 2. Nn 1135/ Pn 9157

On the (Pic. 2) we clearly see how the Pn line goes up, almost 9 times bigger than Nn . There is liner dependence between Pn and Nn , which shows $Nn/Pn=0,????$

But we see here that Natural Number line also comes off from X axis. So It is difficult to say lines are straight or curve.



Picture 3.

Let's review the (Pic. 3), which also is built as a relationship/dependence between Nn and Pn .

The red line (Prime Numbers) retires from Natural Number lines, and it is not linear, and look like as graphic of the function $Y = \sqrt{X}$. It also proves that Nn/Pn will seek to zero as well, and Pn numbers are going to infinity.

So we found that Pn are bigger than $Nn/Pn=0$, which proves that difference between Pn and Nn will be increasing at biggest numbers as well.

We just need to prove how the Prime Numbers are distributed, or how are being distributed in the numbers row, in the numbers line. And now let's some time on the (Pic. 5)

This picture is taken from Wikipedia which describes the involute or Evolent.

Numbers $B1, B2, B3$ and etc. is the Prime Numbers location/allocation in the Number Systems.

And now let's move Involute world of Prime Numbers:

Please some statements from Wikipedia and/or internet.

n mathematics, an **involute** (also known as an **evolvent**) is a particular type of curve that is dependent on another shape or curve. An involute of a curve is the locus of a point on a piece of taut string as the string is either unwrapped from or wrapped around the curve [1].

It is a class of curves coming under the roulette family of curves.

The evolute of an involute is the original curve.

The notions of the involute and evolute of a curve were introduced by Christiaan Huygens in his work titled *Horologium oscillatorium sive de motu pendulorum ad horologia aptato demonstrationes geometricae* (1673) [2].

There is a circle of diameter $\{ \displaystyle d \}$ d centered at $\{ \displaystyle O \}$ O . This circle is divided into twelve equal parts. At points 2, 3, 4, ... draw tangents to the circle, directed in one direction. We find the involute points based on the fact that when the circle is expanded, the point $\{ \displaystyle B$

$\wedge \{ 2 \}$ $\{ \displaystyle B \wedge \{ 2 \}$ must be separated from point 2 by a distance equal to the length of the arc between points 1 and 2, and the point $\{ \displaystyle B \wedge \{ 3 \}$ $B \wedge \{ 3 \}$ must be separated from point 3 by a distance equal to the length of the arc between points 1 and 3 (two lengths of the previous arc), etc.

We obtain the exact position of the involute points by plotting along the tangents the lengths of the corresponding arcs. The length of the arc between points 1 and 2 is determined by the formula $a = p \cdot d / m$, $a = 3.14159XD / M$ where d is the diameter of the circle, m is the number of parts into which the circle is divided. Having received a number of points of involute, we connect them with a smooth line. In this case, the circle of diameter $\{ \displaystyle d \}$ d is an evolute to this involute.

If $\vec{x} = \vec{c}(t)$, $t \in [t_1, t_2]$ is the parametric representation of a regular curve in the plane with its curvature nowhere 0 and $p(t)$ its curvature radius and $\vec{n}(t)$ the unit normal pointing to the curvature center, then

- $\vec{E}(t) = \vec{c}(t) + p(t)\vec{n}(t)$

Describes the evolute of given curve.

For $\vec{c}(t) = (x(t), y(t))^T$ and $\vec{E} = (X, Y)^T$ one gets

- $$X(t) = x(t) - \frac{y'(t) \cdot (x'(t)^2 + y'(t)^2)}{x'(t) \cdot y''(t) - x''(t) \cdot y'(t)}$$
 and
- $$Y(t) = y(t) - \frac{x'(t) \cdot (x'(t)^2 + y'(t)^2)}{x'(t) \cdot y''(t) - x''(t) \cdot y'(t)}$$

If we put natural numbers on the 1st circle, and Prime numbers on the second circle, we can find the relationship between these 2 numbers (natural and prime).

On external circle I put natural numbers from 1 to 36. Natural numbers are blue colored. Red line is Prime Numbers. Prime number against 36 is 151.

Let's increase the numbers of Natural Numbers and Prime numbers accordingly.

Pic. 6 is the same graphic with natural number 5133 and prime number 49999 accordingly.

Let's look at attentively. Yes, that is an Involute. Yes, Prime Numbers are being distributed as an involute.

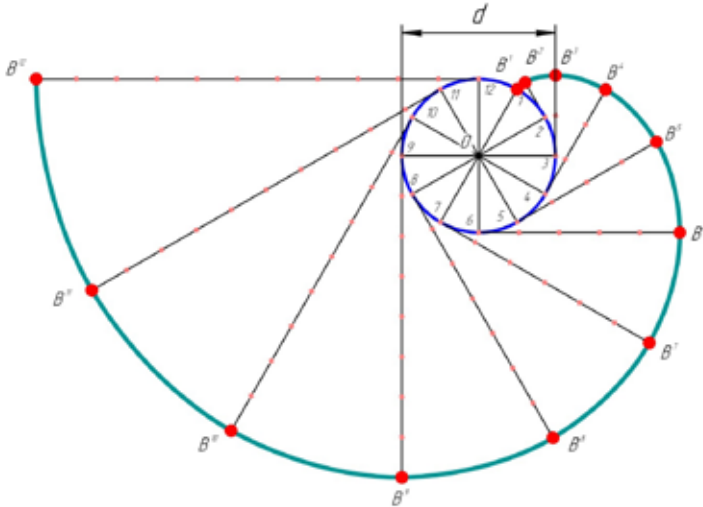


Figure 4.

Blue lines are Natural Numbers and Red Lines are Prime numbers. It shows the relationship between Nn and Pn . **Prime numbers are being created and distributed as an involute relatively to Natural Numbers. That is low which is proved.**

We can allocate them in different ways:

1) Natural numbers will be on axis X , and **involute** (also known as an **Evolent**) **spiral** will be on parallel line to Natural Numbers.

2) Natural and Prime Numbers will be allocated on 2 spirals with the different radiuses.

3) Spirals of Natural and Prime Numbers will be on parallel spaces.

Involute also is known as a trajectory of rocket (or any items), which leaves the Earth with 3rd Escape Velocity, more than 11.2 km/sec, and trajectory is set as a Hyperbola, also Evolent, goes forward and rotates, and never comes back.

But is another topic, which I am going to describe on my next manuscript,

Table above shows involute for 10000.

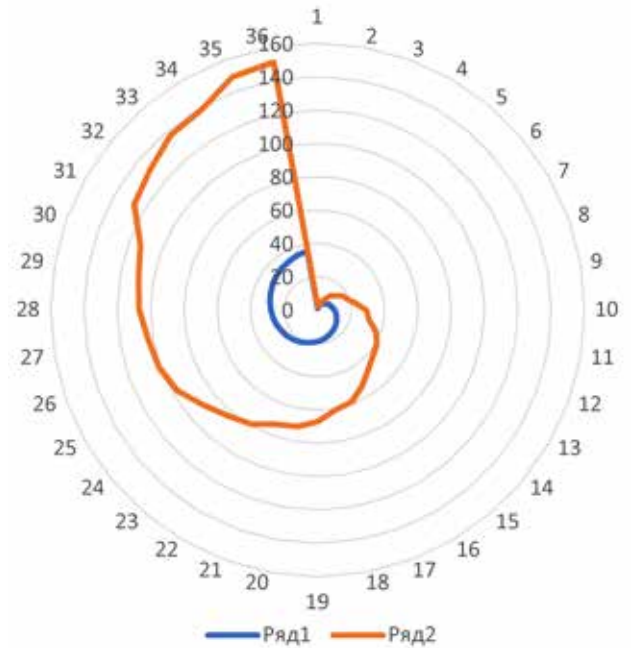


Figure 5.

On this picture above we clearly see that the relationship is being proved:

- 1–2
- 2–3
- 3–5
- 4–7
- 5–11
- 6–13
- 7–17
- 8–19
-
- 29–103
- 30–113

This shows Prime Number against Natural number for first 36 numbers, which is 151.

Tis table above shows for 75 Numbers of Natural Number row. So, between figures 5 degree.

$$360/72=5 \text{ degree.}$$

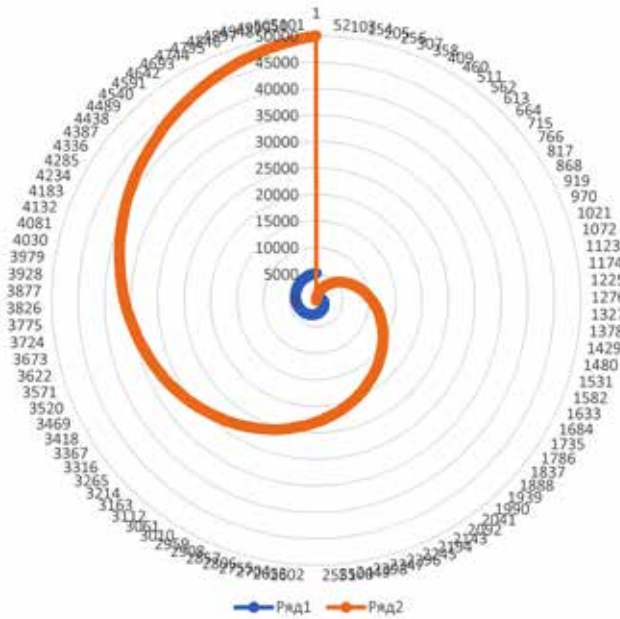


Figure 6.

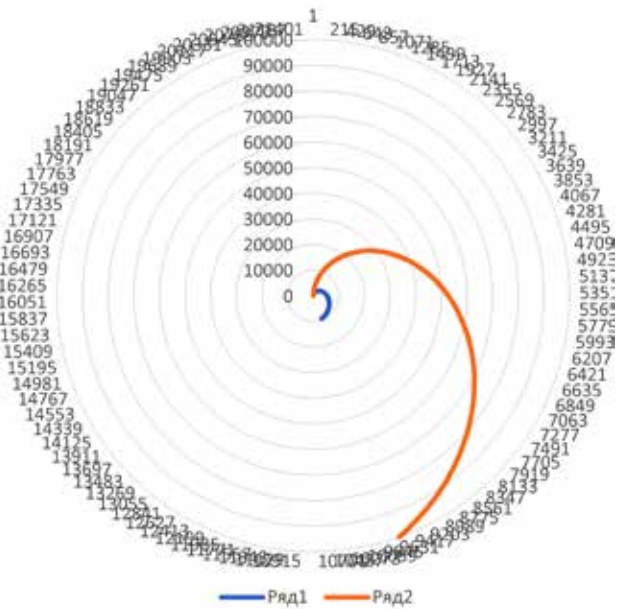


Figure 7.

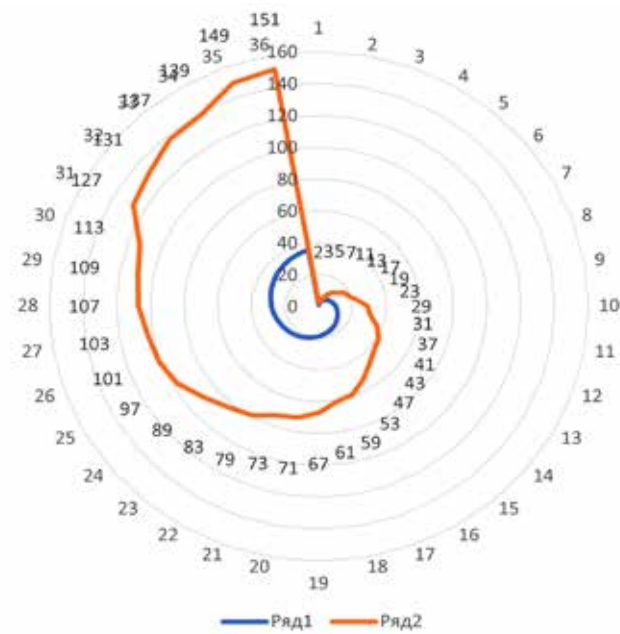


Figure 8.

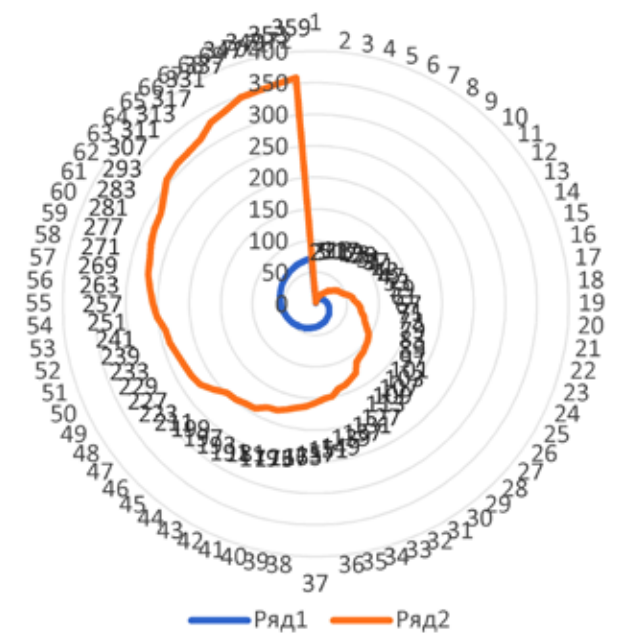


Figure 9.

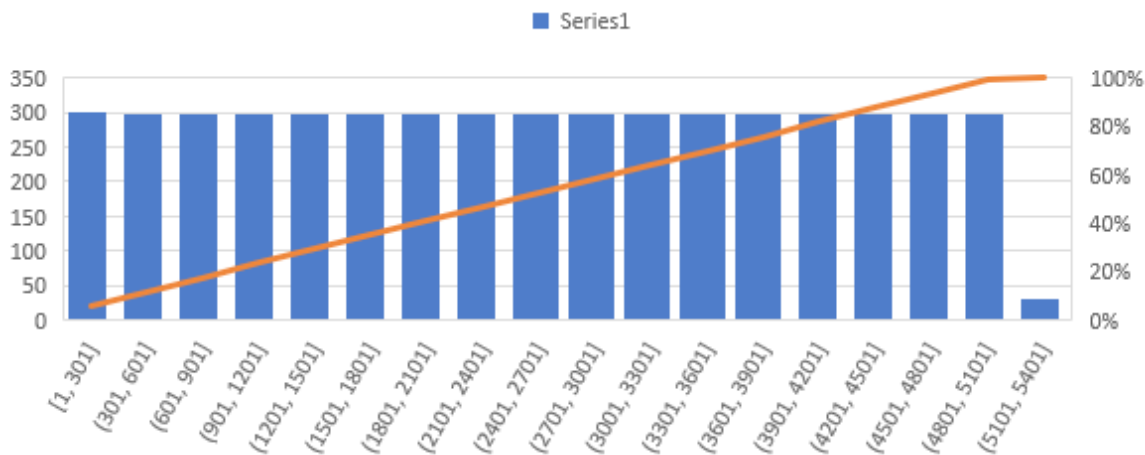
Figure 8.

So above, we see different graphics of involute (or evolute), which clearly shows that PRIME NUMBERS ARE BEING DISTRIBUTED BY INVOLUTE NATURE/FORM. SO, THERE IS A PRIME NUMBER AGAINST EVERY NATURAL

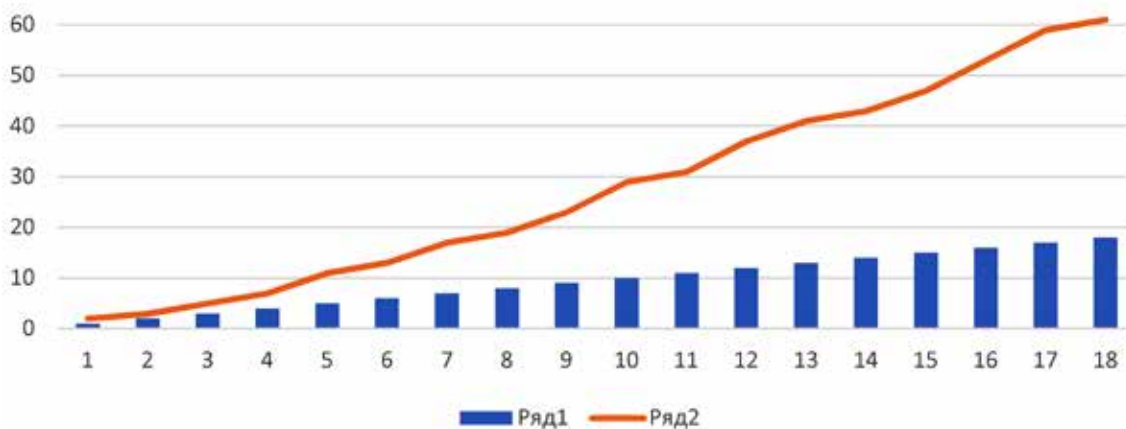
NUMBER ON THE CURVE, IT IS NOT LINE, IT IS A CURVE.

And below some slides/graphics which I used for my calculations:

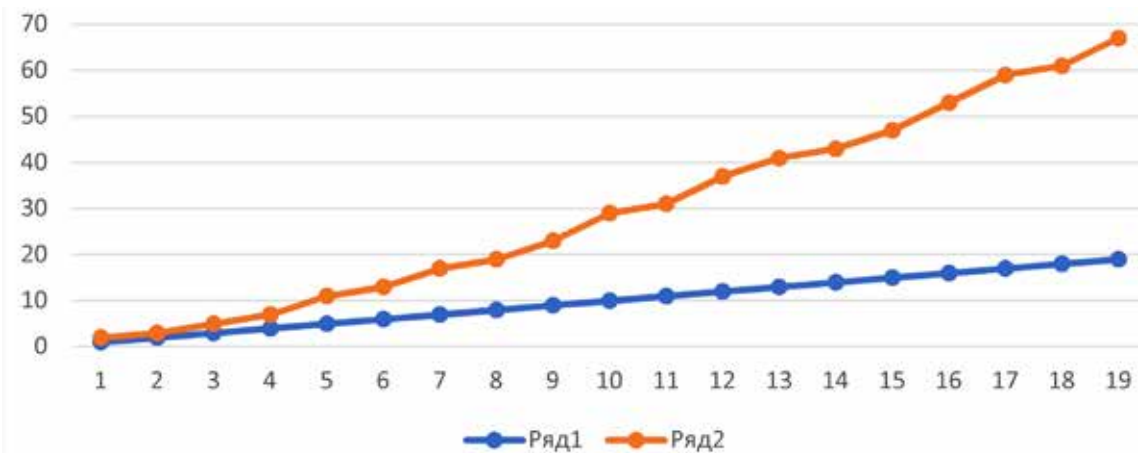
Picture of Prime Number distribution relatively to Natural Numbers.



Picture 10. Chart Title



Picture 10.



Picture 11.

This picture clearly shows that red line (Prime Numbers) should be on space, and can't be on plane,

Another statement.

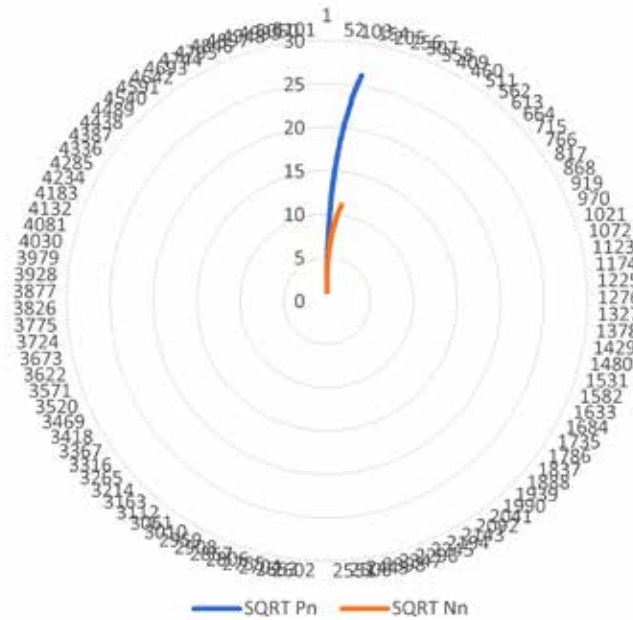
2. The Riemann hypothesis There are so-called prime numbers, for example, 2, 3, 5, 7, etc., which are divided only by themselves. How

many of them are not known? Riemann believed that this can be determined, and the regularity of their distribution can be found. Whoever finds will also provide a cryptography service.

Prime Numbers are distributed in accordance to Involute nature/principles.

I think that it is proven.

Waiting for your comments and corrections. This graphic shows the relationship between Square Roots of P_n and N_n . Also not linear and can't be on plane.



Picture 112.

References:

1. Rutter J.W. Geometry of Curves. CRC Press. 2000. – P. 204. ISBN 9781584881667.
2. Mc Cleary John. Geometry from a Differentiable Viewpoint. Cambridge University Press. 2013. – 89 p. ISBN 9780521116077.

Section 2. Medical science

<https://doi.org/10.29013/AJT-22-3.4-11-13>

Shermatova G. D.,

Eshbakova K. A.,

Narbutaeva D. A.,

Karakulova A. M.,

*Institute of the Chemistry of Plant Substances
named after Acad. S. Yu. Yunusov AS of Uzbekistan*

ANTIOXIDANT AND ANTIHYPOXIC ACTIVITY OF EMODIN AND CHRYSOPHANOL

Abstract. The aim of this research is to study the biological activity of phenolic compounds of *Rumex pamiricus* plant in Uzbekistan. Two known anthraquinone derivatives, chrysophanol and emodin has been isolated from the chloroform fraction extract of *Rumex pamiricus* roots. Chrysophanol and emodin were tested *in vitro* for antioxidant and antihypoxic activity.

Keywords: *in vitro*, antioxidant, antihypoxic, anthraquinone, chrysophanol, emodin, *Rumex pamiricus* Rech. f., *Polygonaceae*

1. Introduction

Herbal remedies play an important role in modern medicine and it appears feasible that the compounds from herbs can be helpful in prevention or treatment of different diseases [1]. The interest of natural drugs as adjunctive therapy for acute and chronic diseases has grown significantly in the recent years [2]. The phenolic compounds are of great importance in terms of various biological activities in the research work in this area. Phenolic compounds are probably the most explored natural compounds due to their potential health benefits as demonstrated in a number of studies. Continuing these studies, we began to study the phenols of the plant *Rumex pamiricus* in order to isolate natural compounds from local plant raw materials and study biological activity [3].

Plants of the genus *Rumex* L. (sorrel, dock) are widely distributed in North America, Central and

Eastern Europe, Kazakhstan, the Far East and partly in the Caucasia, Russia and East Asia [4; 5; 6; 7]. This genus includes more than 250 species distributed worldwide. 16 species grow in Uzbekistan [3; 8; 9]. The herb *Rumex pamiricus* belongs to the family of *Polygonaceae*, which is widespread in Central Asia (Pamir-Alay, Tian Shan, Dzungarian Alatau), Kashgaria. One of the most common types of *Rumex* in Uzbekistan (Tashkent, Samarkand and Kashkadarya regions) [2]. It grows along wet mountain meadows, along the banks of mountain rivers and lakes. Perennial herbaceous plant reaching 60–100 cm in height (Figure –1) [3]. Since ancient times, concoction or tea from various parts of this herb has been used in folk medicine to treat diarrhea, dysentery, stercoral ulcer, as appetizer, analeptic medicine for lever, heart, as antihemorrhagic, to treat hepatitis, fever and other diseases [2]. Plants belonging to the *Polygonaceae* are

known to produce a large number of biologically important secondary metabolites, such as anthraquinones, flavonoid glycosides, phenolic acids, naphthalenes, stilbenoids, steroids and leucoanthocyanidins [10]. Among wild plants, *Rumex* plants have a great potential [3]. They are already widely used as food, fodder, melliferous, and medicinal plants [6; 11; 12].



Figure 1. *Rumex pamiricus* Rech. f. Location: Beldersay, Chimgan mountains (Ugam Chatkal National Park), Tashkent region. (Pictures author: G. D. Shermatova)

2. Experimental part

2.1. Antioxidant activity of emodin and chrysophanol

The antioxidant activity of the studied substances was determined by their effect on the intensity of lipid peroxidation (LPO) processes, which was assessed by the accumulation of malondialdehyde (MDA) in *in vitro* experiments. The content of malonic dialdehyde (MDA) in experiments *in vitro* was determined by color reaction with thiobarbituric acid [209, p. 66–68]. LPO was induced with 10 μ M FeSO₄ in the presence of 200 μ M ascorbate in a medium containing 145 mM KCl, 25 mM Tris HCl, pH 7.4. All studied samples at a dose of $1 \cdot 10^{-5}$ mg/ml were dissolved in 95% ethyl alcohol. An oily solution of pharmacy vitamin E (10%) at a concentration of $1 \cdot 10^{-5}$ mg/ml was used as a reference drug.

Antioxidant activity *in vitro* of the studied compounds is presented in Table 1.

Table 1. – Antioxidant activity of emodin and chrysophanol

Compounds	10^{-5} g/ml	
	MDA (n/mol/mg)	Effect in%
Control	0.98±1.25	–
Vitamin E	0.23±0.012	76.0
Emodin	0.56±0.010*	42.0
Chrysophanol	0.68±0.009*	31.0

Note: *statistically significant differences were noted compared with the corresponding control: at $p < 0.05$.

Discussion: As can be seen from the table, their inhibitory effect on the processes of lipid peroxidation in experiments *in vitro* was manifested in the range of 31.0–76.0%. The antioxidant effect of the two studied substances (emodin and chrysophanol) was 42.0–31.0%. The reference drug vitamin E (76.0%) has a more pronounced antioxidant activity.

2.2. Antihypoxic activity of emodin and chrysophanol

The antihypoxic activity of emodin and chrysophanol and the reference drug mildronate was studied on white mice of both sexes under normobaric hypoxic hypoxia. Animals were placed in a hermetic chamber 2 hours after drug administration. The results are presented in table 2.

Table 2. – Antihypoxic activity of emodin and chrysophanol

Compounds	Dose, mg/kg	Lifespan, min	Effect, %	P
1	2	3	4	5
Control	–	16.3±0.58		

1	2	3	4	5
Emodin	50 mg/kg	20.3±0.67	24.5%	p<0.1
Chrysophanol	50 mg/kg	21.7±1.02*	33.0%	p>0.05
Mildronate	100 mg/kg	23.5 ± 0.88*	44.0%	p>0.05

Discussion: An analysis of the experimental data presented in Table 2 indicates that, with a preliminary single administration under conditions of acute normobaric hypoxic hypoxia, the studied substances to one degree or another contribute to an increase in the lifespan of animals. The most pronounced increase in life expectancy under the influence of chrysophanol-33.0% (21.7±1.02 min). A slightly less pronounced effect was observed in emodin, its effect was 24.5% (20.3±0.67

min). Both compounds are inferior to mildronate in antihypoxic action – 44.0% (23.5 ± 0.88).

3. Conclusion

1. Emodin and chrysophanol have moderate antioxidant activity (42 and 31%, respectively) compared to the reference drug vitamin E (76%).

2. Chrysophanol has antihypoxic activity (33%) at the level of the almost control drug mildronate (44%). Emodin showed moderate activity (24%).

References:

1. Shermatova G.D., Zhang Y.J., Davranov K. Antibacterial and Antifungal Activities of Rumex Confertus Willd. International Journal for Research in Applied Science & Engineering Technology.– 9/12. 2021.– P. 1855–1856.
2. Shermatova G. Emodin, an anthraquinone derivative from Rumex pamiricus Rech. f. Universum: chemistry and biology.– 3/93. 2022.– P. 28–31.
3. Shermatova G. D., Bobakulov Kh.M., Shamuratov B. A., Mavlyanov S. M., Zhang Y.J., Eshbakova K. A., Azimova Sh.S., Sasmakov S. A. Phenolic Compounds of Rumex L: Aerial Part Fractions and Essential Oil Results of In vitro Screening for Antimicrobial Activity. Chemical Science International Journal.– 31/1, 2022.– P. 15–25.
4. Kołodziejek J. Growth performance and emergence of invasive alien Rumex confertus in different soil types. Scientific Reports.– 9/1. 2019.– P. 1–13.
5. Kholmatov H. Kh., Habibov Z.N., Olimkhodjaeva N. Z. In book: Medicinal herbs of Uzbekistan. Ibn Sino. 1991.– P. 93–94.
6. Podgurskaya V. V., Luksha E. A., Gushchina E. S., Savchenko I. A., Korneeva I. N., Kalinkina G. I. Biological activity of the genus Rumex (Polygonaceae) plants. Chem. Plant Raw Mater.– 2. 2021.– P. 59–78.
7. Shermatova G. D., Rakhimova Sh. Kh., Komilov B. J., Abdul-Azizovich B. M. Protein content of Some Rumex Species (Polygonaceae). Austrian Journal of Technical and Natural Sciences.– 1/2. 2022.– P. 3–7.
8. Shermatova G. D., Shamuratov B. A. Flavonoids of Rumex pamiricus. Bulletin of National University of Uzbekistan.– 4/2. 2013.– P. 232–233.
9. Rao K. N. V., Ch S., Banji D. A study on the nutraceuticals from the genus Rumex. Hygeia. J. D. Med.– 3/1, 2011.– P. 76–88
10. Jeelani S. M., Farooq U., Gupta A. P., Lattoo S. K. Phytochemical evaluation of major bioactive compounds in different cytotypes of five species of Rumex L. Industrial Crops and Products.– 109. 2017.– P. 897–904.
11. Bello O. M., Fasinu P. S., Bello O. E., Ogbesejana A. B., Adetunji C. O., Dada A. O., Ibitoye O. S., Aloko S., Oguntoye O. S. Wild vegetable Rumex acetosa Linn. Its ethnobotany, pharmacology and phytochemistry. A review. S. Afr. J. Bot.– 125. 2019.– P. 149–160.
12. Vasas A., Orbán-Gyapai O., Hohmann J. The Genus Rumex: Review of traditional uses, phytochemistry and pharmacology. J. Ethnopharmacol.– 175. 2015.– P. 198–228.

Section 3. Mechanics

<https://doi.org/10.29013/AJT-22-3.4-14-16>

*Kalmova Maria,
Senior Lecturer of the Department of Structural Mechanics,
Engineering Geology, Foundations and Foundations
Samara State Technical University,*

THE SCOPE OF APPLICATION OF DEVICES WHOSE OPERATION IS BASED ON TAKING INTO ACCOUNT THE CONNECTIVITY OF THERMOELECTROELASTIC FIELDS

Abstract. The work highlights devices whose operation is based on taking into account the connectivity of thermoelectroelastic fields. Sensors of various classes based on piezo- and pyroeffect are considered. The designated areas of application of the considered measuring instruments and calculation methods allow us to analyze the connectivity of temperature, electric and elastic fields.

Keywords: piezoelectric elements, thermoelectroelasticity, piezoceramic cylinder.

Currently, devices whose operation is based on taking into account the connectivity of fields of different physical nature are widely used. At the same time, the piezo- and pyroelectric effect based on the coupling of thermoelectroelastic fields is used as the basis for the operation of temperature sensors.

The scope of application of such sensors is very wide in medicine. For example, cylindrical actuators of reinforced type are used in microdosing devices, in scanning microscopy, in microsurgical and ocular operations for accurate instrument feeding.

Multilayer piezoactuators, which are used for internal combustion engines, are widely used in the automotive industry, thereby ensuring the smooth operation of the engine. A multilayer piezoelectric actuator can be used to manufacture a generator that converts mechanical forces into electrical signals.

Shell-less piezo-package actuators, manufactured in the form of a disk or ring, are widely used in industry, in high-frequency positioning systems for

instrumentation, as well as optoelectronic systems for monitoring and controlling technological processes in microelectronics at the submicron level; in manipulators of various robots, in optomechanical devices for micro-displacements of the slide table (control of gas analyzers-dosimeters) [1; 2].

The elements based on the piezoelectric effect have high performance, are less susceptible to interference, and are technologically advanced in manufacturing. The use of piezoelectric materials in electronics makes it possible to reduce the geometric characteristics of device elements and contributes to the creation of efficient energy converters. The use of pyroelectric elements allows you to measure the temperature and analyze other characteristics of devices and structures. The effects of temperature stresses must be taken into account in the designs of aerospace technology, for example, in solid-fuel charges of rocket engines, which are thick-walled hollow cylinders, etc. The pyroelectric effect belongs

to a wide class of thermoelectric phenomena that manifest themselves externally as the electrification of dielectrics when their temperature changes. To date, pyroelectric converters of various types, such as thermal radiation detectors, chromatographic detectors, anemometers, shock wave sensors, etc. are used in industry.

Thermal imaging and thermography methods are used to remotely measure the temperature of objects [3]. Thermal imaging is based on determining the location of objects and recognizing their shape (even in complete darkness), but without taking into account temperature. Thermography performs the functions of thermal imaging and provides quantitative radiometric measurements of the temperature of this object. Therefore, the devices used in industrial and medical diagnostics are divided into two main classes: thermal imagers and measuring thermographs. Thermal imagers (infrared cameras) are most often used as night vision devices. For accurate diagnostics in engineering and medicine, measuring thermographs are used, with the help of which data of the thermal field of the object is obtained. Thermal imaging devices help to identify dangerous defects that show a violation of the normal operation of the object by identifying hot or cold places in the temperature field. Thermal imaging is of great importance: in industry, medicine, military equipment, transport, scientific research and everyday life. Pyroelectric thermal imagers are used in aerial photography of fires. Miniature pyroelectric X-ray generators find applications in radiography and radiation calibration.

Thermometric converters are used to measure thermal parameters. These include pyroelectric temperature meters (pyro-thermometers), heat capacity and thermal conductivity meters (pyrocalorimeters), heat content and heat exchange meters with the medium (catarometers, anemometers), etc. The pyro-thermometer, depending on the circuit of its inclusion, determines the temperature or the rate of its change. Pyroelectric catharometers are used in

gas chromatographs to analyze gas mixtures by the thermal conductivity of the components of the mixture, pyroelectric anemometers are used to study the features of the movement of liquid or gas media, in particular, in metallurgy.

In modern practical medicine, respiratory parameter sensors are used, which are designed for non-contact recording of the frequency and intensity of breathing and understanding the state of the respiratory system, the operation of which is based on the pyroelectric effect.

The development of space engineering contributed to the creation of pyroelectric shock wave sensors that experience two thermal effects – convective and radiation and mechanical effects, the exposure time does not exceed 1 ms. Such pyroelectric sensors provide simultaneous measurement of all types of impacts with direct reproduction of the form of convective and radiative heat flows.

Based on the above, it can be concluded that applied research has led to the widespread practical use of pyroelectrics in many areas of modern science and technology. Currently, these studies are also continuing to develop quite actively. In order to expand the functionality of devices of this type, there is a need for an in-depth analysis of non-stationary processes, which makes it possible to understand the effect of the interaction of electric, temperature and elastic fields. To do this, various theories are used that analyze this problem with varying degrees of accuracy. At the same time, as a rule, thin elastic systems are used as computational models of the structures under consideration when performing kinematic hypotheses. The task becomes significantly more complicated when studying the construction of finite rigidity in a three-dimensional formulation. In this case, a system of non-conjugate differential equations is formed, the integration of which is associated with great mathematical difficulties, but only such an approach allows us to fully take into account the connectivity of electroelectroelastic fields [4].

References:

1. Bobtsov A. A. SPb GU ITMO: Actuators and systems for micro-displacements, 2011.
2. Dzhagupov R. G. – St. Petersburg: Polytechnic, 1994.
3. Bush A. A. State educational institution of higher professional education “Moscow State Institute of Radio Engineering, Electronics and Automation (Technical University)”: Pyroelectric effect and its applications. 2005.
4. Shlyakhin D. A., Kalmova M. A. The nonstationary thermoelectric elasticity problem for a long piezoceramic cylinder. PNRPU Mechanics Bulletin, – Vol. 2. 2021. – P. 181–190.

Section 4. Food processing industry

<https://doi.org/10.29013/AJT-22-3.4-17-22>

*Rakhmonov Kakhramon Sanokulovich,
Bukhara Engineering Technological Institute, Bukhara, Uzbekistan*

*Khudaikulov Anvar Shavkatovich,
Atamuratova Tamara Ivanovna,
Karshi Engineering Economics Institute, Karshi, Uzbekistan*

TECHNOLOGICAL ASPECTS OF THE PRODUCTION OF WHEAT BREAD VARIETIES USING SPONTANEOUS FERMENTATION STARTERS

Abstract. The article substantiates the expediency of using in the production of bread to adjust the baking properties of the main raw materials, improve the quality of finished products and prevent microbial infection of the last natural bioadditives – starter cultures. The data of specialized information sources on promising types of starter cultures are considered, the reasons limiting their use in the baking industry are established. The expediency of using starter cultures of spontaneous fermentation, especially for regions with a hot climate, is substantiated. The results of a study of the biotechnological properties and composition of the microbiota of polystrain spontaneous fermentation starters (PSSB) are presented, using the example of pea-star anise starter culture traditionally used in the preparation of Uzbek flatbread. It has been established that PZSB affect the state of the main flour biopolymers, the intensity of their acid hydrolysis, the rheological properties of the dough, and the quality of the finished product.

Keyword: bread, sourdough, microbial contamination, pea and star anise sourdough.

Introduction

The most ancient method of biological loosening of the dough is the use of wheat, hop, wine, pea-star anise, pea-anise and other starter cultures, the microflora of which developed spontaneously. But even today, wheat sourdoughs are a means of increasing acidity, intensifying the dough preparation process, improving taste and aroma, preventing potato disease in bread and molding.

Satsaeva N. K. developed a technology for making wheat bread resistant to microbial contamination based on hop sourdough. The conditions for sour-

dough cultivation were optimized, the possibility of stabilizing the microbiological composition of the latter by using hop broth containing 90.8% isohumulone and wheat bran was established.

The use of concentrated lactic acid starter (CLSC) is recommended for enterprises with intermittent operation, since this starter does not require forced cooling or other preservation methods during non-working hours. The preparation of KMCZ is carried out according to the Leningrad scheme using liquid cultures of lactic acid bacteria *L. plantarum* – 30, *L. casei* – 26, *L. brevis* – 1, *L. fermenti* – 34 or dry lactobacterin (1–10).

Acidophilic starter consists of bacteria *L. acidophilus*-146 and yeast strain “Ryazanskiye-17” adapted to high temperatures (40...450 °C) on the basis of the Ryazan race. A high level of amino acids was found in the starter: the content of lysine is 1585 mg/100 g, leucine – 1275 mg/100 g, valine – 510 mg/100 g. The use of this starter is effective for improving the quality of products with strong gluten, with accelerated dough preparation technologies [10–15].

On the international market, Ernst Böcker GmbH & Co. KG (Germany) offers a wide range of both starter products and inactivated starter cultures (paste-like, liquid and dry) ready for use. The company’s product range includes various inactivated sourdoughs: Böcker Germe – dry sourdough for the production of wheat and wheat-rye bread; “Böcker Direkt25” – liquid sourdough for wheat bread; “Böcker Sprossenpaste Weizen” – a pasty sourdough containing germinated wheat grains; “Böcker Wellness-Krauter” – pasty sourdough, which includes a unique composition of herbs (ramson, basil, dandelion, nettle, violet, watercress, cornflower); “Böcker Kartoffelpaste” – pasty potato sourdough with potato cubes [15–18].

The expediency of using various composite mixtures based on barley subjected to bioconversion in the preparation of starter cultures has been established. With this method of processing grain raw materials, all pathogenic microflora is destroyed, while the value of the product increases by 1.4 ... 1.8 times, unlike its analogue.

Lebedenko T. E. et al. carried out a comparative assessment of methods for preparing dough from wheat flour to ensure high quality of finished products, duration, laboriousness of the process, etc., the advantages and disadvantages of each of them, as well as rational conditions of use.

The range of use of starter cultures is very wide, but their biotechnological potential has not yet been sufficiently studied. It should be noted that the technology of breeding sourdoughs is complex; in

the breeding cycle, “pure” cultures of acid-forming bacteria and yeast are needed, which is not always possible in the conditions of bakeries in regions remote from the center, as well as for small producers of bakery products. In addition, in the conditions of the hot climate of Uzbekistan, it is very difficult to maintain the stable required technological parameters, and, consequently, the quality indicators of starter cultures.

New prospects for the industry open up the possibility of using polystrain spontaneous fermentation starters (hereinafter referred to as PZSB), which are characterized by their availability and the absence of the need to purchase “pure” cultures for the breeding cycle. However, they are practically not used in the production of mass varieties of bread due to the production of products of reduced volume with insufficiently loosened crumb.

As a result, it is necessary to develop technological solutions to stabilize the microbiological composition of this type of starter cultures in order to obtain high-quality products.

Purpose of the study

The aim of the work was to study the microbiological composition of PZSB and its effect on the main flour biopolymers, dough properties and the quality of bread from wheat flour of the 1st grade.

Objects of study: pea-star anise sourdough (hereinafter GBZ), wheat bread.

Methods and materials

GBZ was prepared according to the recipe and technological parameters presented in table 1 [12, p. 263-264].

Previously, a mixture of peas and star anise in a ratio of 1.0:0.1 was poured into 1 liter of hot water at a temperature of 80 ± 20 °C, sprinkled with flour, then kept at a temperature of 30 ± 10 °C for 24 hours. in a ratio of 1:1.

The resulting starter was accumulated to the required amount by periodic refreshment, observing the proportions of the recipe and technological parameters of the second phase of the breeding cycle. To

prepare the nutritional mixture, wheat flour of the second grade and water were mixed in a ratio of 1:2, the enzyme preparation Amilorizin P10x was added in an amount of 0.01% to the mass of flour in the mixture.

Table 1. – Consumption of raw materials and semi-finished products and the mode of preparation of the starter culture in the breeding cycle

Name of raw materials, semi-finished products and process indicators	Breeding phase	
	I	II
Peas peeled crushed	1.0	–
star anise	0.1	–
Wheat flour II grade	–	10.0
Milk serum	–	10.0
Water	1.0	10.0
Leaven	–	2.1
Humidity,%, no more	–	72.0 ... 75.0
Initial temperature, °C	30	35 ... 40
Acidity final, hail, no more	–	18.0 ... 22.0
Fermentation duration, h	24	8 ... 12

The nutrient mixture was thoroughly mixed with pre-sour starter, placed in a thermostat and incubated at a temperature of $28 \pm 10\text{C}$ for 20 ... 24 hours until the final acidity was 22.0 deg. Then, every 12 hours, a selection of 50.0% of the finished starter was made and a similar amount of the nutrient mixture was added [19–23].

Titrate acidity was determined by titration with a 0.1 mol/dm³ solution of sodium hydroxide, active acidity was determined on a pH-meter brand pH-673; the number of bacteria – in the Goryaev counting chamber using a ZSM microscope (Poland); bacterial activity – to restore methylene blue; species and quantitative composition of the microflora – by phase-contrast microscopy after preliminary incubation on specialized agar media. A series of trial baking was carried out according to the generally accepted method according to GOST 27669–88 “Baking wheat flour.

Method of trial laboratory baking of bread. GBZ was prepared according to the generally accepted method [122, p. 263–264], wheat dough – by non-dough and sponge methods. The mass fraction of sugar in semi-finished products was determined by an accelerated semi-micro method; the amount of gluten washed from the dough – according to GOST 27839–88 “Wheat flour. Methods for determining the quantity and quality of gluten, water-soluble proteins – by colorimetric method. The quality of bread was analyzed for compliance with the requirements of GOST 27842–88 “Bread from wheat flour. Specifications” [24–30].

Results and discussion

We studied the traditional technology for the preparation of GBZ, which belongs to the group of PZSB. Every 24 hours for 8 days in the starter without renewal, the dynamics of changes in acidity, the composition of microflora and its activity was determined (Table 2).

Table 2. – Quality indicators of starter cultures during spontaneous fermentation

The name of indicators	Values of indicators of the quality of the starter when diluted during, days								
	initial	1	2	3	4	5	6	7	8
Acidity, hail	1.6	10.0	12.6	15.0	17.5	17.0	22.0	26.8	32.4
pH	6.30	3.70	3.65	3.55	3.50	3.50	3.40	3.00	2.80
Quantity	–	226	1329	2320	2385	2769	2851	2512	2192
acid-forming bacteria, mln/g	–	70	65	50	40	35	55	60	75

It was found that the studied starter culture reached its optimal acidity on the 4th... 5th day. At the same time, the bacteria were distinguished by the best reducing activity (40–35 min), which then naturally decreased.

Rod-shaped bacteria and yeast microorganisms were found in the studied sourdough. At the same time, bacteria of the Enterobacteriaceae R. family, which belong to the natural microflora of flour, dominated. As a result of increasing the acidity of the starter and lowering the pH value to 3.5... 3.7, the rest of the microflora weakened or was inhibited, the medium became elective and acid-resistant, rod-shaped bacteria began to dominate in it. At the same time, the number of gram-negative bacteria of the Enterobac-

teriaceal group decreased, and the number of gram-positive rod-shaped bacteria belonging to the genus *Lactobacillus* naturally increased. Simultaneously, yeast cells began to multiply in the medium, which at the beginning of the process were present only in single copies. As the period of incubation of the starter increased, a gradual death of yeast cells of both genera was noted, so after 3 days the number of cells of the cultural yeast race *Saccharomyces* dropped to $15.8 \cdot 10^6$, a *Zygomycetes* – to $3.4 \cdot 10^6$ cells in 1 g of sourdough [31–35].

The ratio of bacteria and yeast on days 1.3 and 5 of dilution was about 13:1, 151:1 and 1025:1, respectively. After 3 days, coccal forms of bacteria and mold fungi began to develop in the sourdough (Table 3).

Table 3. – Species and quantitative composition of microorganisms in sourdough

Time incubation leaven, days	Number of microorganisms ($N \times 10^6$ in 1 g of sourdough) in a nutrient medium	
	MPA	SA
Through 4 h	15.4 (baker's yeast <i>Sacch. cerevisiae</i>)	17.8 (baker's yeast <i>Sacch. cerevisiae</i>) 12.0 (wild yeast <i>Zygomycetes</i>)
1	16.0 (<i>Sacch. cerevisiae</i>) 10.0 (wild yeast <i>Zygomycetes</i>)	18.0 (<i>Sacch. cerevisiae</i>) 12.0 (<i>Zygomycetes</i>)
2	14.5 (<i>Sacch. cerevisiae</i>) 15.0 (<i>Zygomycetes</i>)	17.5 (<i>Sacch. cerevisiae</i>) 18.0 (<i>Zygomycetes</i>)
3	5.8 (coccal forms of bacteria <i>Sarcina</i>) 12.6 (<i>Zygomycetes</i>)	15.8 (<i>Sacch. cerevisiae</i>) 3.4 (<i>Zygomycetes</i>)
4	5.2 (<i>Sarcina</i>)	5.6 (<i>Sacch. cerevisiae</i>) 5.8 (<i>Zygomycetes</i>)
5	2.6 (<i>Zygomycetes</i>) 0.7 (<i>Sarcina</i>)	2.7 (<i>Sacch. cerevisiae</i>) 2.0 (<i>Zygomycetes</i>)
6	0.7 (<i>Sarcina</i>) 0.2 (mushrooms <i>Aspergillus</i>)	2.3 (<i>Sacch. cerevisiae</i>) 1.9 (<i>Zygomycetes</i>)

Further, the properties of the dough and the state of the main biopolymers of wheat flour of the 1st grade were investigated in variants without sourdough, on sourdough without yeast, on sourdough and yeast. With a non-dough method of dough preparation, 8.0% was added to the dough, and 4.0% of sourdough was added to the prescription amount of flour with a sponge method. Samples without yeast and sourdough served as controls. The results of the analyzes are given in (table 3).

Analysis of the data in Table 4 showed that after 3 hours of ripening, the residual amount of sugars in the dough in variants with sourdough exceeded similar values in the variants with yeast and yeast with sourdough, respectively, by 1.4 ... 0.8 and 0.9 ... 0, 5%. An increase in the duration of ripening of semi-finished products in variants with sourdough and yeast, even up to 5 hours, did not lead to depletion of the mass fraction of sugars, moreover, in these variants, their amount exceeded similar values

in semi-finished products with yeast by 1.5 ... 0.9 ... 1.4% (rel.) – with the sponge dough method.

Conclusion

Thus, it was found that it is advisable to use the biologically active mixture after three days. During five days of cultivation, a variety of microflora was preserved in the starter: cocci, rod-shaped bacteria, yeast, mold fungi, etc. With longer cultivation,

acid-resistant rod-shaped bacteria began to dominate. There was a process of displacement of the original microflora of the spontaneously fermented sourdough. Particularly effective is the joint use of yeast and starter cultures in the sourdough dough method, which will intensify the technological process of making bread, reduce the pH of semi-finished products to 5.5 ...

References:

1. Dorosh A. P. Study of the antagonistic properties of sourdough with directed cultivation and evaluation of microbiological indicators of bread based on it / A. P. Dorosh, N. N. Gregirchak // *Technique and technology of food production.* – V. 37. – No. 2. 2015. – P. 10–15.
2. Lebedenko T. E. Modern approaches to choosing a method for preparing wheat dough / T. E. Lebedenko, A. Ya. Kaminsky, R. P. Shchelakova, N. Yu. Sokolova // *Kharchova science and technology.* – No. 1(10). 2010. – P. 46–52.
3. Satsaeva I. K. Improving the quality of wheat bread on the basis of improving the technology of hop sourdough // *Dissertation.... Cand. tech. Sciences.* – Eagle: State. tech. un-t, 2004. – 106 p. – Scientific library of dissertations and abstracts: disser Cat URL: <http://www.dissercat.com/content>
4. Amiraslanov N. I. Influence of the duration of intensive kneading of liquid dough on the kinetics of fermentation // *Bakery and confectionery industry.* – No. 2. 1987. – P. 35–37.
5. Matveeva I. V. Biotechnological bases of bread preparation / I. V. Matveeva, I. G. Belyavskaya. – M.: DeLi print, 2001. – 150 p.
6. Eremin S. F. Modern technologies for the production of bakery products // *Food and rational use of raw materials.* – No. 5. 2002. – 3 p.
7. Ravshanov S. S. The Effect of Drinking And Activated Water on Field Scales of Wheat Grains Grown In Arid Climatic Conditions // Rakhmonov K. S. Ergasheva H. B., Yuldasheva Sh. J. // *European Journal of Molecular & Clinical Medicine.* – Vol. 7. – Issue 3. 2020. – P. 3065–3070.
8. Rakhmonov K. S., Confectionery Products for Therapeutic and Preventive Purpose with Medicinal Herbs Uzbekistan // L. N. Khaydar-Zade, N. SH. Kuliev, G. H. Sulaymonova // *Annals of the Romanian Society for Cell Biology.* – Vol. 25. – Issue 2. 2021. – P. 4126–4140.
9. Oltiev Azim. The role of catalysts in fat transesterification technology // Matluba Kamalova., Kakhramon Rakhmonov, Orifjon Mamatqulov // *IOP Conf. Series: Earth and Environmental Science* – 848. 2021. – 012220 p.
10. Rakhmonov K. S. Wheaten ferments spontaneous fermentation in biorechnological methods // Isabayev I. B. // *Austrian Journal of Technical and Natural Sciences.* – No. 7–8. 2016. – P. 9–12.
11. Rakhmonov K. S. Methods for improving the composition of the nutrient medium of sourdough cultures for bakery products from wheat flour // T. I. Atamuratova. Isabaev I. B. // *Bakery of Russia.* – No. 2. 2016. – P. 22–24.
12. Rakhmonov K. S. Optimization of the recipe composition of wheat breads using spontaneous fermentation starter cultures // Isabaev I. B., U. M. Ibragimov, Molchanova E. N. // *Bakery of Russia.* 2018. – № 3. – S. 33–37.

13. Ravshanov S. S., Rakhmonov K. S., Ergasheva H. B., Yuldasheva Sh. J. The Effect of Drinking and Activated Water on Field Scales of Wheat Grains Grown in Arid Climatic Conditions // European Journal of Molecular & Clinical Medicine.– Vol. 07.– Issue 03. 2020.– P. 3065–3070.

<https://doi.org/10.29013/AJT-22-3.4-23-29>

*Yulchiev Aslbek,
Department of Chemistry, Andijan State University,
Andijan, Republic of Uzbekistan*

*Serkayev Qamar,
Department of Food Technology,
Tashkent Institute of Chemical Technology,
Tashkent, Republic of Uzbekistan*

*Mirzaev Abdugappor,
Department of Biotechnology, Tashkent State Technical University
named after I. Karimov, Tashkent, Republic of Uzbekistan*

*Asqarov Ibrokhim,
Department of Chemistry, Andijan State University,
Andijan, Republic of Uzbekistan*

TECHNOLOGICAL SCHEME OF REFINING OF COTTONSEED OIL PURIFIED FROM GOSSYPOL

Abstract. The article deals with the technological scheme of refining cottonseed oil purified from gossypol. In the experiments, oil samples purified from gossypol containing monoethanolamine (MEA) were refined in two stages using sodium hydroxide. According to the research, the optimal temperature for the refining process was increased from 25 °C to 50–55 °C at the end of the process, the concentration of the alkaline solution was 200 g/l, and the amount of water supplied to moisten the soapstock was formed 0.5–1.0% by weight of oil. To completely purify the oil from gossypol and its derivatives, urea solutions with a concentration of 20–25% in the amount of 0.3–0.7% are given using capacity (5a) instead of water supplied in the process of alkaline refining. The results of the study showed that high gossypol cottonseed oil was treated with monoethanolamine in the amount of 0.2% by weight of oil, as well as when treated with urea solution in the amount of 0.5% by weight of oil for complete refining of gossypol refined oil, it has been found that positive results such as obtaining oils containing gossypol content of up to 0.002% can be achieved.

Keywords: cottonseed oil, refining process, gossypol, purification of cottonseed oil from gossypol, monoethanolamine, forrafination.

Introduction

Several scientists have researched the separation of gossypol from the composition of cottonseed oil with high gossypol. In particular, scientists of the Institute of Bioorganic Chemistry named after O. S. Sodikov of the Academy of Sciences of the Republic of Uzbekistan U. A. Saidakhmedov, A. S. Ibra-

gimov and others managed to obtain gossypol acetate with a purity of 85% by processing acetylene acetic acid in different proportions in the separation of gossypol acetic acid [1; 2; 3].

In addition, methods have been developed in which the anthranilate gossypol content is reduced in processes compared to the conventional method,

and the yield of the final finished product gossypol is higher [2; 4; 5].

Research has also been conducted on the conversion of gossypol in cottonseed oil from oil to shrot by combining it with various components in cottonseed. In the research, the technology of low-gossypol cotton shrot and lightly refined oil production by hydrothermal treatment of cottonseed meal using a solution of urea and sodium silicate was introduced. Today it is used in 23 oil companies of the republic.

Processing of urea solution in cottonseed meal is one of the patented scientific inventions of the Intellectual Property Agency for the invention of IAP 03125 "Method for obtaining lightly refined cottonseed oil and low-content gossypol" [4; 7; 9].

Materials and methods

The method proposed by us has been studied to obtain high gossypol cottonseed oil by converting gossypol to maximum oil by processing the seed pulp using ultra-high frequency rays [5–9].

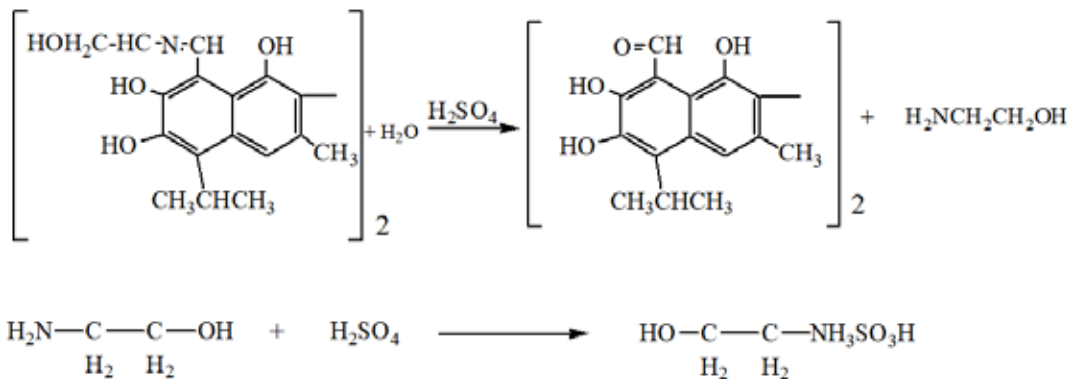


Figure 1. The chemical reaction of separating gossypol from a derivative of gossypol with MEA

As can be seen from Figure 1, when the gossypol product is treated with sulfuric acid, the acid initially acts as a catalyst. Monoethanolamine is released by accelerating the hydrolysis of the product under the influence of water [21–25].

It then interacts with the separated MEA to form the sulfuric acid salt of MEA and precipitates. The following are the technological schemes for the separation of technical gossypol from the combination of gossypol with MEA and complete refining of gossypol degreased oil using urea solution (Figure 2).

Studies have been carried out on the formation of a monoethanolamine compound of gossypol in isolated high gossypol cottonseed oil and its separation with gossypol as a separate commodity by treatment with sulfuric acid [10–17].

In the study, high-gossypol cotton oil with a high gossypol content of 1.46–1.68%, obtained using ultra-high frequency processing, was forrafinated by adding 0.2% monoethanolamine to its mass, followed by complete refining with urea solution. a decrease in the amount of gossypol was observed until traces were detected [18–21].

The processing of two fractions – ethanolamin-gossypol and gossypol degreased oils – formed as a result of the treatment of high-gossypol cotton oil with monoethanolamine (MEA) requires the development of two separate technological sequences. The chemical reaction of high-gossypol cottonseed oil treated with MEA and its separation from technical gossypol with sulfuric acid is as follows:

The pressed high gossypol cotton oil obtained by ultra-high frequency processing falls into the tank (2). From there, the pump (3) is transferred by its own flow to the reactor (1) using a filter regulator (4). The capacity of the reactor is 1000 kg of oil. The lower part of the reactor is equipped with a stirrer and a coating to heat the mixture and stir it for 50–60 rpm to proceed with the forrafination process. The mixer is equipped with an individual electric motor via a separate reducer.

Once the required amount of high gossypol cotton oil has been loaded into the reactor, the mixer is

switched to operating mode and water or steam is supplied to heat or cool the oil (if necessary). The

temperature of the oil is monitored using a thermometer installed in the reactor.

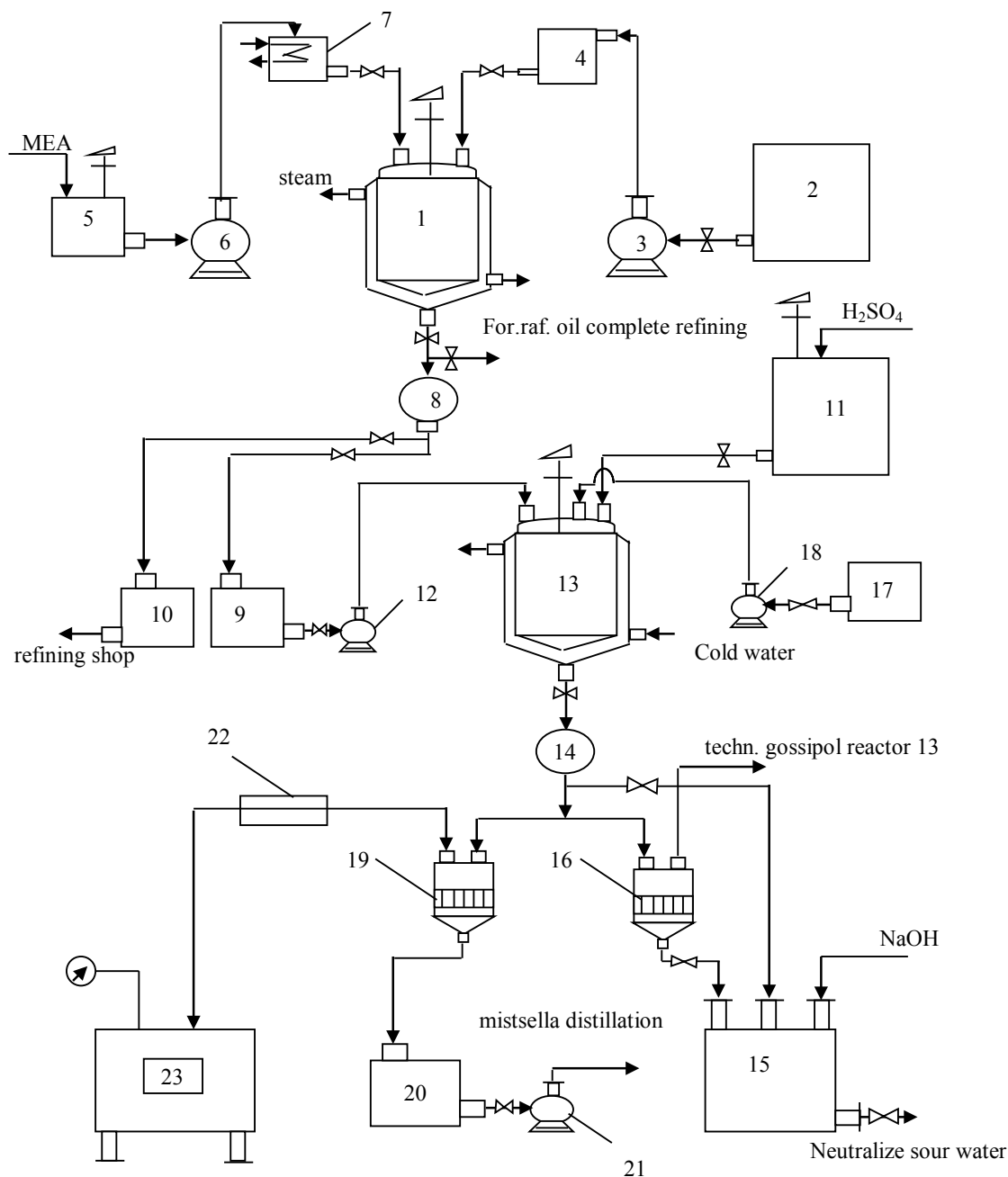


Figure 2. Technological scheme of processing and technical gossypol separation of high gossypol cotton oil with MEA

Results and discussion

We know that in the traditional technology when the periodic forrafination process is carried out periodically, the temperature of the oil starts at 20–25 °C and ends at 50–55 °C. In traditional technology, the refining process takes 20–25 minutes. In our

research, high gossypol cottonseed oil was refined in a stepwise manner. During the study, forrafination of high gossypol cottonseed oil was carried out at different temperatures, and it was found that the optimal temperature for the maximum sedimentation of gossypol is 45–50 °C. Studies have shown that

treatment with MEA at a rate of 0.2% relative to the oil mass is mainly effective.

The reactor (1) is treated with MEA through the tank (5), pump (6) and regulator (7), calculated relative to the oil mass as mentioned above. The processing and mixing time is 15–20 minutes. MEA is gradually added to the high gossypol cotton oil with constant stirring. After the addition of the required amount of MEA, the reaction mixture is allowed to stand for 1.5–3.0 hours. The liquid soapstock and oil are separated into two phases at the bottom of the reactor. Because the liquid is heavier than the soapstock mass, it collects at the bottom of the reactor, while the oil collects in the top layer. Extreme care must be taken in separating the phases of degassed oil and liquid soapstock. The liquid collected at the bottom of the reactor is collected in the soapstock tank (9) through a valve and observation window (8) designed to separate the soapstock. The degassed oil is sent through the valves for complete refining. Partial emulsification is observed between the soapstock and the decomposed oil, and the resulting emulsion is collected in a separate tank (10) and returned to the refining process.

The MEA product (soapstock) of the gossypol collected in the tank (9) is transferred to the reactor (13) using a pump (12) in order to separate the gossypol as a separate commodity. To return the compound of gossypol formed from MEA to gossypol to the reactor (13), the working sulfuric acid prepared for treatment with 5% sulfuric acid is prepared in a tank (11) and transferred to the reactor (13) by its own flow.

The soapstock collected in the tank (9) is transferred to the reactor (13) using a pump (12). The disposable liquid soapstock load on the reactor (13) is 245 kg. The reactor (13) is a mixer with a speed of 50–60 rpm and the bottom part is covered with a coating so that the reactor is heated or cooled if necessary. A valve is installed at the bottom of the reactor (13) to separate the reaction mass. In this case, the pH of the interior of the reactor is checked using a universal indicator and the environment is

controlled to be around 4.5–5.0. To separate the technical gossypol, the reactor (13) is cooled to 20–25 °C using cold water. As a result of the cooling of the reaction mixture, the technical gossypol rises to the top layer of the mixture. The mixture is allowed to stand for 1 hour to completely separate the technical gossypol in the reaction mixture. To separate the technical gossypol, the sour water is first collected in the tank (15) using a valve, controlled by means of an observation window (14) mounted on the bottom of the reactor (13). To separate the technical gossypol from the intermediate emulsion containing gossypol residues, the nutch is passed through a filter (16) and the gossypol residues are retained. The remaining technical gossypol in the reactor (13) is washed with water until it reaches a neutral point. The leachate from the leaching is cleaned of gossypol residues using a nutch filter (16) and sent to the tank (15) for sour water. The sour water collected in the tank (15) is neutralized with sodium alkali and discharged into the sewer.

The technical gossypol residues trapped by the Nutch filter (16) are returned to the reactor (13). The technical gossypol, washed with water to a neutral medium, is processed with extraction gasoline to remove fatty acids and other water-insoluble raw materials. In the reactor (13), the technical gossypol in a neutral environment is supplied with extraction gasoline using a tank (17) and a pump (18). The reactor (13) performs several functions simultaneously. This serves to avoid the use of redundant equipment in the technological cycle and reduce the cost of the product. The capacity of the reactor (13) was 245 kg for liquid soapstock and 50 kg for technical gossypol. The reactor is treated with 210 kg of extraction gasoline in terms of oil mass and the process is continued for 25–30 minutes. A mixture of technical gossypol and extraction gasoline is trapped in a nutch-filter (19) containing technical gossypol. The mistsella cleaned from the technical gossypol is sent to distillation using a tank (20) and a pump (21). Gasoline collected during distillation is returned to

the process. Using technical gossypol hand cocktail collected in the Nutch filter (19), parchment paper is spread on 3–4 cm thick sheets. Partially dried technical gossypol of the same thickness is taken to the table (22) after one day for complete drying

and dried for 10 hours at 50–60 °C using dry air in a vacuum dryer (23). The yield of technical gossypol is 16.5–16.8 kg per 1000 kg of high gossypol oil. The technological scheme of complete refining of degassed oil is given below.

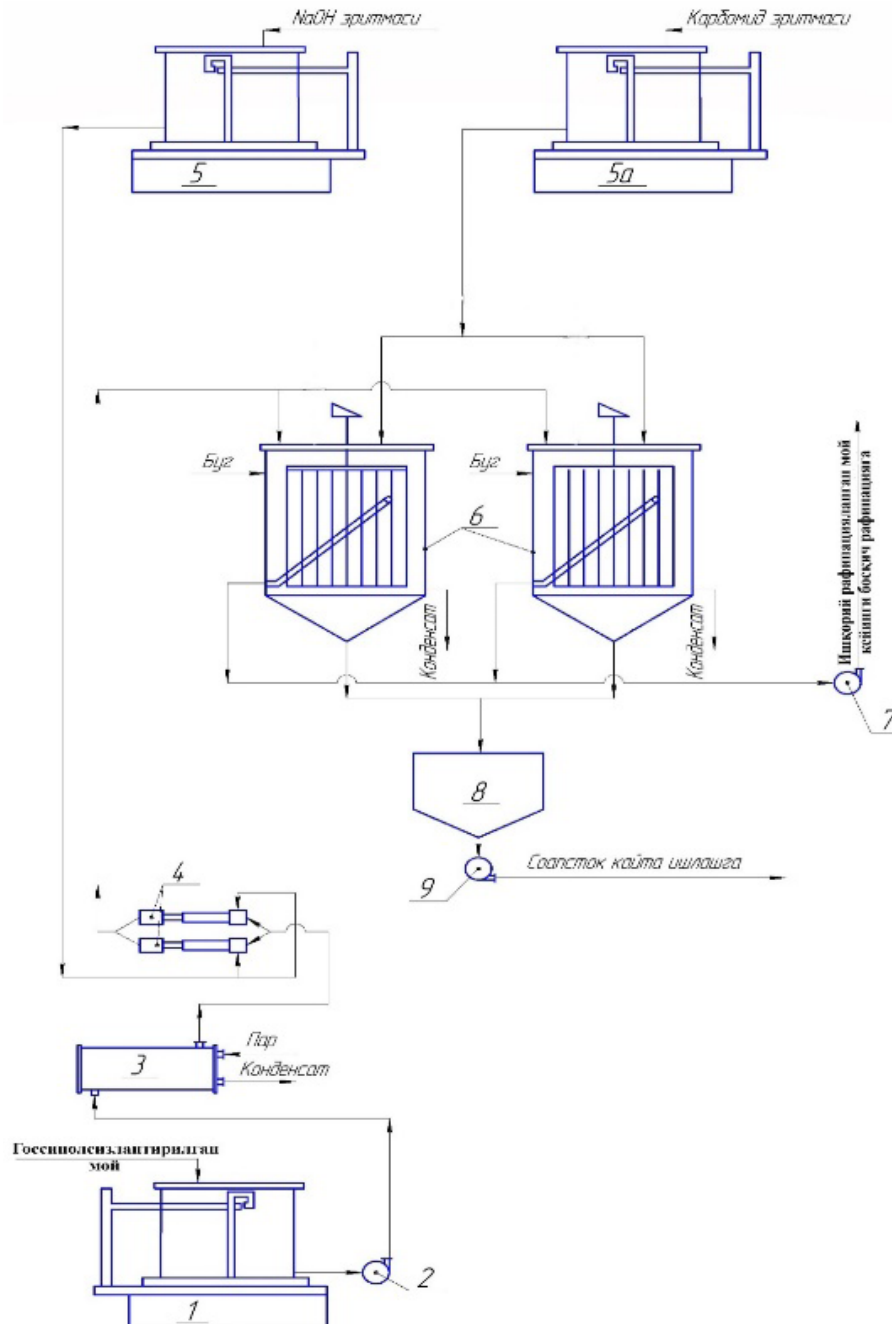


Figure 3. Technological scheme of refining oils purified from gossypol using urea solution

The oil purified from the gossypol (Fig. 4) falls into the weighing tank (1). The temperature is then adjusted to 20–25 °C using a pump (2) and a heat

exchanger (3). Adjusting the temperature of the oil serves to ensure the optimal course of the refining process and the complete purification of the accompany-

ing substances in the oil. The adjusted oil is transferred to the reactor-turbulizer (4). In the reactor-turbulizer unit, the oil and alkali solution are intensively mixed. The reactor turbulizer unit, on the other hand, is supplied with a calculated amount of working alkali solution based on the acid number of the oil.

In the experiments, oil samples purified from gossypol containing monoethanolamine were refined in two stages using sodium hydroxide. According to the research, the optimum temperature for the refining process was increased from 25 °C to 50–55 °C at the end of the process. The concentration of the alkaline solution was 200 g/l, and the amount of water supplied to moisten the soapstock was 0.5–1.0% by weight of oil. The refining process took 23–25 minutes. The working alkaline solution is continuously transferred to the recuperator turbulizer using the weighing tank (5). A mixture of oil and alkali is fed to the periodic neutralizer (6). To completely purify the oil from gossypol and its derivatives, urea solutions with a concentration of 20–25% in the amount of 0.3–0.7% are given using capacity (5a) instead of water supplied in the process of alkaline refining. The alkaline refined oil is transferred to the next stage of refining using a pump (7). The soapstock collected at the bottom of the neutralizers (6) is sent to the soapstock for processing using a tank (8) and a pump (9).

Conclusion

The results of the study showed that high gossypol cottonseed oil was treated with 0.2% MEA of oil mass, while gossypol oil was treated with 0.5% urea solution for complete refining of gossypol refined oil. It has been found that positive results can be obtained, such as obtaining oil in the state.

The proposed technological scheme allows for the simultaneous forrafination of high-hemp cotton oil using MEA and the separation of technical hemp as a separate commodity. The advantage of the proposed technology is that the complete refining of oil refined from forrafinated gossypol using a urea solution does not significantly change the existing technological process, but the possibility of obtaining high-quality oil.

Acknowledgements

The authors acknowledge the immense help received from the scholars whose articles are cited and included in references to this manuscript. The authors are also grateful to the authors/ editors/publishers of all those articles, journals and books from where the literature for this article has been reviewed and discussed.

The authors report no conflicts of interest.

The Source of funding is nil.

References:

1. Nazirov N. Science and cotton. Publishing house "Uzbekistan".– Tashkent. 1977.– 276 p.
2. Markman A. L., Rzhekhin V. P. Gossypol and its derivatives. – Moscow: Food Industry, 1965.– 244 p.
3. Patent. № IAP 03125–2006 y. A method of obtaining lightly refined cottonseed oil and shrot with a low content of gossypol.
4. Julchiev A. B. Mehanizm poluchenija pressovogo vysokogossipol'nogo hlopkovogo masla s ispol'zovaniem SVCh-nagreva [Mechanism for producing high-pressure cottonseed oil using microwave heating]. Universum: Engineering Sciences,– 4 (49). 2018.– P. 10–10. (in Russian).
5. Julchiev A. B. Jeksperimental'nye rezul'taty i optimizacija pererabotki hlopkovoj mjatki v SVCh-ustanovke. Universum: tehniicheskie nauki, [Experimental results and optimization of the processing of cottonseed in a microwave unit],– 7–2 (76). 2020.– P. 46–50. (in Russian).
6. Adams R., Geissman T. A., & Edwards J. D. Gossypol, a pigment of cottonseed.– 60(6). 1960.–P. 555–574.
7. Yulchiev A. B., Rakhmanov D. T., & Jamolov K. Sh. W. Influence of carbamide solution on the purification of sunflower oil. Universum: Engineering Sciences,– 7–2(88). 20213.– P. 7–41.

8. Sh I. S. Research of changes in the quality indicators of bleached cottonseed oil and its products. *Austrian Journal of Technical and Natural Sciences*, – (3–4). 2019. – P. 16–19.
9. Yulchiev A. B., & Normatov A. M. (). Microwave installation for moisture-thermal treatment of cottonseed. *Universum: Engineering Sciences*, – 7–2(76). 2020. – P. 51–57.
10. Aslbek Y., Qamar S., & Abdugappor M. The operator model of high gossypol cotton oil extraction, functional scheme of technical gossypol extraction and oil refining. *Universum: химия и биология*, – 3–2 (93). 2022. – P. 42–47.
11. Lin H., Wedegaertner T. C., Mao X., Jing X., & Roa-Espinosa A. A method to refine crude cottonseed oil using non-toxic polyamine-based cationic polymers. *Chinese Journal of Chemical Engineering*, – 23(2). 2015. – P. 379–383.
12. Yulchiev A. B., Abdurakhimov S. A., & Serkaev Q. P. (). Operator models of technology for producing cottonseed oil with high content of gossypol using. *European applied sciences*, – (3). 2015. – P. 77–79.
13. King W. H., & Thurber F. H. An improved procedure for the purification of gossypol. *Journal of the American Oil Chemists Society*, – 30(2). 1953. – P. 70–74.
14. Yulchiev A. B. Influence of microwave treatment of cottonseed oil on the parameters of press oil and cake. *Fat and oil industry*, – (3). 2015. – P. 13–17.
15. Lipstein B., & Bornstein S. Studies With Acidulated Cottonseed-Oil Soapstock: 2. Attempts to Reduce its Gossypol Content. *Poultry Science*, – 43(3). 1964. – P. 694–701.
16. Yulchiev A. B. Optimization of the process of obtaining high-grade cottonseed oil using microwave processing of mint. *Fat and oil industry*, – (5). 2015. – P. 20–22.
17. Kim H. Isolation, purification and partial characterization of a gossypol related brown pigment from cottonseed pigment glands (Doctoral dissertation, Oklahoma State University). 1966
18. Yulchiev A. B. Gossypol localization modification in the cotton mash during the process of microwave manufacturing. *Europaische Fachhochschule*, – (9). 2015. – P. 55–57.
19. Castillon L. E., Hall C. M., & Boatner C. H. Preparation of gossypol from cottonseed pigment glands. *Journal of the American Oil Chemists' Society*, – 25(7). 1948. – P. 233–236.
20. Yulchiev A. B. On the economic efficiency of the introduction of technology for obtaining high-pressure cottonseed oil by microwave radiation. *Volga Scientific Bulletin*, – 7 (47). 2015. – P. 35–38.
21. Pons Jr. W. A., Berardi L. C., & Frampton V. L. Kinetic study of gossypol fixation in cottonseed oil. *Journal of the American Oil Chemists' Society*, – 36(8). 1959. – P. 337–339.
22. Aslbek Y., & Ibrokhim A. Problems and prospects of classification and certification of cottonseed oil fractions on the nomenclature of goods of foreign economic activity in terms of chemical composition. *Universum: химия и биология*, – 3–2 (93). 2022. – P. 38–41.
23. Bahtiyorbekovich Y. A., Abdurakhmanov A. S., & Pardayevich S. Q. The change of gossypol composition during the moisture heat processing of cottonseed cake by different methods. *Austrian Journal of Technical and Natural Sciences*, –(1–2). 2015. – P. 118–121.
24. Jia G., Zhan Y., Wu D., Meng Y., & Xu L. An improved ultrasound-assisted extraction process of gossypol acetic acid from cottonseed soapstock. *AIChE Journal*, – 55(3). 2009. – P. 797–806.
25. Yulchiev A. B., Abdurahimov S. A., & Serkaev K. P. Study of the method of hydrothermal treatment of cottonseed with the use of microwave radiation. *Chemical technology control and management*, – (2), 2011. – P. 47–50.

Section 5. Technical sciences

<https://doi.org/10.29013/AJT-22-3.4-30-34>

*Akhmedov Ulug Karimovich,
Doctor of Chemical Sciences, Professor
Institute of General and Inorganic Chemistry
of the Academy of Sciences of the Republic of Uzbekistan
Head of the laboratory "Surfactants"*

*Kurambaev Sherzod Raimberganovich,
Doctor of Technical Sciences, Urgench State University
Associate Professor of the Department of Food Technology*

*Bakhtiyarov Sardorbek Bakhtiyarovich,
PhD of Technical Sciences, Urgench State University
Senior Lecturer of the Department of Food Technology*

OBTAINING COTTONSEED OIL THAT MEETS THE REQUIREMENTS OF FOOD SAFETY OF THE POPULATION

Abstract. Access to sufficient, safe and nutritious vegetable oil-based food is essential to sustain life and improve the health of the population. Adsorbents for the adsorption purification of vegetable oils, in particular cottonseed oil, are brought to the oil and fat plants of Uzbekistan from abroad.

In order to obtain a highly effective adsorbent from natural kaolin Sultan-Uvays, the authors developed a technology for modifying kaolin, the resulting modified adsorbent was used in the adsorption purification of cottonseed oil in miscella, and positive results were obtained in terms of the degree of purification and yield of finished cottonseed oil.

Keywords: Safe, vegetable, natural, mineral, adsorbent, modification, degree, soapstock, organoleptic, physico-chemical.

Introduction

Obtaining cottonseed oil by extraction that meets safety requirements is the most important factor for maintaining life and improving the health of the population. Unsafe vegetable oils containing disease-causing concomitant substances or harmful chemicals are the cause of many diseases.

Every year in low- and middle-income countries, the economic cost of lost productivity due to

employee illness and subsequent medical costs increases.

Issues of food safety with vegetable oils and food products based on them are inextricably linked. Unsafe vegetable oils give rise to various diseases when they are fed, which especially affects all generations of the world's population. Foodborne diseases are an obstacle to social and economic development.

National businesses and agencies responsible for ensuring food safety play a key role in ensuring that every population can eat safe food. Through appropriate food safety regulations, in particular cottonseed oil, they can assist in the management of food safety issues at all stages of the food chain.

Because proper processing, storage, and safety of vegetable oils preserves their nutritional value, minimizes spoilage, and ensures food safety.

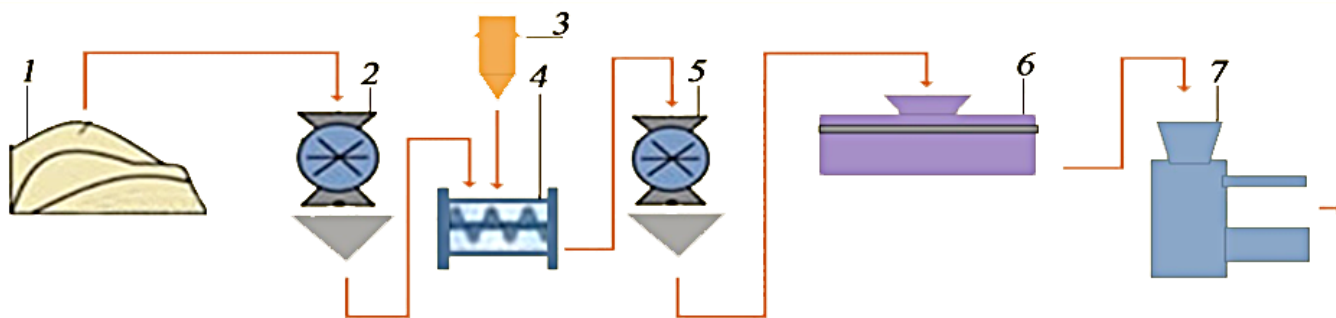
Objective of work.

Adsorbents for the adsorption purification of vegetable oils in oil and fat plants of Uzbekistan are brought from abroad. In Uzbekistan, there are deposits of natural minerals that are rich in kaolin, bentonite, flask and others. The natural mineral kaolin Sultan-Uvays has not yet found its practical application in the adsorption purification of cottonseed oil [1, p. 183–184].

The adsorption properties of natural Sultan-Uvays kaolin in its natural form are low. To obtain a highly effective adsorbent from natural kaolin Sultan-Uvays, the authors developed a technology for modifying kaolin. The resulting modified adsorbent from kaolin was used in the adsorption purification of cottonseed oil in miscella. At the same time, positive results were obtained in terms of the degree of purification and the yield of finished cottonseed oil [2, p 61–65].

Materials and methods.

To accomplish this task, the authors decided to use the natural mineral kaolin Sultan-Uvays in the adsorption purification of cottonseed oil. For the adsorption purification of cottonseed oil in a miscella obtained by the extraction method, a modified adsorbent from natural kaolin Sultan-Uvays was obtained, the technological scheme of which is given in Drawing No. 1.



Drawing 1.

Drawing No. 1. Technological scheme for obtaining a modified adsorbent from natural kaolin Sultan-Uvays. 1. Natural kaolin Sultan-Uvays. 2. Chopper. 3. Storage tank for whey from curdled milk. 4. Bake. 5. Chopper. 6. Separator. 7. Packing machine.

The technological processes for obtaining a modified adsorbent are as follows: grinding of natural kaolin, adding filtered whey from curdled milk to kaolin, followed by drying, grinding and sifting, and packaging of the resulting modified adsorbent.

Also, the authors have developed an effective technology for improving the refining and deodorization of cottonseed oil obtained by the extraction method, which is given in Drawing No. 2.

Drawing No. 2. Technological scheme for improving the refining and deodorization of cottonseed oil obtained by the extraction method. 1. Tank for miscella. 2. Bleach separator. 3. Filter press. 4. Distiller. 5. Deodorizer. 6. Oil cooler. 7. Filter press. 8. Packing machine.

The technological processes for improving the refining and deodorization of cottonseed oil obtained by the extraction method are as follows: cottonseed oil miscella receiving, adsorption purification by the proposed modified adsorbent, oil filtering to separate the adsorbent, alkaline refining, miscella distillation, deodorization, oil cooling, filtering, container packing of ready-made cottonseed oil that meets the

requirements of the standard. In this improvement technology, adsorption refining is applied to the 60% concentration miscella instead of the traditional 35–40% concentration miscella, to save time and energy,

and increase productivity. During adsorption treatment with the proposed modified adsorbent, the adsorbent is introduced in an amount of up to 1–8% by weight of the miscella.



Drawing 2.

Results and discussions.

Using the technology for improving the refining and deodorization of cottonseed oil, the authors de-

termined the color indices of the miscella before and after adsorption purification with a modified adsorbent, the indices of which are given in Table No. 1.

Table 1. – Color indices of the miscella before and after adsorption purification with a modified adsorbent

Nº	Color of the miscella before adsorption purification, red units	The color of the miscella after adsorption purification with a modified adsorbent, red units	The color of the miscella after adsorption cleaning with the control adsorbent, red units
1	Sample N ^o 1. 21	17	18
2	Sample N ^o 2. 32	28	30

According to (table 1), we can conclude that the modified adsorbent and the control adsorbent reduced the amount of coloring pigments of cottonseed oil, which affects the decrease in the color of cottonseed oil miscella samples. Table 1 shows the average values of cotton miscella samples. The modified adsorbent is introduced into the miscella of cottonseed oil in an amount of 1–8% by weight of the miscella until the required color of the oil is obtained during the subsequent alkaline refining, since the adsorption efficiency of the proposed modified

adsorbent affects the optimization of further alkaline refining and distillation. Since the impact of the external environment on cotton seeds during their long-term storage affected the change in the quality indicators of cottonseed oil, the proposed modified adsorbent is introduced in an increased amount over the course of the year [3, p. 93–96, 4, p. 51–52].

The authors determined the final indicators after alkaline refining of cottonseed oil, which has undergone adsorption refining, the indicators of which are given in (table 2).

Table 2. – Indicators after alkaline refining of cottonseed oil purified by the proposed modified adsorbent

№	The name of indicators	Indicators of cottonseed oil not passed adsorption purification	Indicators of cottonseed oil not passed adsorption purification	Indicators of cottonseed oil that passed adsorption cleaning with a control adsorbent
1	Chromaticity, red units at 35 yellow	10	4–5	9
2	Soapstock quantity, %	5.2–8.5	1.8–3.6	3.4–7.2

According to the indicators of table No. 2, we can conclude that adsorption cleaning with a modified adsorbent had a positive effect on the further process of alkaline refining. The color of cottonseed oil meets the safety requirements, the amount of soap stock is the smallest compared to other samples [5, p 45].

Organoleptic and physico-chemical parameters of cottonseed oil obtained by the extraction method, refined and deodorized by the proposed technology, are given in (Tables 3 and 4).

Table 3. – Organoleptic characteristics of cottonseed oil obtained by the extraction method, refined and deodorized by the proposed technology

№	The name of indicators	Indicators for refined, deodorized cottonseed oil of the highest grade, norm according to GOST	Indicators of cottonseed oil obtained by the proposed technology
1	Smell	Without smell	Without smell
2	Taste	no taste	no taste
3	Transparency	Transparent	Transparent

From (table 3), we can conclude that the use of technology to improve the refining and deodorization

of cottonseed oil obtained by the extraction method gave positive results in terms of organoleptic indicators.

Table 4. – Physical and chemical indicators of cottonseed oil obtained by the extraction method, refined and deodorized by the proposed technology

№	The name of indicators	Indicators for cottonseed oil of the highest grade, standard according to GOST	Oil indicators obtained by the proposed technology
1	Chromaticity, no more than red units, with 35 yellow units	5	4–5
2	Acidity, mg KOH/gr, no more	0.2	0.15
3	Moisture and volatile substances, %, no more	0.1	0.08
4	Mass fraction of non-fatty substances, (sediment by mass) %, no more	Absent	Absent
5	Soap (quality indicators)	Absent	Absent
6	Unsaponifiable substances, % no more	1.0	0.7
7	Peroxide value, mmol/kg, $\frac{1}{2}$ «O», no more	10	4.5
8	Flash point, °C no more	Absent	Absent
9	Determination of solvent (gasoline) in oil	Absent	Absent

From table No. 4 we can conclude that the use of technology for improving the refining and deodorization of cottonseed oil obtained by the extraction method gave positive indicators in terms of the degree of clarification and in all physicochemical parameters [6, p. 5–6].

Conclusion

During the adsorption purification of cottonseed oil in miscella, a modified adsorbent obtained from natural kaolin Sultan-Uvays was used.

The use of technology to improve the refining and deodorization of cottonseed oil obtained by the extraction method gave positive results in terms of organoleptic indicators, according to the degree of clarification and according to all physical and chemical indicators to obtain cottonseed oil that meets the requirements of food safety of the population.

References:

1. Aripov E. A. Natural mineral sorbents, their activation and modification. – Tashkent, 1970. – P. 183–184.
2. Akhmedov A. N., Suvanova F. U., Abdurahimov S. A., Pardaev G. E. Efficient technology for processing low-grade cotton seeds. 2019 FAN. – Tashkent. From 61–65, – P. 76–83 p.
3. Usmanov B. S., Kadirov Z. Z., Ibragimov L. A. Methods for using high-frequency rays during long-term storage of raw materials for the production of vegetable oils. Universum Technical sciences. From – 2021. – P. 93–96.
4. Mustafaev S. K., Smychagin E. O. Prospects for the use of innovative technology for post-harvest seed treatment in the production of vegetable oils. 13th International Conference “Fat and Oil Industry-2013”. Collection of conference materials. October 23–24. 2013. – P. 51–52.
5. Akhmedov A. N., Suvanova F. U. Improving the refining process of extracted cottonseed oil miscelles. 2021 g. 2021/2 (42). Innovative technologies. – 45 p.
6. State standard of the Republic of Uzbekistan. O’z DSt 816: 2015. Refined cottonseed oil. Specifications. – Tashkent. 2015. – P. 5–6.

<https://doi.org/10.29013/AJT-22-3.4-35-43>

Soliev L.,

Jumaev M. T.,

Nizomov I. M.,

Makhmadov Kh.R.,

Olimdzonova N. V.,

Muzafarova D. V.,

Tajik State Pedagogical University

named after Sadriddin Aini, Dushanbe, Tajikistan

FORMATION OF INVARIANTE QUILIBRIA IN MULTICOMPONENT SYSTEMS AND DETERMINATION OF SOLID PHASE CRYSTALLIZATION PATHWAY

Abstract. The structure of a phase complex of the six-component mutual system of Na, K, Mg, Ca||SO₄, Cl-H₂O at 50 °C in the anhydrite (CaSO₄) crystallization region is studied by translation method. The variants of the formation of invariantequilibria (invariantfields) at transition from the five to the six component state and possibleways for solid phasecrystallization with anhydrite (CaSO₄) participation are shown.

Keywords: multicomponent systems, translation method, phase complex, geometric images.

Introduction

Laws, determining the structure of the phase complex (phase equilibria) of multicomponent systems, are a theoretical basis for the creation of optimal processing conditions of polymineral natural and complex technical raw materials. Experimental establishment of the seregularitiesrequiresconsiderable material and time costs. There are also problems in displaying the establishedpatterns in the form of state diagrams (phase equilibrium diagrams) of the system using the geometricfigures of the real three-dimensional space [1], identification of solid phasesbecause of their diversity. The methodsdeveloped for the study of multicomponentsystems [2] have limitedapplication. For example, the method of determiningphaseassociations of “marine” system of Na, K, Mg, Ca||SO₄, Cl-H₂O at 25 °C developed by the authors [3–7], based on minimizing the Gibbs energy, can satisfactorilydetermine the possible phase associations in the four-component systems. When using

the method for five-and more component systems, according to the authors, the resultsobtained will be unreliable. In addition, it is impossible to construct a phaseequilibrium diagram of the studiedsystem on the basis of the obtaineddata.

Objects and methods

Kurnakovwrote N. S. the following about the nature of diagrams of multicomponentsystems: “... any diagram of multicomponentsystem can be considered as formed from the diagram of systems with smaller number of components, complicated by introduction of new components or otherconditions of equilibrium, and characteristicelements of more simple diagram do not disappear, but only take anothergeometrical image...”. [8; 9]. Ya. G. Goroshchenkohavingtheoreticallygrounded N. S. Kurnakov’sideas in addition to the two known basicprinciples of physicochemicalanalysis (principles of correspondence and continuity) proposed the third one, the principle of compatibility of geometricalimages of pi (n+1) component sys-

tems in one diagram [10; 11]. Based on the principle of compatibility we have developed the translation-method [12] to predict the phase equilibria in multicomponent systems followed by the construction of their phase complex diagrams (phase equilibria). The translation method is recognized by specialists as one of universal methods for investigations of multicomponent systems [2] and has been extensively tested in the study of five-component and fragmented six-component systems [13–19].

The experience of application of translation method for investigation of fragments of six component system Na, K, Mg, Ca||SO₄, Cl-H₂O [19] has shown the different nature of geometrical images-formation in multicomponent systems. For example, the study of formation conditions of nonvariant equilibria in the five-component system of NaCl-KCl-MgCl₂-CaCl₂-H₂O at 25 °C [20] demonstrated that increasing the component system promotes the appearance of additional nonvariant point formation, which is accompanied by the formation of «qua-

sitots» having definite size. The study of sylvium-fragment method of six-component system of Na, K, Mg, Ca||SO₄, Cl-H₂O at 50 °C [21] has shown that monovariant curves can form both at translation of nonvariant points of five-component systems to six-component composition level and for binding of nonvariant points at this component level.

Results and their discussion

In the present paper, we considered the possible variants of the formation of divariant fields (divariant equilibria) of the six-component system Na, K, Mg, Ca||SO₄, Cl-H₂O at 50 °C in the anhydrite (CaSO₄) crystallization domain established by translation. The six-component system under study includes 6 five-component systems in 4 of which anhydrite is an equilibrium phase at 50 °C. The list and phase composition of precipitation of nonvariant points of the system Na, K, Mg, Ca||SO₄, Cl-H₂O at 50 °C in the area of crystallization of anhydrite (CaSO₄) which were taken from [19; 22] are given in (table 1).

Table 1. – Phase composition of the precipitation of the nonvariant points of the system Na, K, Mg, Ca||SO₄, Cl-H₂O at 50 °C in the area of crystallization of anhydrite (CaSO₄)

Nonvariant points	Phase composition of precipitation	Nonvariant points	Phase composition of deposits system
System Na ₂ SO ₄ -K ₂ SO ₄ -MgSO ₄ -CaSO ₄ -H ₂ O		E ₃₆ ⁵	An+Ac+Cc+Lev
E ₉ ⁵	An+Ac+Pg+Sc	E ₅₇ ⁵	An+Ki+Lev+Sk
E ₁₀ ⁵	An+As+Gb+Gz	E ₅₈ ⁵	An+Ga+Ki+Lev
E ₁₁ ⁵	An+Gz+Pg+Ps	System K, Mg, Ca SO ₄ , Cl-H ₂ O	
E ₁₆ ⁵	An+Gz+As+Pg	E ₆₂ ⁵	An+Pg+Ps+Ci
System Na, K, Ca SO ₄ , Cl-H ₂ O		E ₆₄ ⁵	An+Gf+Kr+Ci
E ₄₁ ⁵	An+Ga+Gb+Gz	E ₆₅ ⁵	An+Bi+Kr+Tx
E ₄₂ ⁵	An+Gz+Pg+Ci	E ₆₆ ⁵	An+Gf+Tx+Ca-2
E ₄₅ ⁵	An+Ga+Gf+Ci	E ₆₇ ⁵	An+Ki+La+Cc
E ₄₆ ⁵	An+Ga+Gf+Ca-2	E ₆₈ ⁵	An+Bi+Ki+Kr
E ₄₇ ⁵	An+Ga+Gz+Ci	E ₇₀ ⁵	An+Pg+La+Cr
System Na, Mg, Ca SO ₄ , Cl-H ₂ O		E ₇₁ ⁵	An+Gf+Kr+Tx
E ₄₈ ⁵	An+Ga+Bi+Tx	E ₇₃ ⁵	An+Kai+Kr+Ci
E ₄₉ ⁵	An+Ga+Tx+Ca-2	E ₇₅ ⁵	An+Kai+Ki+La
E ₅₀ ⁵	An+As+Ga+Lev	E ₇₆ ⁵	An+Kai+Ki+Kr
E ₅₁ ⁵	An+As+Ga+Gb	E ₇₇ ⁵	An+Kai+Cn+Cy
E ₅₄ ⁵	An+B+Ga+Ki	E ₇₈ ⁵	An+Kai+La+Pg

In (Table) 1 and below, E is the designation of a nonvariant point, where its upper index indicates the multiplicity of the point (system component), and the lower index indicates the ordinal number of the point. For convenience, the ordinal numbers of the points are preserved as in [19, 22]. The following notation of the equilibrium solid phases is accepted [23, 24]: An – anhydrite (CaSO_4); As – astrachanite ($\text{Na}_2\text{SO}_4 \cdot \text{MgSO}_4 \cdot 4\text{H}_2\text{O}$); Bi – bischofite ($\text{MgCl}_2 \cdot 6\text{H}_2\text{O}$); Ga – halite (NaCl); Gb – glau-

berite ($\text{Na}_2\text{SO}_4 \cdot \text{CaSO}_4$); Gz – glaserite ($3\text{K}_2\text{SO}_4 \cdot \text{Na}_2\text{SO}_4$); Gf – hydrophilite ($\text{KCl} \cdot \text{CaCl}_2$); Kai – kainite ($\text{KCl} \cdot \text{MgSO}_4 \cdot 3\text{H}_2\text{O}$); Ki – kiserite ($\text{MgSO}_4 \cdot \text{H}_2\text{O}$); Cr – carnallite ($\text{KCl} \cdot \text{MgCl}_2 \cdot 6\text{H}_2\text{O}$); La – langbeinite ($\text{K}_2\text{SO}_4 \cdot 2\text{MgSO}_4$); Lev – leveite ($\text{Na}_2\text{SO}_4 \cdot \text{MgSO}_4 \cdot 2,5\text{H}_2\text{O}$); Pg – polyhalite ($\text{K}_2\text{SO}_4 \cdot \text{MgSO}_4 \cdot 2\text{CaSO}_4 \cdot 2\text{H}_2\text{O}$); Ps – pentasolite ($\text{K}_2\text{SO}_4 \cdot 5\text{CaSO}_4 \cdot \text{H}_2\text{O}$); Si – sylvin (KCl); Sk – sakyite ($\text{MgSO}_4 \cdot 6\text{H}_2\text{O}$); Tx – tachhydrite ($2\text{MgCl}_2 \cdot \text{CaCl}_2 \cdot 12\text{H}_2\text{O}$); Ca-2 – $\text{CaCl}_2 \cdot 2\text{H}_2\text{O}$.

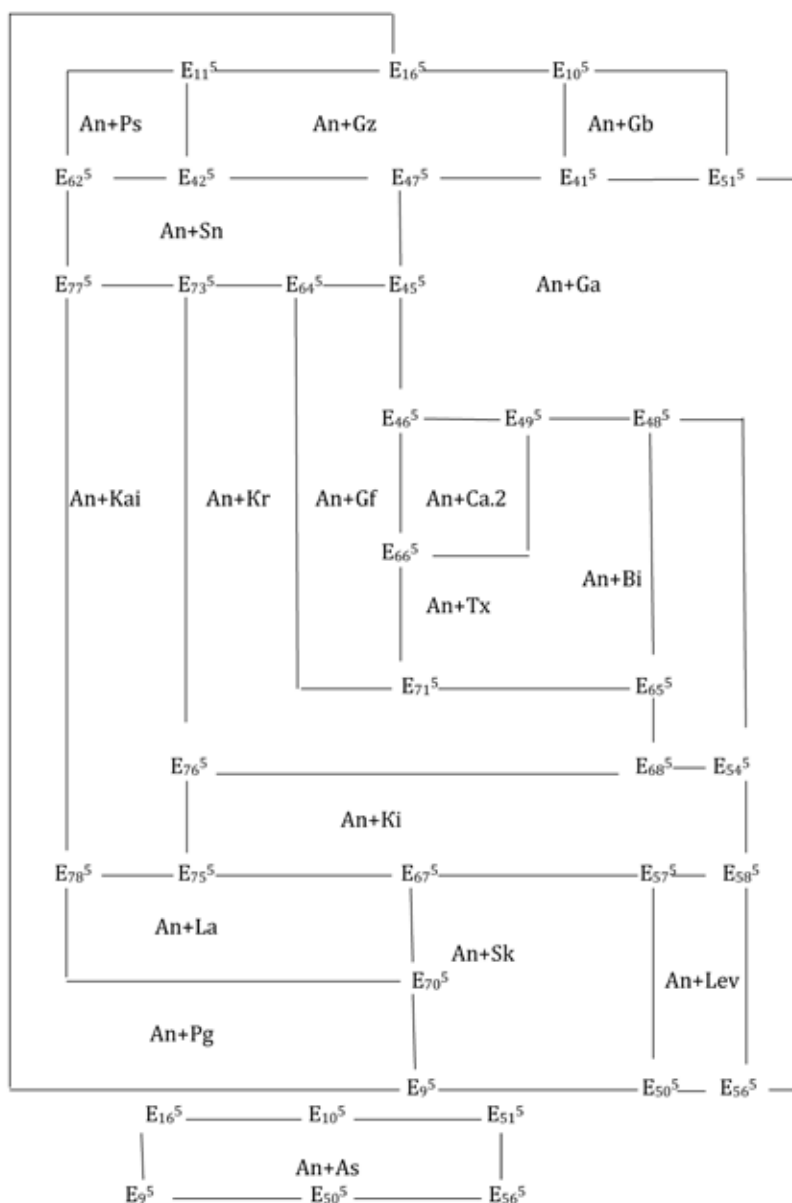
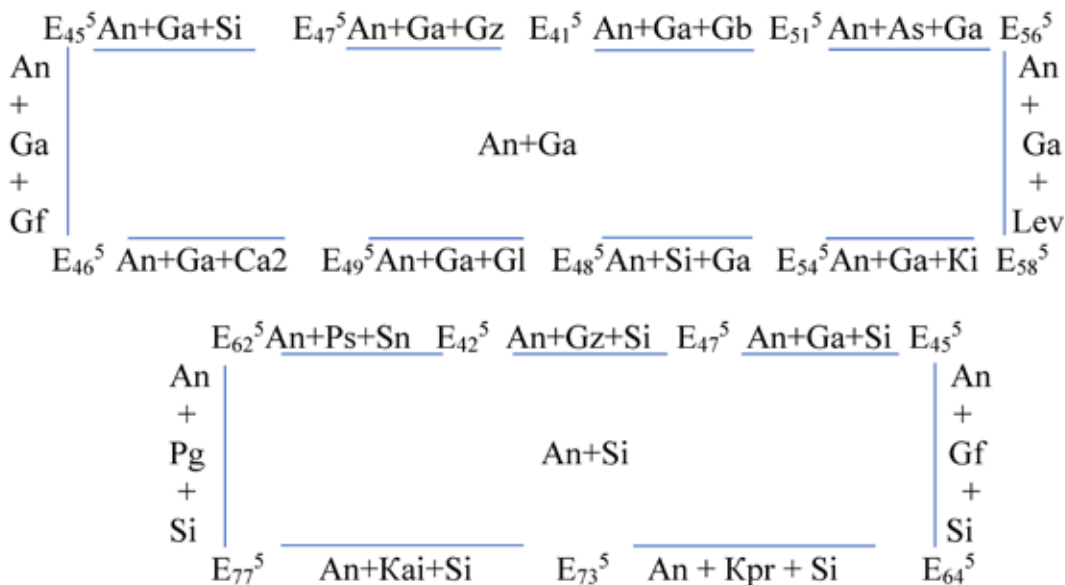


Figure 1. Composition of the phase complex diagram of the 50 °C isotherm of the system $\text{Na, K, Mg, Ca} \mid \text{SO}_4, \text{Cl-H}_2\text{O}$ at the five-component composition in the anhydrite (CaSO_4) crystallization region, constructed by the translation method

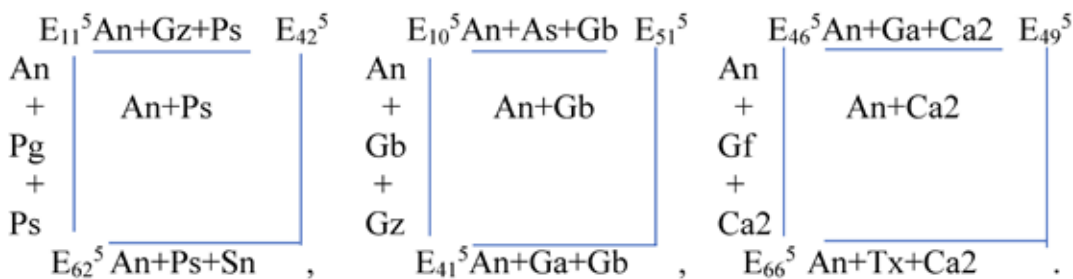
Drawing corresponding (according to Gibbs rule of phases) monovariant curves between five-point nonvariant points we obtain a phase complex diagram of the system Na, K, Mg, Ca||SO₄, Cl-H₂O at 50 °C in the area of crystallization of anhydrite (CaSO₄) at five-component composition. Such diagram is shown in (Fig. 1) where the five nonvariant points, monovariant curves and divariant fields containing anhydrite (CaSO₄) as one of equilibrium solid phases and mutual location of these geometrical images are shown.

As can be seen from (Fig. 1), the invariant fields are contoured with different numbers of nonvariant points and monovariant curves. Obviously, the greater the number of nonvariant points and monovariant curves involved in the contouring of the divariant fields, the more significant are the parts of the system under study occupied by these fields. For example, 10 nonvariant points and 10 monovariant curves take part in contouring of a divariant field with equilibrium solid phases An+Ci (Fig. 1) and 7 nonvariant points and 7 monovariant curves take part in contouring of a divariant field with equilibrium solid phases An+Ci:



This indicates that the first invariant field in the given conditions occupies a larger part of the system than the second divariant field.

The invariant fields with equilibrium solid phases An+Ps, An+Gb and An+Ca.2 are contoured by three five-valued nonvariant points and the same number of monovariant curves:



This indicates that they separately occupy a much smaller part of the investigated system under the given conditions than the divariant fields with equilibrium solid phases An+Ga and An+Si.

At transition of system from a five-component level on a six-component level (for example, by addition of the sixth component in any of four five-component systems where one of equilibrium phases is anhydrite),

transformation of geometrical images of five-component systems with their subsequent translation (transfer) to a level of six-component composition occurs. Further the translated geometrical images participate in formation of elements of a structure diagram of researched system at a six-component level [19; 22].

In accordance with the principle of compatibility [10; 11], combining the geometrical images of the five and six component levels of the system Na, K, Mg, Ca|SO₄, Cl-H₂O at 50 °C in the anhydrite (CaSO₄) crystallization area, we obtain its combined diagram of the phase complex (Fig. 2).

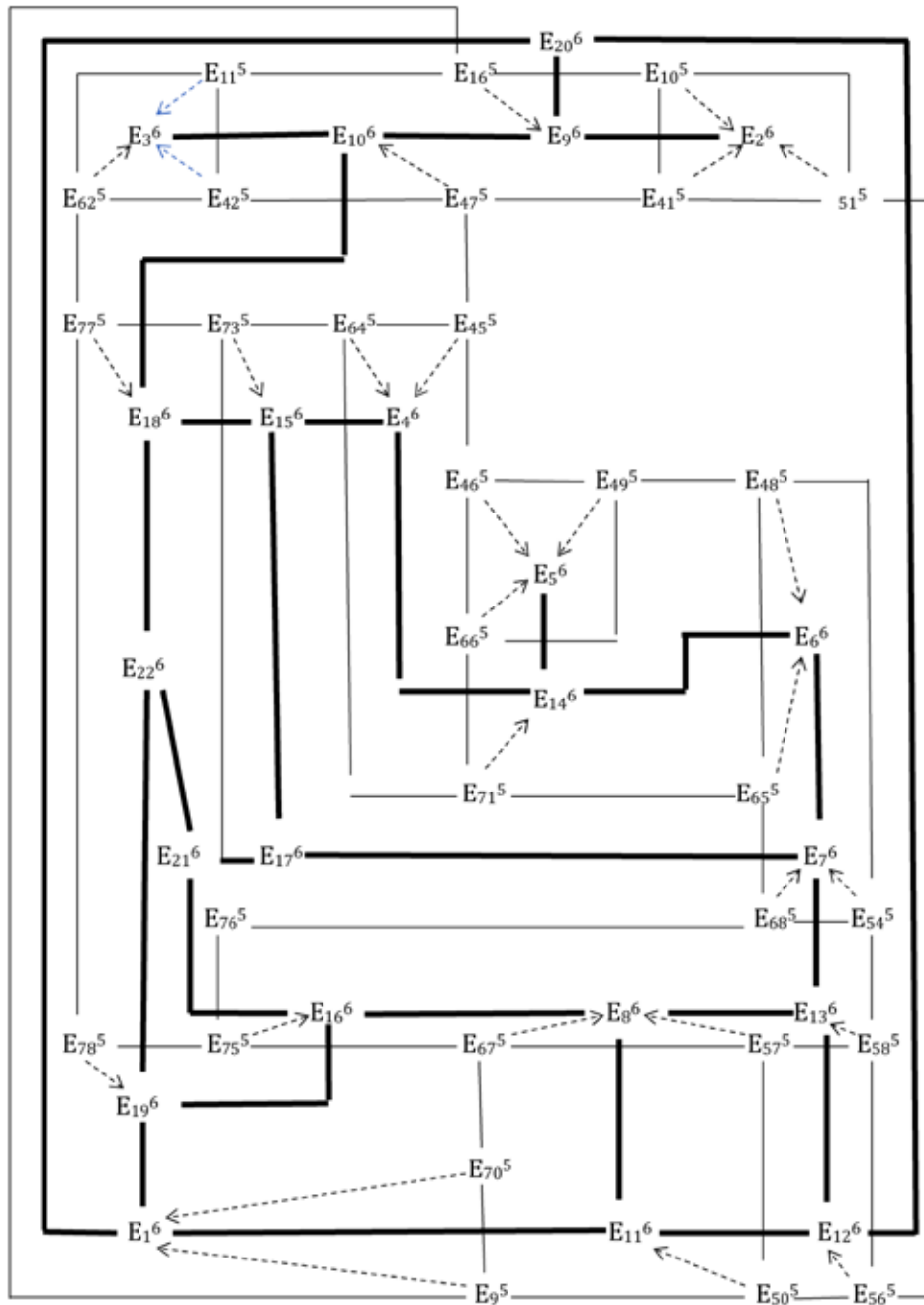


Figure 2. Structure of the combined diagram of the phase complex of the 50 °C isotherm at the level of five-six-component composition in the anhydrite (CaSO₄) crystallization area by the translation method

Such combined diagram of the phase complex reflects the interrelation between all geometrical images of the five- and six-component levels of the system under study in the considered conditions. For example, in (Fig. 2), the thin solid lines represent the monovariant curves of the five-component composition level (they run between the five non-variant points). The dotted lines are the monovariant level curves of the six-component composition. They are formed by the translation of the five-not-variant points to the level of the six-component composition, and the arrow points to the direction of translation. The bold solid lines are also monovariant curves of the six-component composition level. They run between the six-component non-variant points. The six-valued nonvariant points are formed by interrupting (following Gibbs' phase rule) the monovariant level curves of the six-component composition.

The analysis of the joint diagram of the system Na, K, Mg, Ca||SO₄, Cl-H₂O at 50°C in the anhydrite (CaSO₄) crystallisation range [19; 22] demonstrates that it is characterised by the following number of geometrical patterns at the five component (A) and six component (B) compositions under given conditions (Table 2).

Table 2.– Number of geometrical patterns of the system Na, K, Mg, Ca || SO₄, Cl-H₂O at 50 °C in the area of crystallisation of anhydrite (CaSO₄) at levels of five (A) and six (B) components determined by method of translation

Geometric images System	Components	
	A	B
Non-variant points	30	22
Monovariant curves	44	58
Divariant fields	18	47

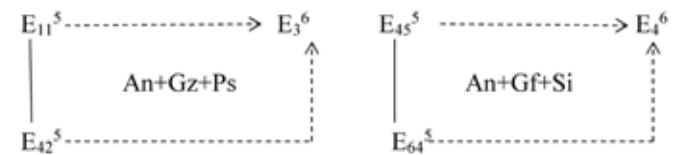
The conditions for the formation of geometric images of the system under study in the given system are discussed in detail in [19; 22]. In this paper, according to the task, we will consider examples of the formation of the invariant fields (invariant equilibria) and the possibility of determining the crystallization-

path of the solid phases by their structure. A more detailed analysis of constructed combined diagram of phase complexes of the system Na, K, Mg, Ca||SO₄, Cl-H₂O at 50°C in anhydrite (CaSO₄) crystallisation area is considered in [19; 22].

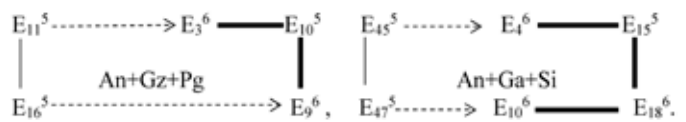
The formation of diadivariant fields on the level of six component composition is realized in two ways. The first way is related to translation of the monovariant curves of the five-component composition level to the level of the six-component composition. The second way is related to contouring of the systems surface with six nonvariant points and monovariant curves passing between them.

The invariant fields formed by translation of the monovariant curves of the five-component composition level to the level of the six-component composition (Fig. 2) can be contoured by

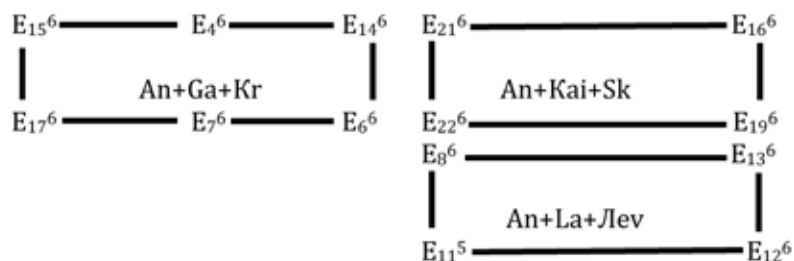
a) Five-not-variant points – monovariant curves formed by translation of five-not-variant points – six-not-variant points passing between them. For instance:



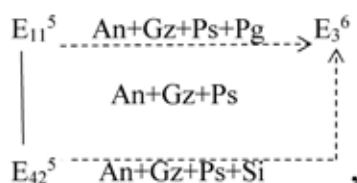
b) five-not-variant points – monovariant curves passing between them – monovariant curves formed by translation of five-not-variant points – six-not-variant points – monovariant curves passing between them. For example:



Analysis of the phase complex diagram of the system Na, K, Mg, Ca||SO₄, Cl-H₂O at 50°C in the anhydrite (CaSO₄) crystallization region shows that three (3) divariant fields are formed along the second path and they have the following contours (Fig. 2):

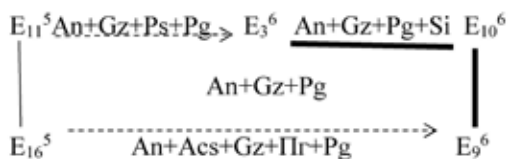


Principles of formation of geometrical images, in particular of the invariant fields, have not only scientific-theoretical value for understanding of regularities determining structures of diagrams of multicomponent chemical systems, but also are extremely important for the solution of practical problems, in particular at establishment of possible ways of crystallization of solid phases. For example, if a figurative point of an anhydrite (CaSO_4) fragment composition of a system under study at 50°C in the beginning of isothermal evaporation is located on the invariant field



then two options are possible (according to the number of monovariant curves of the six-component composition level, which outline this field) further crystallization path: a) towards monovariant curve $E_{11}^5 \rightarrow E_3^6$, upon reaching which Pg (polyhalite) crystallizes as the fourth equilibrium solid phase and; b) towards monovariant curve $E_{42}^5 \rightarrow E_3^6$, upon reaching which Si (sylvin) crystallizes as the fourth equilibrium solid phase. Further the crystallization path ends at nonvariant point E_3^6 with equilibrium solid phases $\text{An}+\text{Gz}+\text{Pg}+\text{Ci}+\text{Ps}$.

Finding the figurative point of the mixture composition on the invariant field



There are four options for the fourth equilibrium solid phase crystallization path (accord-

ing to the number of monovariant curves of the six-component composition level). Further the crystallization path will end at one of the three six nonvariant points. For example, when the crystallization path reaches the $E_{11}^5 \rightarrow E_3^6$ monovariant curve, the quadruple equilibrium solid phase will be Ps (pentasol) and crystallization will terminate at the E_3^6 nonvariant point with equilibrium solid phases $\text{An}+\text{Gz}+\text{Pg}+\text{Ps}+\text{Ci}$. At achievement of a crystallization path of monovariant curve $E_{16}^5 \rightarrow E_9^6$, the quaternary equilibrium solid phase will be As (astrachanite) and the crystallization will terminate at nonvariant point E_9^6 with equilibrium solid phases $\text{An}+\text{Ac}+\text{Ga}+\text{Gz}+\text{Pg}$.

When the crystallization path reaches the monovariant curves $E_3^6 - E_{10}^6$, $E_9^6 - E_{10}^6$ its further movement depends on the process of saturation of the solution with the fifth equilibrium solid phase. For example, if reaching the path of crystallization of monovariant curve $E_3^6 - E_{10}^6$ solution saturation process is accompanied by increasing of solution concentration due to pentasol (Ps), then the crystallization path will be directed towards nonvariant sixth point E_3^6 , upon reaching which equilibrium solid phases will be $\text{An}+\text{Gz}+\text{Pg}+\text{Ps}+\text{Cs}$. If upon achievement of the path of crystallization of monovariant curve $E_3^6 - E_{10}^6$ the process of solution saturation is accompanied by increasing of solution concentration due to halite (Ga), the path of crystallization will be directed towards nonvariant sixth point E_{10}^6 , upon achievement of which equilibrium solid phases will be $\text{An} + \text{Ga} + \text{Gz} + \text{Pg} + \text{Ci}$. In the same way further crystallization paths can be determined on the monovariant curve $E_9^6 \dots - E_{10}^6$.

References:

1. Anosov V. Ya., Ozerova M. I., Fialkov Yu. Ya. Major Methods of Physicochemical Analysis. (Nauka, Moscow); 1976. – 504 p. [in Russian].
2. Goroshenko Ya. G., Soliev L. The main trends in the methodology of physical and chemical analysis of complex and multicomponent systems. *Russ. J Inorg Chem.* – 32(7). 1987. – P. 1676–81.
3. Pitzer K. S., Kim J. Thermodynamics of electrolytes IV. Activity and osmotic coefficients for mixed electrolytes. *Journal American Chemical Society.* – 96(18). 1974. – P. 5701–07.
4. Wood J. R. Thermodynamics of brine-Salt equilibria the systems NaCl-KCl-MgCl₂-CaCl₂-H₂O at 25 °C. *Geochim et Cosmochim Acta.* – 39(8). 1975. – P. 1147–63.
5. Harvie E., Weare J. H. The prediction of mineral Solubilities natural water the Na-K-Mg-Ca-Cl-SO₄-H₂O system from Geochem at *Cosmochim Acta.* – 44(7). 1980. – P. 981–97.
6. Eugster H. P., Harvie C. F., Weare J. H. The prediction of mineral solubilities natural water the Na-K-Mg-Ca-Cl-SO₄-H₂O system from zero to high concentration at 25°C. *Geochem et Cosmochim Acta.* – 44(9). 1980. – P. 1335–47.
7. Harvie C. F., Eugster H. P., Weare J. H. Mineral equilibrium in a six-components seawater system Na-K-Mg-Ca-Cl-SO₄-H₂O at 25 °C II compositions of the soluted solutions. *Geochem et Cosmochim Acta.* – 46(9). 1982. – P. 1603–18.
8. Kurnakov N. S. Some questions of the theory of physical and chemical analysis. *Reports of the USSR Academy of Sciences.* – 25(5). 1939. – P. 38487. [Russian].
9. Kurnakov N. S. The introduction to Physicochemical Analysis. *Izd-vo Akad. Nauk USSR.* – Moscow / Leningrad. 1940. [Russian].
10. Goroshenko Ya. G. Physicochemical Analysis of Homogeneous and Heterogeneous Systems. – Kiev: Naukova Dumka; 1978. [Russian].
11. Goroshenko Ya. G. The Center of Mass Method for Multicomponent Systems Imaging. – Kiev: Naukova Dumka; 1982. [Russian].
12. Soliev L. Prediction of structure of multicomponent water-salt systems phase equilibria diagram by means of translation method. *VINITI № 8990-B87*, 1987. – 28 p. Russian.
13. Soliev L. Phase Equilibria in the Na, K, Mg, Ca||SO₄, Cl-H₂O System at 25 °C in the Region of Glauberite Crystallization. *Rus J Phys Chem.* – 77(3). 2003. – P. 351–54.
14. Soliev L. Phase Equilibria in the Na, K, Mg, Ca||SO₄, Cl-H₂O System at 50 °C in the Crystallization Glazirite (3K₂SO₄·Na₂SO₄). *Rus J Phys Chem.* – 87(9). 2013. – P. 1442–47. DOI: 10.1134/S0036024413090227
15. Tursunbadalov Sh., Soliev L. Phase Equilibria in the quinary Na, K //SO₄, CO₃, HCO₃-H₂O system at 75 °C. *Journal of Solution Chemistry.* – 44(8). 2015. – P. 1626–39. DOI: 10.1007/s10953-015-0368-3.
16. Tursunbadalov Sh., Soliev L. Phase Equilibria in multicomponent water-salt system. *Journal of chemical engineering data.* – 61(7). 2016. – P. 2209–20. DOI: 10.2021/acs.jced.5b00875.
17. Tursunbadalov Sh., Soliev L. Determination of phase Equilibria and construction of comprehensive phase Diagram for the Quinary Na, K, // SO₄, CO₃, HCO₃-H₂O system at 25 °C. *Journal of chemical engineering data.* – 62. 2017. – P. 698–03. DOI: 10.2021/acs.jced.6b00739.
18. Soliev L., Jumaev M. T. Phase complex of the system Na, Ca||SO₄, CO₃, HCO₃-H₂O at 100 °C. *Chemica Techno Acta.* – 7(2). 2020. – P. 192–98. DOI: 10.15826/chimtech.2020.7.2.04

19. Soliev L. Prediction of Phase Equilibria in Multinary Marine-Type Systems by the Translation Method, Book 3. Dushanbe: Er-Graph; 2019. – 232 p. Russian.
20. Soliev L. Invariant Equilibria in Multicomponent Systems. Russ J Inorg Chem. – 64(7). 2019. – P. 894–98. DOI: 10.1134/S0036023619070167
21. Soliev L. Monovariant Equilibria in Multinary Systems. Russ J Inorg Chem. – 65(2). 2020. – P. 212–16. DOI: 10.1134/S0036023620020187
22. Soliev L. Phase Equilibria in the Na, K, Mg, Ca||SO₄, Cl-H₂O system at 50 °C in the Angidrite crystallization. Russ J Inorg Chem. – 56(10). 2011. – P. 1659–65. DOI: 10.1134/S0036023611100238
23. Reference book on experimental data for solubility in multicomponent water-salt systems. – Vol. I., Books. 1–2. – Saint-Petersburg: Khimizdat, 2003. – 1152 p. Russian.
24. Reference book on experimental data for solubility in multicomponent water-salt systems. – Vol. II., Books. 1–2. – Saint-Petersburg: Khimizdat, 2004. – 1247 p. Russian.

<https://doi.org/10.29013/AJT-22-3.4-44-51>

*Nurov Kurbonali Bozorovich,
Candidate of Chemical Sciences, Associate Professor
of the Department of Experimental Physics, TSPU named S. Ayni*

*Dzhuraev Tukhtasun Dzhuraevich,
Doctor of Chemical Sciences, Professor, of the Department
of Metallurgy of the TTU named acad. M. S. Osimi*

*Jafarov Amirsho Sayobidovich,
PG student, of the Department of Technology
and Mechanical Engineering TSPU named after S. Ayni*

INVESTIGATION OF THE REGION OF EXAMINATION OF MELTS IN SYSTEMS In – B^{VI} (B^{VI} – S, Se, Te) BY THE ACOUSTIC METHOD

Abstract. The temperature dependences of the propagation velocity of ultrasound in exfoliating melts of the In-S, In-Se and In-Te systems have been studied. Supercritical phenomena have been found, consisting in an anomalous decrease in the speed of ultrasound with decreasing temperature as one approaches the delamination dome in a short temperature range. It has been established that these anomalies increase gradually as the melt concentration approaches the critical one. The coordinates of the critical point have been established.

Keywords: ultrasonic velocity, delamination, melt, system, delamination dome, critical composition and temperature.

Introduction

The study of stratification of liquids is of interest for at least two important areas: the first is the construction of the stratification dome on the phase diagram and the second is the study of the features of the second-order phase transition liquid-liquid.

The optical method is widely used to study the phenomenon of stratification and to study the structure in transparent liquids. The difference in refractive indices in separating liquids, and the resulting specificity of light propagation, makes it possible to visually observe the boundary between them. Opaque liquids (metal and semiconductor) lack such an effective research method as optical. However, the generality of the laws of wave processes makes it possible to use the propagation of not only electromagnetic waves, but also other types of waves, in particular elastic ones. Elastic waves have even greater

possibilities than light in studying the atomic structure, as well as in studying the separation of liquids, since all real liquid media are always “transparent” in the acoustic sense and not always in the optical sense. Elastic waves are also distinguished by the fact that the speed of their propagation strongly depends on the inertial properties of the particles that make up the medium and, consequently, on the concentration of the components. Considering that the speed of propagation of ultrasound is currently measured with an accuracy of 10^{-4} , it is possible to effectively use this characteristic of the propagation of elastic waves for the precision study of liquids.

Although diffraction methods are methods of direct study of the structure, nevertheless, they do not provide direct information about the structure of melts of metals and semiconductors. Side maxi-

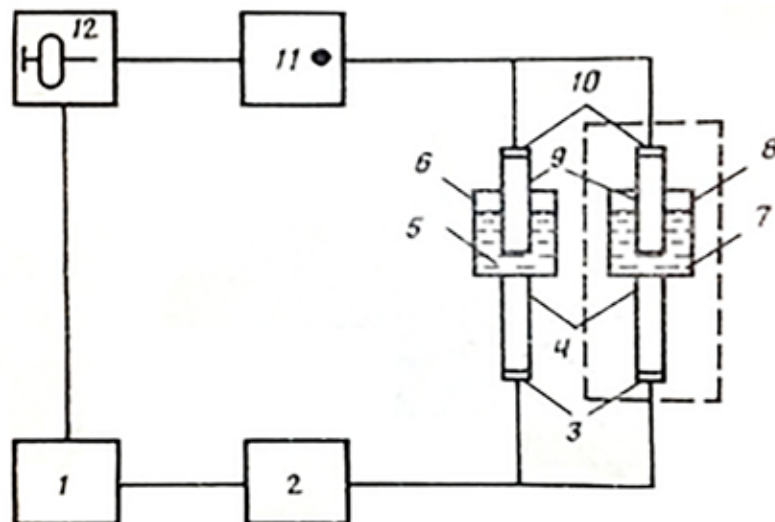
ma or sagging on the scattered X-ray intensity curve only indicate that a superposition of two structures is possible. Processing of experimental X-ray data requires well-known assumptions [1–2]. At the same time, it should be borne in mind that X-ray measurements in high-temperature and chemically aggressive melts are rather complicated, and sometimes not realizable.

Currently, acoustic research is a powerful tool for obtaining information about the structure of melts of metals and semiconductors. In condensed media, the elastic impulse propagates from atom to atom through interatomic bonds, and therefore the change in the latter significantly affects the rate of its propagation. Therefore, the speed of propagation of ultrasound is a fine characteristic, sensitive to changes in the nature of the chemical bond. To study the stratification of liquids and the stratification process itself, a method is needed that makes it possible to measure the ultrasound velocity in each of the existing layers, moreover, at different distances from the boundary between the layers. This method is pulse-phase, which allows you to work on a transmitted wave and change the acoustic base [3–4].

Technique for measuring the velocity of ultrasound in exfoliating melts

The essence of the acoustic method lies in the fact that the propagation velocity of ultrasound ϑ_s is measured depending on the height h of the liquid column and the so-called $\vartheta_s - h$ characteristic is analyzed at a fixed temperature. The set of $\vartheta_s - h$ characteristics at different temperatures and for melts of different initial concentrations provides complete experimental information on the melt separation, i.e., all the necessary data for constructing a separation dome from experimental points.

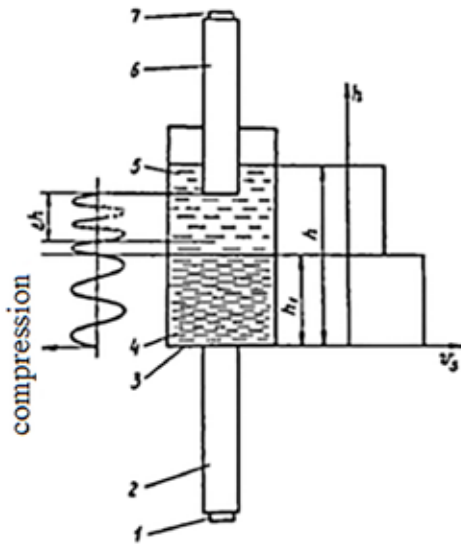
On (pic. 1) A diagram of the installation for measuring the velocity of propagation of ultrasound is presented. The pulse generator 1 modulates the RF voltage of the sinusoidal signal generator 2 into a sequence of rectangular packets with high-frequency filling, which excite the piezoelectric elements 3 of the comparison cell and the measuring cell in parallel (dashed lines). Ultrasonic pulses through the lower fixed sound ducts 4 probe the reference liquid (distilled water) 5 in the container 6 and the investigated melt 7 in the container 8.



Picture1. Functional diagram of the installation for measuring the velocity of propagation of ultrasound in melts

On (pic. 2) representations the scheme of the measuring cell for determining the velocity of propagation

of ultrasound in a separating melt and the nature of the change in velocity with height are presented.



Picture 2. Scheme of the measuring cell for determining the velocity of propagation of ultrasound in the melt and the nature of its change in the height of the melt in the presence of stratification into two liquid phases.

By moving the upper movable sound duct with the help of a micrometer screw at a distance $\Delta h = n\lambda$, we get the opportunity to fix the value of the velocity of propagation of ultrasound in the area Δn .

By successively probing the melt by moving the upper sound duct, one can establish a change in the velocity of propagation of ultrasound along the height of the investigated melt and detect its jump when passing through the phase boundary between regions 4 and 5. In (pic. 2) on the left schematically shows how a sinusoidal plane wave propagates in the melt from the lower to the upper sound duct, the length of which in the lower layer is greater than in the upper one. The spatial distribution of the wave phases has a stationary character, i.e. at any moment of time, a multiple of the period of oscillation $n\tau$ in a plane located at an arbitrary distance from the bottom of the container, the same phase of the wave is realized.

When moving the upper acoustic duct down to a distance $n\lambda$ (in this case $n = 2$) on the screen of an oscilloscope with a differential amplification unit, the second input is fed with a coherent sinu-

soidal signal from the same generator that generates the total displacement $\Delta h = n\lambda$ probing the melt and setting frequency f , speed of ultrasound, we find the voltage, n extinctions of the total signal are observed. Registering according to the ratio $\vartheta_s = f \frac{\Delta h}{n}$, which is identical to the obvious formula $\vartheta_s = f \cdot \lambda$. Since the wavelength, defined as $\lambda = \frac{\Delta h}{n}$, is a component of the melt thickness Δh , the velocity ϑ_s also refers to this melt volume. By probing the melt in the region of delamination at different temperatures, one can detect the disappearance or appearance of a boundary between the layers, i.e. to fix the temperature of the beginning of delamination, and also, using the values of the velocity of propagation of ultrasound in the first and second layers at each given temperature, it is possible to plot the v_s dependence above the delamination region for alloys of a certain composition and extrapolate it to the intersection with the v_s dependence curve along the delamination dome.

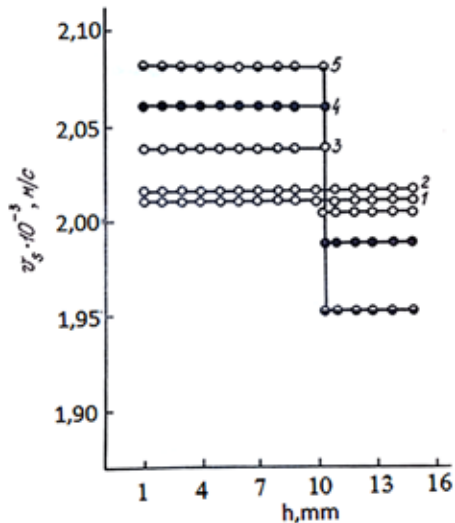
Experimental results

The authors of [1–6] carried out the study using the methods of differential thermal, microstructural and X-ray analysis and the method of measuring microhardness. The alloys were synthesized in evacuated quartz ampoules using In and elemental Se with a purity above 99.9% (by weight).

For the In-Se system, indium (In-000) and selenium-was were used as starting materials for the preparation of alloys. h. Samples were fused in evacuated to -10^{-4} Pa and sealed quartz ampoules. At the melting temperatures of indium and selenium, the samples were kept for 2 hours, the main fusion was carried out at 950K for 3 hours with intensive mechanical stirring, and finally, they were cooled in air while shaking the ampoules until the samples solidified. The measurements were carried out in a high-purity argon atmosphere in the frequency range 1–3 MHz.

On (pic. 3) presents the results of an experimental study of the ultrasound propagation velocity ϑ_s as a function of the height h of the liquid column of a

sample with the initial composition $\text{In}_{0.83}\text{Se}_{0.17}$ at various temperatures. It can be seen that at 930 and 917 K (lines 1 and 2, respectively), the ϑ_s-h characteristics are straight lines parallel to the h axis, the speed of propagation of ultrasound does not depend on height, which indicates the homogeneity of the melt.



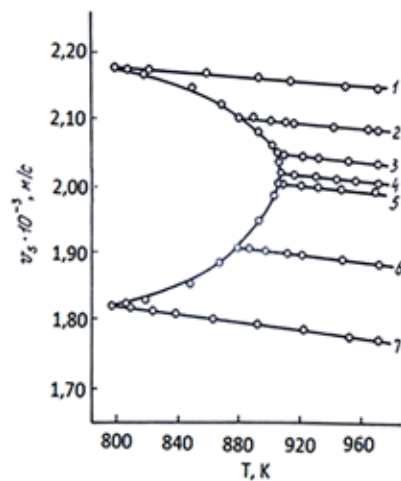
Picture 3. The change in the velocity of propagation of ultrasound along the height of the liquid column in the melt of the initial composition $\text{In}_{0.83}\text{Se}_{0.17}$ 1–5 correspond to temperatures of 930, 917, 910, 903, 893 K

But at 910 K on the ϑ_s-h characteristic (line 3) there is a velocity jump of ultrasound. The step unambiguously establishes the fact of stratification of the melt into two liquid phases, which differ in the velocity of ultrasound propagation. Further, at 903 and 893 K, the step size $\Delta\vartheta_s$ increases successively (Pic. 3, lines 4 and 5), which indicates an increase in the concentration gap in the coexisting layers with decreasing temperature.

As seen in (pic. 3), steps ϑ_s-h characteristics 3–5 are fixed with great accuracy at the same height. The fact that the boundary between the layers is kept in one position with a change in temperature only indicates a redistribution of the atoms of the components without changing the volume of the phases. Therefore, it can be suggested that this composition is critical. Since the delamination temperature is fixed quite accurately, the temperature ϑ_s-h

-characteristic 3 (910 K) can be considered close to critical.

The data presented in (pic. 3), make it possible to plot the dependence of the velocity of propagation of ultrasound along the line of monovariant liquid-liquid equilibrium. This requires values corresponding to the upper and lower branches of the ϑ_s-h characteristics in (pic. 3), submit according to temperature. As a result, we obtain a general curve corresponding to the dependence of the ultrasound propagation velocity along the delamination dome (see pic. 4).



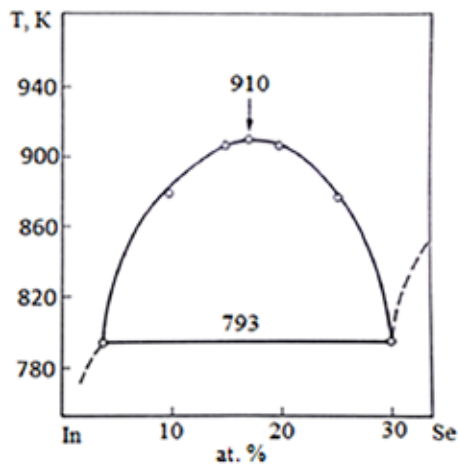
Picture 4. Temperature – concentration dependence of the speed propagation of ultrasound in melts of the In-Se system. Polytherms 1–7 correspond to samples containing 4, 10, 15, 17, 20, 25, and 30 at.% Selena

This result, in turn, makes it possible to construct a line of monovariant liquid-liquid equilibrium on the state diagram of the In-Se system. To do this, it is necessary to establish the dependence of the ultrasound propagation velocity on temperature for melts of various compositions at various temperatures above the delamination region and extrapolate this dependence to the intersection with the curve characterizing the dependence of ϑ_s along the delamination dome. The intersection points and determine the coordinates of the figurative points of the line of monovariant equilibrium liquid – liquid.

Based on this, we studied the temperature dependence of the propagation velocity of ultrasound ϑ_s 7 compositions (see pic. 4). It can be seen from the figure that the temperature dependences of the ultrasound propagation velocity above the delamination temperature (pic. 4, polytherms 1–7, respectively) are linear, which allows them to be reliably extrapolated to the intersection with the curve of the dependence of the ultrasound propagation velocity along the delamination dome.

From (pic. 4) shows that at $T > T_{cr}$ all polytherms have a negative slope to the temperature axis. Such a change in the speed of propagation of ultrasound at $T > T_{cr}$ is quite understandable, since above T_{cr} (critical temperature) there is a homogeneous solution. As can be seen from the figure, no anomalies were found on the polytherms. They decrease linearly with temperature starting from the delamination temperatures.

In accordance with the conclusions in [5–6], this fact indicates that there is no pronounced development of large-scale concentration fluctuations in the melts of this system. Built according to the data presented in (pic. 4), the curve of monovariant liquid-liquid equilibrium in the In-Se system is shown in (pic. 5) as a fragment of the phase equilibrium diagram.



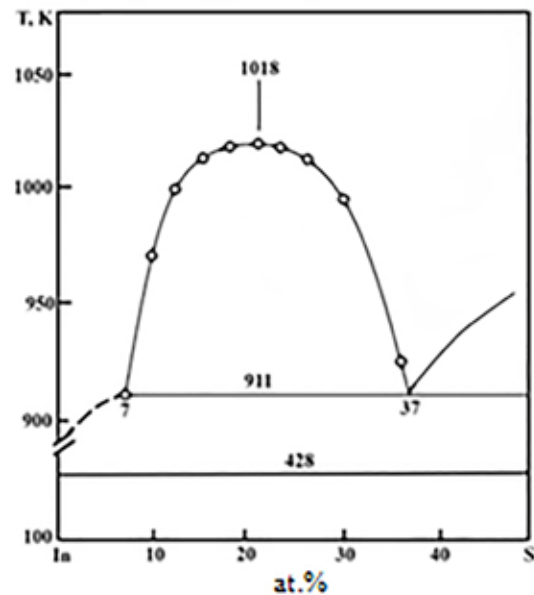
Picture 5. Fragment of the state diagram of the In-Se system in the area of melt separation

It can be seen that the curve of monovariant liquid-liquid equilibrium in the indium-selenium system is characterized by a symmetrical binodal. In

this system, the coordinates of the critical point are set: temperature – 910 K, composition – 17 at.% Se.

Alloys of the In – S system were studied in [11–12] in the concentration range from 0 to 70% at. S by microstructural, X-ray, and differential thermal analyses. Alloys were prepared by heating mixtures of components in evacuated quartz ampoules. The study used In with a purity of 99.999% (by mass) and crystalline S with a purity of 99.999% (by mass).

State diagrams of the In-S system were constructed in a similar way. On picture 6 shows the state diagrams of the In-S system in the region of melt separation. According to the obtained experimental data, the delamination dome in this system is symmetrical and rests on a monotectic horizontal with extreme points at compositions of 7 and 37 at.% sulfur. In the In-S system, the following coordinates of the critical point are set: temperature – 1018 K, composition – 21 at.% S.



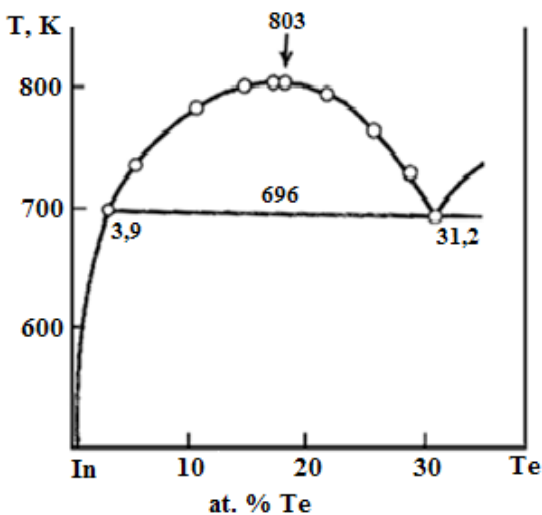
Picture 6. A fragment of the diagram of phase equilibria of the In-S system illustrating the position of the curve of monovariant liquid-liquid equilibrium in combination with a monotectic horizontal

The In – Te state diagram is described in [13–16]. It has been established that the interaction between In and Te is characterized by limited mis-

cibility of the components in the liquid state with monotectics at a temperature of 423 °C and a content of 28% (at.) Te and the formation of a number of compounds in the solid state, regarding which there are discrepancies in the literature.

In the In-Te system, this method was used to study the temperature dependence (ϑ_s-h) – characteristics in melts containing 6, 11, 15, 18, 18.35, 22, 26, 29 at.% Te.

In the In-Te system, anomalies were found on the ϑ_s polytherms, the essence of which is that the dependence $\vartheta_s \sim f(T)$ passes through a gentle maximum before becoming linear. These anomalies extend over a fairly wide temperature range and are most pronounced in the alloy of critical composition (18.35 at% Te).



Picture 7. A fragment of the diagram of phase equilibria of the In-Te system illustrating the position of the curve of the monovariant liquid-liquid equilibrium in combination with the monotectic horizontal

According to [7–8], melts of the In-Te system are semi-metallic; interatomic bonds in them are realized not only by the metallic type, but also by the covalent one. The presence of covalent bonds in melts is due to the presence of tellurium atoms, which are prone to the formation of these bonds due to the well-known specificity of the structure of the

outer electron shells. We suggest that the observed anomalies in the velocity of ultrasound propagation in the melts of this system are due precisely to the possibility of the coexistence of two types of interatomic bonds, which, along with concentration fluctuations, should contribute to the formation of significant density fluctuations. The nature of the changes in the latter during heating of the melts, in fact, should be the physical reason for the occurrence of anomalies in the temperature dependence of the ultrasound propagation velocity.

The results of the studies carried out provide complete experimental information, on the basis of which it is possible to construct a monovariant equilibrium curve that limits the separation region on the phase equilibrium diagram of the In-Te system.

On (pic. 7) shows the results of such a construction.

For the In-Te system, the following critical point coordinates are established: temperature – (803 ± 2) K, composition – 18.35 at.% Te. the rest In.

Conclusions

Thus, using the ultrasonic method, the area of delamination in the systems In – B^{VI} (where B^{VI} – S, Se, Te) was investigated and refined. Curves of monovariant equilibrium were constructed, limiting the indicated area. Experimental result We have shown that the delamination dome for all the studied systems is practically symmetrical.

It is shown that the study of the propagation velocity of ultrasound is an effective and reliable method for constructing curves of monovariant liquid-liquid equilibrium in high-temperature melts of binary metal and semiconductor systems.

In conclusion, we note that the acoustic method has sufficient reliability and high information content in the case of: studies of the stratification of melts of metals and semiconductors, supercritical phenomena occurring in them; construction and refinement of state diagrams; finally, the study of the structure of metallic and semiconductor melts.

References:

1. Slavnova G. K., et al. New data on the phase diagram of the indium-selenium / G. K. Slavnova, N. P. Luzhnaya, Z. S. Medvedeva // *Journal of Inorganic chemistry*.– V. 8. 1963.– P. 1199–1203.
2. Slavnova G. K., Eliseev A. A. X-ray study of indium-selenium alloys / G. K. Slavnova, A. A. Eliseev // *Journal of Inorganic Chemistry*.– V. 8. 1963.– P. 1654–1660.
3. Slavnova G. K., Eliseev A. A. X-ray study of indium-selenium alloys / G. K. Slavnova A. A. Eliseev // *Journal of Inorganic Chemistry*.– T. 8.– Pub 7. 1963.– P. 1654–1660.
4. Slavnova G. K. // *Journal of Inorganic chemistry*.– T. 8. 1963.– P. 2217–2221.
5. Guliev T. N., Medvedeva Z. S. // *Journal of Inorganic chemistry*.– T. 10. 1965.– P. 1520–1524.
6. Osamura K., Murakami Y., Tommie Y. // *J. Phys. soc. Japan*.– V. 21. 1966.– 1848 p.
7. Glazov V. M. And other Equipment and methods for studying the acoustic properties of electronic melts / V. M. Glazov, V. I. Timoshenko, S. G. Kim // *Factory laboratory*.– T. 51.– No. 3. 1985.– P. 22–26.
8. Glazov V. M. et al. Investigation of melt separation in the Sb-Se system by the acoustic method / V. M. Glazov, S. G. Kim., K. B. Nurov // *Proceedings of the Academy of Sciences of the USSR, Inorganic materials*.– T. 26.– No. 3. 1990.– P. 526–529.
9. Khodzhaev F. K., Nurov K. B. Investigation of the delamination area in the Cu-Pb system by the pulse-phase method / F. K. Khodzhaev, K. B. Nurov // *Bulletin of the South Ural state university, metallurgy series*.– V. 19.– No. 4. 2019.– 4 p.
10. Glazov V. M., Kim S. G., Nurov K. B. Acoustic study of the area of melt separation in the In-Se system / V. M. Glazov, S. G. Kim., K. B. Nurov // *Proceedings of the Academy of Sciences of the USSR. inorganic materials*.– T. 25.– No. 5. 1989.– P. 859–861.
11. Hahn H., Klinger W. // *Z. Anorg. All. chem*.– Bd. 260. 1949.– P. 97–109.
12. Stubbs M. F., Schufle J. A., Thompson A. J. et al. // *J. Amer. chem. Soc*.– V. 74.– No. 6. 1952.– P. 1441–1443.
13. Grochowski E. G., Mason D. R., Schmitt G. A., Smith P. H. // *J. Phys. Chem. Solids*.– Vol. 25.– No. 6. 1964.– P. 551–558.
14. Palatnik L. S., Atrashenko L. V., Galchinetskiy L. P., and Koshkin V. M. Reports Academy of sciences of the USSR.– T. 165. 1965.– P. 809–812.
15. Galchinetsky L. P., Atrashchenko L. V., Koshkin V. M., Sysoev L. A. // *Edition by Academy of Sciences of the USSR. Inorganic materials*.– Vol. 6.– No. 5. 1970.– P. 860–863.
16. Vol A. E., Kagan I. K. Structure and properties of binary metal systems.– M.: Science.– T. 3. 1976.– 815 p.
17. Glazov V. M., Kim S. G. Study of supercritical phenomena in exfoliating melts of Ga-Te and In-Te systems by acoustic method/ V. M. Glazov, S. G. Kim // *Journal of Physical chemistry*.– T. 61.– No. 8. 1987.– P. 2171–2178.
18. Glazov V. M., Kim S. G. Acoustic studies of delamination and supercritical phenomena in electron melts / V. M. Glazov, S. G. Kim // *Paper of Academy of Sciences of the USSR*.– T. 290.– No. 4. 1986.– P. 873–876.
19. Regel A. R., Glazov V. M., Kim S. G. Acoustic studies of structural changes during heating of melts of semiconductors and semimetals / Regel A. R., Glazov V. M., Kim S. G. // *Physics and technology of semiconductors*.– T. 20.– No. 8. 1986.– P. 1353–1376.
20. Glazov V. M., Kim S. G. Investigation of the separation of melts by the acoustic method / Glazov V. M., Kim S. G. // *Reports of the Academy of Sciences of the USSR*.– T. 282.– No. 5. 1985.– P. 1170–1174.

21. Nurov K. B., Jafarov A. S. Study of binary systems from singular temperature points / Nurov K. B., Jafarov A. S. // Reports of the Academy of Sciences of the Republic of Tajikistan, – T. 64. – No. 7–8. 2021. – P. 442–448.
22. Nurov K. B., Jafarov A. S., Juraev T. J., Toshev M. T. Mukhabbatov H. K. Investigation of the region of limited solubility in the liquid state in binary systems of indium with selenium and tellurium / Nurov K. B., Jafarov A. S., Juraev T. J., Toshev M. T. Mukhabbatov H. K. // Materials of the international conference “The main problems of metallurgical production” Dushanbe, – TTU. 2021. – P. 85–90.

<https://doi.org/10.29013/AJT-22-3.4-52-58>

*Radkevich Maria Viktorovna,
D. Sc. in Engineering, Professor,
National Research University
“Tashkent Institute of Irrigation and
Agricultural Mechanization Engineers”,
Republic of Uzbekistan, Tashkent*

*Shipilova Kamila Bakhtiyarova,
PhD, Senior Lecturer,
National Research University
“Tashkent Institute of Irrigation and
Agricultural Mechanization Engineers”,
Republic of Uzbekistan, Tashkent*

*Abdukodyrova Malokhat Noridzhonovna,
Associate professor,
National Research University
“Tashkent Institute of Irrigation and
Agricultural Mechanization Engineers”,
Republic of Uzbekistan, Tashkent,*

A REVIEW OF METHODS FOR ASSESSING THE EVAPORATION OF LIQUID DROPS UNDER VARIOUS CONDITIONS

Abstract. The article discusses methods for estimating the evaporation of liquid droplets under various environmental conditions. All estimation methods can be divided into three groups: evaporation of a stationary levitating drop, evaporation of a falling drop, and evaporation of a drop lying on a solid surface. The possibility of using the considered models and data in the design of local climate control systems is assessed.

Keywords: evaporation, drop, water vapor, surface, airflow.

Introduction. The problem of evaporation of liquid droplets is constantly studied by scientists all over the world due to a variety of practical tasks. Knowledge of evaporation processes of single droplets under various environmental conditions allows to design and improve technical cooling systems, microclimate installations, various energy and heating systems [3, 4, 26].

The purpose of this article is to review existing models for evaluating liquid droplet evaporation for

further application in designing a local climate control system.

The first drop evaporation model was proposed by Maxwell in 1887 [4]. This model was very simple and was constructed under the assumption that the evaporation process is limited to vapor diffusion. Expression for calculation of vapor flux from the drop surface was obtained by integration of vapor flux equation from liquid surface and has the form:

$$j_w = 4\pi r_0 D_v (\rho_{vs} - \rho_{v0}) \quad (1)$$

where j_w is flux of number of vapor molecules from drop surface, r_0 is drop radius, $D_v \rho_{vS}$ and ρ_{v0} are vapor diffusion coefficient and its density on surface and in ambient gas.

This model is suitable only for stationary conditions, which are practically never met in reality, as the drop size inevitably changes during evaporation.

Based on the same assumptions as the Maxwell model, the Spalding model was built, which takes into account the change in droplet diameter over time. This model was called “law d^2 ” and found wide application in practical calculations [4]:

$$\left(\frac{d}{d_0}\right)^2 = 1 - \frac{8D_v \rho_0}{d_0^2 \rho_{\infty}} \ln(1 + b_{1d})t \quad (2)$$

However, Maxwell and Spalding models describe only the functional dependence of drop size change with time and are applicable only to diffuse evaporation.

Hertz and Knudsen models are developed to describe the kinetic or free-molecular mode of evaporation [4].

$$I = \frac{1}{4} \pi r_p^2 \frac{M}{RT} \sqrt{\frac{8RT}{\pi M}} \alpha_m (p_s - p_{\infty}) \quad (3)$$

where α_m is the fraction of the number of falling vapor molecules condensing into the liquid phase, M is the molar mass of vapor, R is the universal gas constant

Given classical models can not solve all variety of practical problems of drop evaporation. Therefore, for each newly emerging problem researchers look for a suitable solution, as a rule, by experiment. Let's consider different approaches to estimation of evaporation of droplets.

Evaporation of a stationary droplet in an air stream.

The simplest case of evaporation of droplets immobile in relation to medium, which excludes influence of hydrodynamic factor, was considered by N.A. Fuchs [25]. He found that for sufficiently small droplets their motion is not reflected in the evaporation rate, i.e. the evaporation process is quasi-stationary.

In some works, evaporation of a stationary droplet in an air stream was studied for different droplet diameters at high temperatures of air or superheated steam [5; 15; 17, 22–24, 27; 29].

For example, it is noted in [29] that in most real cases evaporation of a droplet is significantly affected by conductive component of heat flow spent on heating or cooling to adiabatic evaporation temperature.

Studies of evaporation of a stationary droplet in an air stream were conducted by N. E. Shishkin, V. V. Terekhov, M. A. Pakhomov et al. [22–24].

In [22] evaporation processes of droplets in streams of different types were compared. It was found that during evaporation of a droplet in a vapor-gas flow, heat transfer is more intense compared to single-component vapor-droplet flow and single-phase vapor flow.

When studying droplets with diameter not more than 3 mm of pure liquids of water, ethanol and acetone suspended motionless in an aerodynamic channel in an air flow directed from below upwards, it was noted that the surface temperature of the droplets was non-uniform. Evaporation of droplets in a stationary medium (at an air temperature of 19.8°C) was of a similar nature. It was found that for all pure liquids at the initial moments of time the droplet surface temperature was close to the adiabatic evaporation temperature [27]. In further studies [23], evaporation of a suspended droplet in a stream of hot (300°C) air was investigated when the flow rate changed from 0 to 6 m/s. It was found that for water droplets the ratio $\frac{j_w}{p_0 V_0}$ (ratio of flow of evaporating liquid to initial mass) remains unchanged for a long time.

This data is of some interest for the design of microclimate systems, but in real conditions the droplet cannot remain stationary and the airflow will not be strictly vertical.

Evaporation of a falling droplet in an air stream.

Research on evaporation of the falling drop of liquid is of practical interest. Such researches were

carried out by Spiglazova A. S., Mezentsev A. V., Antonov A. S., Zhailubaev J. D. et al. [1; 14; 16; 17; 21].

As a result of experimental studies in [17] for the movement of water droplets in a stream of hot gases (temperature above 1000 K), were established integral characteristics of the evaporation of droplets and droplet evaporation constants for the known models of heat and mass transfer. The obtained values can be used in practical calculations and numerical simulation of evaporation processes for the conditions of high-temperature cleaning of liquids, polydisperse fire extinguishing, etc.

In the work of Zhailubaev Zh. [14] gives the basis for calculating the surface temperature of evaporating droplets for the entire period of nonstationary evaporation (when a vortex heat flow occurs), in which two stages are highlighted:

1 – propagation of thermal and concentration perturbations from the contact surface to the depth of the phases (the duration of the first stage of evaporation is equal to the contact time of the surface element with the gas phase and does not exceed 10^{-3} – 10^{-4} s for atomized liquid droplets);

2 – stage of nonstationary evaporation, during which the resistance created by the gas phase to exchange processes remains constant. Temperature of liquid in the second stage approaches the value of adiabatic evaporation temperature, achievement of which is considered as the beginning of stationary evaporation of droplets.

Experiments carried out by the authors with suspended droplets 0.56 to 2.5 mm in diameter at air velocities up to 6.5 m/s allowed to obtain solution of the thermal conductivity equation from which the expression for calculation of evaporation rate was derived:

$$q = A(T_1) \cdot r + \varepsilon_K \cdot B(T_1) \cdot r^2 \quad (4)$$

T – temperature; ε_K – thermal conductivity coefficient; r – current radius (coordinates); A , B – constants.

Despite the apparent simplicity of the considered model, its practical use requires a number of

experiments to determine the calculated values of constants A and B .

In the work of Spiglazova A. S. [21] studied the influence of air resistance on evaporation of a falling drop. Analytical expressions were obtained for different ratios of evaporation rate and proportionality factor for the drag force. The use of these models in real conditions is difficult because of the difficulty of accurately assessing the conditions of resistance of the medium to the movement of the droplet.

The kinetics of evaporation of water droplets free-flying in an air stream was analyzed in [13] in order to formulate requirements for the optimal droplet size in an air-droplet mixture designed for cooling production equipment. The following features arise when droplets are forcibly injected into the air stream:

- the droplet expends its mass during evaporation until it disappears;

- small droplets that are in suspension are noticeably affected by viscous frictional forces and therefore their relative velocity in the air is low;

- a stable boundary layer of laminar type is formed around a droplet, which practically excludes the influence of convection and turbulence, so the diffusion of steam from the droplet surface into the ambient air occurs mainly at the molecular level.

Once in the air flow, the droplet very quickly reaches the psychrometric temperature, and further evaporation proceeds mainly at a steady temperature. It was found that the duration of existence of water droplets injected into the air stream is inversely proportional to their initial radius. For example, time of evaporation of a drop with initial radius $r_0 = 0.01$ mm in the flow is $\tau \cong 0.5$ s.

Some authors [2, 20] investigated possibilities of influencing droplet evaporation processes by means of electric fields. In [2] influence of electric field on intensity of evaporation of levitating drops of liquid was simulated and empirical expression for calculation of time of complete evaporation for drops with size $d = 4$ – 5 mm was obtained:

$$t = 1.64f - 40.9, \quad (5)$$

where f is the relative humidity of the air.

It has been experimentally established that constant electric field of 3 kV/cm maximally intensifies processes of evaporation of water drop suspended in air flow.

Model (5) is notable for its simplicity and ease of use in practical calculations, however, this model is not suitable for calculations of microclimate systems as it was developed for evaporation of large drops only.

Comparison of evaporation processes of superheated and cold water was carried out by D. V. Marinichev [19], who found that fine atomization of superheated water with predominance of microdroplets with a diameter less than 3 microns can be achieved by using the technology of explosive boiling of strongly superheated liquid. It was proved that when superheated water is sprayed into an air stream at a velocity of up to 40 m/s, the droplet size distribution has a pronounced bimodal character. Atomizing water temperature of 220–240 °C about 65–70 mass percent of the droplets have diameter less than 3 microns, and the average diameter of large droplets is about 8 microns which is about 1.5–2.5 times less than atomizing cold water. When spraying with cold water (up to 150 °C) droplet size distribution remains unimodal. Data on the droplet size and nature of droplet distribution can be very useful in the calculation of microclimate systems.

Evaporation of droplets from a solid surface.

The process of evaporation of liquid droplets from various surfaces has been studied by many authors [16; 18; 20; 28; 30]. For the purposes of designing microclimate systems, processes of evaporation from surfaces are significant from the point of view that when spraying coolants into the air, a significant proportion of droplets inevitably settles on various surfaces and there continue to evaporate. Therefore further we shall consider results of researches of evaporation of liquid from surfaces of soil, leaves and various solid materials.

Many authors considering evaporation of water droplets from solid surfaces point out that:

- The evaporation rate increases with increasing surface temperature and is highly dependent on the roughness of the wall [30];

- evaporation of droplets smaller than 500 μm directly depends on the thermal conductivity of the substrate [28];

- changes in the electrokinetic potential of particles affect the evaporation of droplets [20]: an increase in the electrokinetic potential of particles leads to a change in the evaporation scenarios of a droplet located on a solid surface: the adhesion of the droplet to the underlying surface weakens, the droplet begins to move with a change in the surface shape, which leads to either acceleration or slowdown of evaporation.

A wide range of studies of evaporation from soil surface was carried out at Research Institute of Hydrometeorology (Uzbekistan) [6–11]. To estimate these processes, theoretical analysis of soil moisture evaporation process was made [11] based on equations of particle number balance and speed of their motion, mathematical dependencies between characteristic particle size of its area and volume were obtained [8]. In [9; 10], based on the generalized equilibrium equation and material balance of particles as well as the equations of hydrodynamics for a continuous medium and energy for air, a multiphase model of interaction between different kinds of underlying surface and air flows in the surface layer and upper atmosphere is analyzed. For these conditions the amount of vapor evaporating from a particle per unit time is calculated.

The problem of estimating the time of evaporation of raindrops and dewdrops from the surface of plant leaves was considered in [12]. To create microclimate systems in arid areas, it is important to be able to manage the time of evaporation of water from plant leaf surfaces. Thomson formula is used to estimate the dependence of saturated vapor pressure over a small droplet:

$$P = P_{\infty} e^{\frac{2M\sigma V_M}{aRT}} \quad (6)$$

where M is the molecular mass, a is the changing drop radius, T is the thermodynamic temperature, V_M is the molar volume, σ is the surface tension of the liquid formed by vapor condensation.

From the above expression it can be concluded that the saturated vapor pressure over the convex surface of the droplets will be greater than over the flat one. Based on this statement the author [12] analyzed the evaporation time of a spherical droplet of small size lying on the surface of a solid body (sheet) at relative humidity f at temperature T :

$$t = \frac{RT \rho_{liq}^2 a_0^3 (2 - 3 \cos \theta + \cos^3 \theta)}{24DM\sigma\rho_{sat}f} \quad (7)$$

θ – contact angle, ρ_{sat} – saturated vapor density, D – diffusion coefficient, r – drop radius, a_0 – initial radius.

An example of calculation of time of evaporation of a water droplet with initial radius $a_0 = 0.1$

mm evaporating from solid surface at contact angle $\theta = 120$ degrees and temperature $T = 293$ K resulted in $t = 325$ hours. This result raises certain doubts about the adequacy of the proposed model. The approach suggested by the author is of interest, however, the model obtained obviously requires refinement.

Conclusion. Many of the considered computational schemes are in principle not stable in practical calculations, or give calculation results which are inadequate to the physical rules of substance movement in a gas flow.

Nevertheless, the data and models obtained by Balakrova S. B., Dokhov M. P., Shishkin N. E., Marinichev D. V. may be recommended (after clarification in real conditions) for calculation and design of microclimate systems based on atomization in the air of water droplets.

References:

1. Антонов А. С. Сравнительный анализ моделей испарения капли жидкости в потоке газа. – Электронный ресурс. Режим доступа: URL: <https://pandia.ru/text/80/589/10200.php>. Дата обращения: 12.06.2022.
2. Балкарова С. Б. Экспериментальное исследование процессов теплообмена капель воды, кристаллизующихся в потоке воздуха. Автореф. дисс. ... к.ф.-м.н. – Нальчик: Кабардино-Балкарский Государственный университет. – 17 с.
3. Береснев С. А., Грязин В. И. Физика атмосферных аэрозолей: Курс лекций. – Екатеринбург: Изд-во Урал. ун-та, 2008. – 227 с
4. Васильев П. С. Теплообмен при капельном кипении жидкостей в технологических аппаратах. Диссертация на соискание учёной степени кандидата технических наук. – Волгоград, 2018.
5. Войтков И. С., Волков Р. С., Кузнецов Г. В., Стрижак П. А. Высокотемпературное испарение капель воды в газовой среде. Журнал технической физики, – Том 87. – Вып. 12. 2017.
6. Денисов Ю. М. Математическая модель переноса влаги. Метеорология и гидрология – № 3. 1978. – С. 67–93.
7. Денисов Ю. М. Некоторые эвристические соотношения по оценки потоков импульса, тепла и пара // Труды Среднеазиатского научно-исследовательского гидрометеорологического института. – Выпуск 160 (238). – Ташкент, 1999.
8. Денисов Ю. М. Основы теории образования и движения аэрозолей // Труды Среднеазиатского научно-исследовательского гидрометеорологического института. Оценка загрязнения природной среды Среднеазиатского региона. – Выпуск 155(236). – Ташкент, 1998.
9. Денисов Ю. М., Джураев А. А. Математическая модель некоторых микрофизических процессов в облаке. Математическое моделирование гидрологических процессов. Средне-Азиатский региональный научно-исследовательский гидрометеорологический институт – Выпуск 63(144). 1979.

10. Денисов Ю. М., Овчаренко В. П. Многофазная магнитодинамическая модель атмосферы. Труды. Вопросы гидродинамики атмосферы. Средне-Азиатский региональный научно-исследовательский гидрометеорологический институт – Выпуск 21(102). – Ленинград, 1975 г.
11. Денисов Ю. М., Сергеев А. И., Безбородов Г. А., Безбородов Ю. Г. Испарение почвенной влаги с оголенных почвогрунтов // Труды Среднеазиатского научно-исследовательского гидрометеорологического института. Математическое моделирование процессов стока горных рек. – Выпуск 163(244). – Ташкент, 2001.
12. Дохов М. П. Влияние кривизны на испарение малых капель жидкостей // Фундаментальные исследования, – № 5. 2006. – С. 83–84.
13. Емельянов А. Л., Платунов Е. С. Кинетика испарения капель в системах охлаждения теплонагруженных элементов приборов // Изв. Вузов. Приборостроение. – Т. 54. – № 1. 2011. – С. 84–88.
14. Жайлаубаев Ж. Д. Нестационарное испарение капель при фазовом переходе. Вестник ПГУ – № 2. 2010.
15. Жорнова О. Н., Гальперин Л. Г. Расчет скорости испарения капель воды в потоке перегретого водяного пара. – Электронный ресурс. URL: https://elar.urfu.ru/bitstream/10995/57869/1/eir_2017_035.pdf/ Дата обращения: 24.05.2022.
16. Кашеев В. М., Муранов Ю. В., Юрьев Ю. С. Определение потока испарения при дисперсно-кольцевом и дисперсном режимах течения (по результатам численного эксперимента). Физико-энергетический институт – 1330. 1982. – 18с.
17. Кузнецов Г. В., Куйбин П. А., Стрижак П. А. Оценка численных значений констант испарения капель воды, движущихся в потоке высокотемпературных газов, ТВТ, – том 53. – выпуск 2. 2015. – С. 264–269.
18. Кузнецов Г. В., Феоктистов Д. В., Орлова Е. Г. Испарение капель жидкостей с поверхности анодированного алюминия Теплофизика и аэромеханика, – Том 23. – № 1. 2016.
19. Мариничев Д. В. Экспериментальное исследование тонкодисперсного распыла перегретой воды. Дисс... кандидата техн. наук. – Москва: Объед. ин-т высок. температур РАН, 2013. – 116 с.
20. Молчанов С. П., Чернова-Хараева И. А., Сенчихин И. Н. Влияние электрокинетического потенциала на испарение капель коллоидных дисперсий. коллоидный журнал, – Том 81. – № 2. 2019. – С. 202–211.
21. Спиглазова А. С., Мезенцев А. В. Движение равномерно испаряющейся капли жидкости с учетом действия силы тяжести и двух различных сил сопротивления – Электронный ресурс. URL: https://elar.urfu.ru/bitstream/10995/94067/1/978-5-91256-506-9_2020_018.pdf/ Дата обращения: 5.06.2022.
22. Терехов В. И., Пахомов М. А., Чичиндаев А. В. Влияние испарения жидких капель на распределение параметров в двухкомпонентном ламинарном потоке. Прикладная механика и техническая физика. – Т. 41. – № 6. 2000.
23. Терехов В. И., Терехов В. В., Шишкин Н. Е. Экспериментальное и численное исследование нестационарного испарения капель жидкости // I Minsk International Heat and Mass Transfer Forum, MIF 2008. – Minsk, May 19–23. 2008.
24. Терехов В. И., Шишкин Н. Е. Испарение капель водных смесей легко – и высококипящих жидкостей в воздушном потоке. Сборник научных статей Современная наука. 2010.
25. Фукс Н. А. Испарение и рост капель в газообразной среде. Издательство Академии наук СССР. – Москва. 1958.

26. Шиляев М. И., Хромова Е. М., Григорьев А. В., Тумашова А. В. Физико-математическая модель конденсационного процесса улавливания субмикронной пыли в форсуночном скруббере. *Теплофизика и аэромеханика*, – Том 18. № 3. 2011.
27. Шишкин Н. Е. Аэродинамика и тепломассообмен в пристенных закрученных одно- и двухфазных струях. Дисс. ... доктора техн. наук. Новосибирск: Институт теплофизики им. С. С. Кутателадзе, 2016. – 266 с.
28. Bazargan V. Effect of substrate cooling and droplet shape and composition on the droplet evaporation and the deposition of particles. Thesis. The University of British Columbia. March, 2014.
29. Guang Jin, Rui Tian, Xingwang Song, Wenfei Wu. Theoretical and Experimental Studies of Droplet Evaporation in High-Temperature Air. The Second China Energy Scientist Forum. 2010.
30. Misyura S. Y., Morozov V. S. Droplet Evaporation on a Heated Structured Wall. *Thermal Science: Year – Vol. 23.* – No. 2A. 2019. – P. 673–681.

Section 6. Chemistry

<https://doi.org/10.29013/AJT-22-3.4-59-66>

Ergashev Dilmurod Adiljonovich,
Associate Professor, Department of Chemical Technology
Fergana Polytechnic Institute,
Khamdamova Shokhida Sherzodovna,
Doctor of Technical Sciences, Professor,
Department of Chemical Technology
Fergana Polytechnic Institute,
Mirzaolimov Akmal Nabiyevich,
Assistant, Department of Chemical Technology
Fergana Polytechnic Institute
Eshpulatova Matluba Boymuradovna,
Junior researcher of the Institute
of General and Inorganic Chemistry of the Academy
of Sciences of the Republic of Uzbekistan

THE SOLUBILITY OF COMPONENTS IN THE SYSTEM $\{99.7[30 \text{MgSO}_4 + 70\% \text{H}_2\text{O}] + 0.3\% \text{HNO}_3 \cdot$ $\cdot \text{NH}_2\text{C}_2\text{H}_4\text{OH} - (\text{NH}_4)_6\text{Mo}_7\text{O}_{24} \cdot 4\text{H}_2\text{O}$

Abstract. The heterogeneous phase equilibrium in an aqueous system consisting of magnesium sulfate, monoethanolamine nitrate, and ammonium molybdate has been studied. It has been established that the system, including magnesium sulfate and monoethanolamine nitrate, belongs to a simple eutonic type, where the salting-out effect of the components on each other is observed. The dependence of changes in the physicochemical properties of solutions in a system containing MgSO_4 , $\text{HNO}_3 \cdot \text{NH}_2\text{C}_2\text{H}_4\text{OH}$ и $(\text{NH}_4)_6\text{Mo}_7\text{O}_{24} \cdot 4\text{H}_2\text{O}$ depending on the composition of the components was studied. A “composition-property” diagram of this system is constructed.

Keywords: fertilizers, MgSO_4 , $\text{MgSO}_4 \cdot 12\text{H}_2\text{O}$ and $\text{MgSO}_4 \cdot 7\text{H}_2\text{O}$, $\text{HNO}_3 \cdot \text{NH}_2\text{C}_2\text{H}_4\text{OH}$, $(\text{NH}_4)_6\text{Mo}_7\text{O}_{24} \cdot 4\text{H}_2\text{O}$, solubility diagram, the composition-properties diagram.

Introduction. In modern intensive technologies for growing field crops, the fertilizer system provides for the introduction of not only N, P_2O_5 , K_2O , but also all the macro- and microelements necessary for the plant. The introduction of sulphur has already become

as common as the introduction of nitrogen, phosphorus and potassium. Somewhat less attention in the nutrition system was paid to providing plants with magnesium and calcium. Recently, scientists and agricultural producers have been persistently and convincingly talk-

ing about the introduction of calcium as a nutrition element at much lower rates – 200–500 kg/ha.

As for magnesium, theoretically, everyone knows about the need to add it. In the composition of fertilizer mixtures, magnesium is contained in a smaller amount, or its content is lower compared to sulphur. Therefore, it is this, somewhat underestimated, an element that can become a limiting factor in the further growth of field crop yields.

Physiological role magnesium is associated with an effect on the activity of many enzymes. It plays an important role in the process of photosynthesis – it activates an enzyme that catalyzes the participation of CO_2 in photosynthesis. It is directly involved in the synthesis of ATP – the energy carrier in plants. Due to the use of the energy of the ATP molecule, the plant synthesizes glucose from carbon dioxide and water – the first link in the complex chain of photosynthesis. It not only participates in the synthesis of carbohydrates, but also ensures their transportation to the underground part of the plant, due to which a well-developed root system is formed, and in winter crops, the sugar content also increases and frost resistance increases [1].

At present, much attention is paid to the production of complex liquid fertilizers containing N, Ca, P_2O_5 , and K_2O , as well as plant protection products, physiologically active substances, etc. Of particular interest is the study of the combined use of liquid fertilizers with physiologically active substances that accelerate the growth and development of plants and increase crop yields. One of such representatives of physiologically active substances is monoethanolammonium nitrate [2; 3].

This article is devoted to research on the production of liquid fertilizer containing Mg, N, Mo, and S and a physiologically active substance. In this regard, the following main research tasks were set and solved:

- Study of solubility in a system consisting of water, magnesium sulfate and monoethanolamine nitrate in a wide temperature and concentration range [4];
- Study of the refractive index, viscosity, density, and pH of the medium at 20 °C in the sys-

tem $[\text{30\%MgSO}_4 \cdot 0,3\text{HNO}_3 \cdot \text{NH}_2\text{C}_2\text{H}_4\text{OH}] - (\text{NH}_4)_6\text{Mo}_7\text{O}_{24} \cdot 4\text{H}_2\text{O}$;

Objects and methods of research. The following were used in the work: $\text{MgSO}_4 \cdot 7\text{H}_2\text{O}$, $\text{HNO}_3 \cdot \text{NH}_2\text{C}_2\text{H}_4\text{OH}$, $(\text{NH}_4)_6\text{Mo}_7\text{O}_{24} \cdot 4\text{H}_2\text{O}$ of analytical grade.

For the study, a 30% aqueous solution of magnesium sulfate was used, which is a transparent solution with a slightly yellowish tint, odourless. The drug dissolves well in water with the formation of homogeneous solutions. Crystallization temperature 19.7–19.9 °C.

The second component is liquid monoethanolamine nitrate (LMEA), which we synthesized based on nitric acid and monoethanolamine [5; 6] at an equimolar ratio of components 1:1. The synthesized compound $\text{HNO}_3 \cdot \text{NH}_2\text{C}_2\text{H}_4\text{OH}$ is a concentrated solution, slightly cinnamon in colour, and highly soluble in water. Boiling point 145 °C, crystallization point –8.0 °C, pH of aqueous solutions 5.35. The third component is the crystalline salt $(\text{NH}_4)_6\text{Mo}_7\text{O}_{24} \cdot 4\text{H}_2\text{O}$. Ammonium molybdate tetrahydrous (analytically pure) was obtained by mixing ethanol with a concentrated ammonia solution of molybdenum (VI) oxide.

When studying the solubility of phases in physicochemical systems, the visual-polythermal method was used [4]. The viscosity of solutions was measured using a VPZh (БПЖ)-type viscometer [7] with a capillary diameter of 1.16–1.32 mm. Results accuracy $\pm 0.0001\text{--}10\text{-lm}^2/\text{s}$. The density of the studied compounds and solutions was determined pycnometrically [8]. The pH of solutions was measured according to the procedure [9] on an FE-20 METTLER TOLEDO pH meter.

Results and discussion. To elucidate the behaviour of the components in the process of obtaining a liquid fertilizer based on magnesium sulfate, nitrate monoethanolammonium and ammonium molybdate, the solubility in the $\text{MgSO}_4 - \text{HNO}_3 \cdot \text{NH}_2\text{C}_2\text{H}_4\text{OH} - \text{H}_2\text{O}$ system (Fig. 1, Table 1.) was studied by the visual-polythermal method [4].

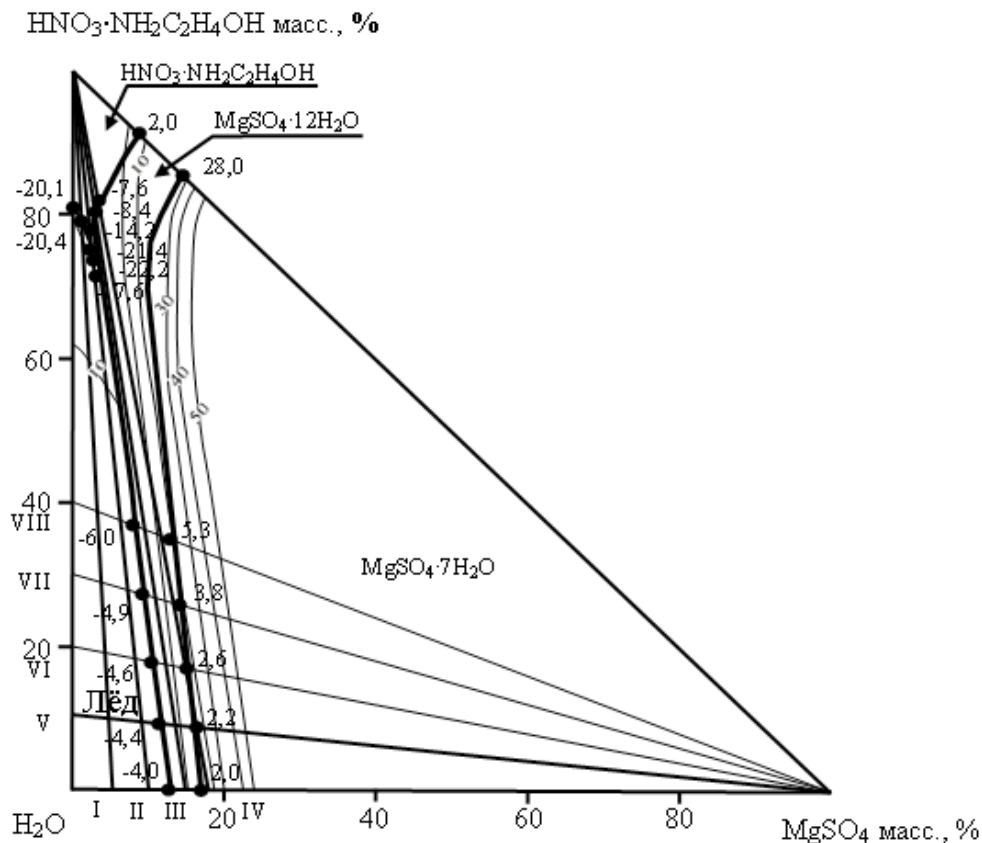

 Figure 1. Polythermal solubility diagram of the system $\text{MgSO}_4\text{-HNO}_3 \cdot \text{NH}_2\text{C}_2\text{H}_4\text{OH-H}_2\text{O}$

 Table 1. – Double and triple points of the $\text{MgSO}_4\text{-HNO}_3 \cdot \text{NH}_2\text{C}_2\text{H}_4\text{OH-H}_2\text{O}$ system

The composition of the liquid phase, wt.%			Crystal temperature, °C	solid phase
MgSO_4	$\text{HNO}_3 \cdot \text{NH}_2\text{C}_2\text{H}_4\text{OH}$	H_2O		
1	2	3	4	5
12.2	–	87.8	–4.0	Ice + $\text{MgSO}_4 \cdot 12\text{H}_2\text{O}$
11.4	9.2	79.4	–4.4	–
10.2	18.0	71.8	–4.6	–
9.1	27.6	63.3	–4.9	–
8.0	37.0	55.0	–6.0	–
3.0	71.8	25.2	–17.6	–
2.8	74.0	23.2	–22.2	Ice + $\text{MgSO}_4 \cdot 12\text{H}_2\text{O}$ + $\text{HNO}_3 \cdot \text{NH}_2\text{C}_2\text{H}_4\text{OH}$
2.0	75.2	21.0	–21.4	Ice + $\text{HNO}_3 \cdot \text{NH}_2\text{C}_2\text{H}_4\text{OH}$
1.2	79.0	19.8	–20.4	–
–	80.6	19.4	–20.1	Ice + $\text{HNO}_3 \cdot \text{NH}_2\text{C}_2\text{H}_4\text{OH}$
1.4	78.0	20.6	–14.2	$\text{HNO}_3 \cdot \text{NH}_2\text{C}_2\text{H}_4\text{OH} + \text{MgSO}_4 \cdot 12\text{H}_2\text{O}$
3.0	80.4	16.6	–8.4	–

1	2	3	4	5
3.7	81.6	14.7	-7.6	-
8.2	91.8	-	2.0	-
16.5	-	83.5	2.0	MgSO ₄ · 12H ₂ O + MgSO ₄ · 7H ₂ O
16.0	9.2	74.8	2.2	-
17.0	9.0	74.0	2.6	-
14.4	23.0	62.6	3.4	-
13.8	26.0	60.2	3.8	-
13.0	35.0	52.0	5.3	-
14.4	85.6	-	28.0	-

On the solubility diagram, the largest field of crystallization belongs to magnesium sulfate heptahydrate, since it has a lower solubility compared to other components of the system. It follows from the given data that no formation of new compounds based on the initial components is observed in the studied system. The system is of a simple type, which means that the components of the system, when presented together, retain their individuality and physiological activity.

The solubility of the binary system of monoethanolammonium nitrate in water was studied from the freezing point of -20.1 to -2.0 °C. Based on the data obtained, the crystallization branches of ice, nitric acid, monoethanolamine and monoethanolamine nitrate were established. The composition and crystallization temperature was determined at figurative points of the system. With the establishment of the quantitative composition of liquid and solid phases, which are given (Table 2., Fig. 2.).

Table 2. – Water solubility data for the HNO₃ · NH₂C₂H₄OH-H₂O system

№	Liquid phase composition, %		Tcr., °C	solid phase
	HNO ₃ · H ₂ NC ₂ H ₄ OH	H ₂ O		
1	2	3	4	5
1	-	100	0	Ice
2	2.8	97.2	-0.2	Same
3	6.3	93.7	-0.4	-
4	11.1	88.9	-0.8	-
5	16.7	83.3	-1.1	-
6	22.5	77.5	-1.8	-
7	30.6	69.4	-2.4	-
8	37.2	62.8	-3.1	-
9	42.2	57.8	-4.4	-
10	46.9	53.1	-5.7	-
11	51.4	48.6	-7.0	-
12	56.0	44.0	-8.2	-
13	61.2	38.8	-10.3	-
14	65.0	35.0	-11.9	-
15	68.2	31.8	-13.2	-
16	72.5	27.5	-15.8	-

1	2	3	4	5
17	76.7	23.3	-17.5	–
18	78.4	21.6	-18.8	–
19	80.57	19.43	-20.1	Ice + HNO ₃ · NH ₂ C ₂ H ₄ OH
20	81.2	18.8	-18.6	HNO ₃ · NH ₂ C ₂ H ₄ OH
21	82.1	17.9	-16.8	Same
22	83.9	16.1	-14.0	–
23	86.0	14.0	-11.2	–
24	88.0	12.0	-8.8	–
25	89.8	10.2	-7.4	–
26	92.0	8.0	-5.8	–
27	93.9	6.1	-4.2	–
28	96.1	3.9	-3.5	–
29	98.0	2.0	-2.4	–
30	100	–	-2.0	–

From the above solubility data, it can be seen (Table 1) that monoethanolamine nitrate is very soluble in water. Based on the data obtained, we have

constructed a polythermal solubility diagram for the binary system HNO₃ · NH₂C₂H₄OH–H₂O.

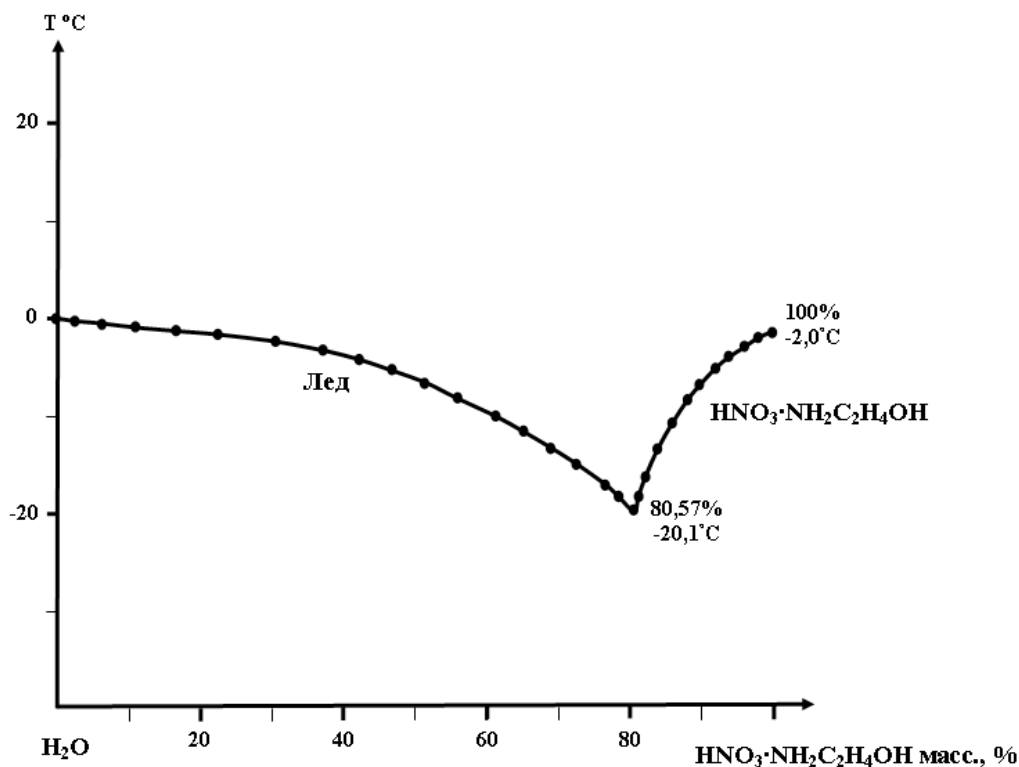


Figure 2. Solubility diagram of the binary system HNO₃ · NH₂C₂H₄OH–H₂O

Solubility in binary systems consisting of sodium tricarbamide chlorate and water, MgSO₄–H₂O and HNO₃ · NH₂C₂H₄OH–H₂O has been studied

by many authors, our results are in good agreement with the literature [10–20].

For the physicochemical substantiation of the process of obtaining sulfur-containing fertilizer with physiological activity, we studied the $\text{MgSO}_4 - \text{HNO}_3 \cdot \text{NH}_2\text{C}_2\text{H}_4\text{OH}$ system. On its polythermal solubility diagram, crystallization branches were revealed: $\text{HNO}_3 \cdot \text{NH}_2\text{C}_2\text{H}_4\text{OH}$, $\text{MgSO}_4 \cdot 12\text{H}_2\text{O}$ and $\text{MgSO}_4 \cdot 7\text{H}_2\text{O}$ (Fig. 3).

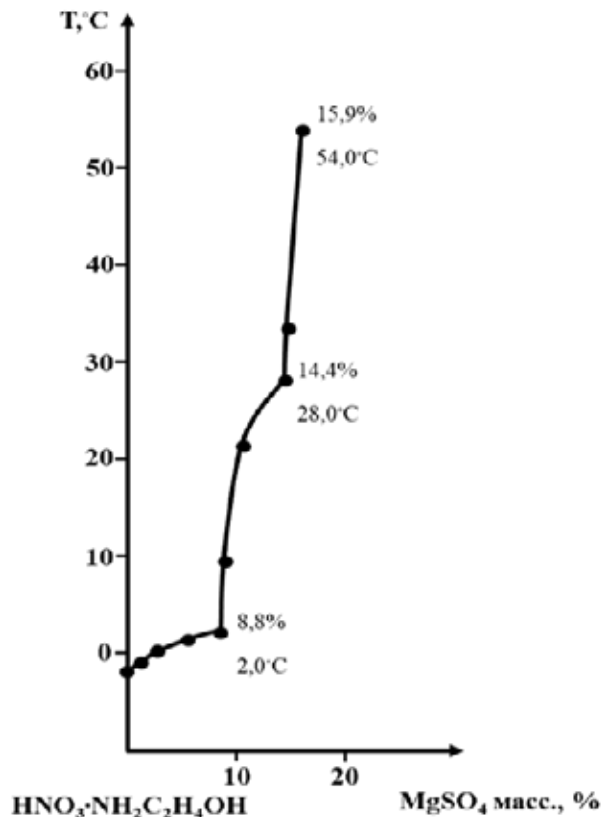


Figure 3. Polythermal solubility diagram of a binary system $\text{HNO}_3 \cdot \text{NH}_2\text{C}_2\text{H}_4\text{OH} - \text{MgSO}_4$

To develop technological standards for the process and recommend a technology for obtaining liquid fertilizer based on magnesium sulfate and a physiologically active substance ($\text{HNO}_3 \cdot \text{NH}_2\text{C}_2\text{H}_4\text{OH}$), the dependence of changes in the rheological properties of solutions on the composition in the $\text{MgSO}_4 -$

$\text{HNO}_3 \cdot \text{NH}_2\text{C}_2\text{H}_4\text{OH} - (\text{NH}_4)_6\text{Mo}_7\text{O}_{24}$ system was studied.

To elucidate the effect of components on the physicochemical properties of solutions of the above system, the dependence of the change in crystallization temperature, medium pH, viscosity and density of solutions on the composition was determined. Based on the data obtained, a “composition-property” diagram of this system was constructed (Fig. 4, Table 3).

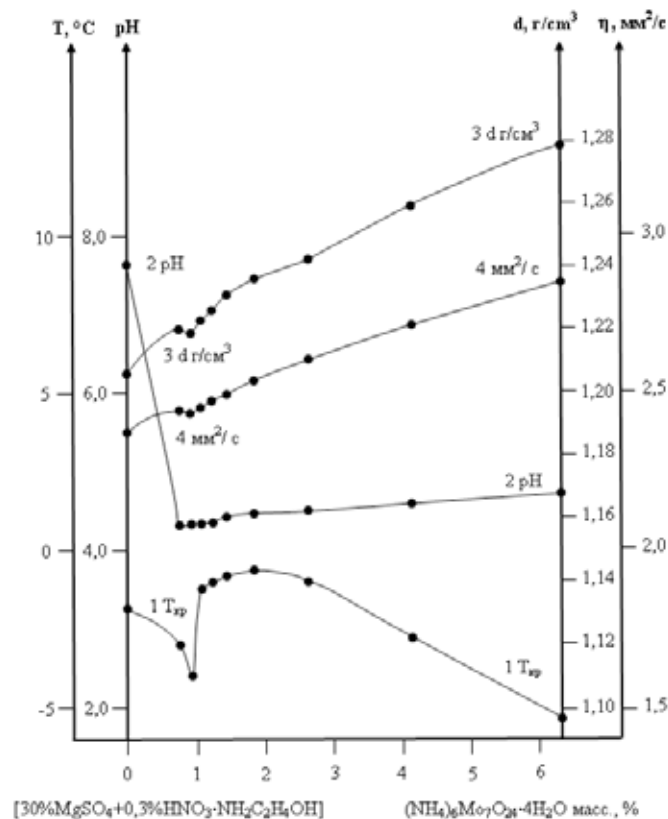


Figure 4. Dependence of the change in crystallization temperature (1), pH (2), density (3) and viscosity (4) of solutions on the composition in the system $\{99.7\%[30\%\text{MgSO}_4+70\%\text{H}_2\text{O}]+0.3\%\text{HNO}_3 \cdot \text{NH}_2\text{C}_2\text{H}_4\text{OH}\} - (\text{NH}_4)_6\text{Mo}_7\text{O}_{24} \cdot 4\text{H}_2\text{O}$

Table 3. – Dependence of the change in the physicochemical properties of solutions on the composition in the $\{99.7\%[30\%\text{MgSO}_4+70\%\text{H}_2\text{O}]+0.3\%\text{HNO}_3 \cdot \text{NH}_2\text{C}_2\text{H}_4\text{OH}\} - (\text{NH}_4)_6\text{Mo}_7\text{O}_{24} \cdot 4\text{H}_2\text{O}$ system

N°	$\{99.7\%[30\%\text{MgSO}_4+70\%\text{H}_2\text{O}]+0.3\%\text{HNO}_3 \cdot \text{NH}_2\text{C}_2\text{H}_4\text{OH}\}$	$(\text{NH}_4)_6\text{Mo}_7\text{O}_{24} \cdot 4\text{H}_2\text{O}$	T_{kr}	pH	$d \text{ g/cm}^3$	mm^2/s
1	2	3	4	5	6	7
1	100	–	–1.8	7.65	1.20661	2.37706

1	2	3	4	5	6	7
2	99.22	0.78	-3.0	4.34	1.22100	2.45001
3	99.08	0.92	-4.0	4.35	1.22003	2.44904
4	98.92	1.08	-1.2	4.36	1.22302	2.450825
5	98.78	1.22	-1.0	4.38	1.226541	2.47510
6	98.54	1.46	-0.8	4.42	1.231830	2.49890
7	98.14	1.86	-0.6	4.47	1.23656	2.54545
8	97.37	2.63	-1.0	4.50	1.24297	2.61480
9	95.85	4.15	-2.8	4.60	1.25954	2.72533
10	93.69	6.31	-5.3	4.74	1.27933	2.85267

Figure 4 shows that in the process of dissolution $\{99,7\%[30\%\text{MgSO}_4+70\%\text{H}_2\text{O}]+0.3\%\text{HNO}_3 \cdot \text{NH}_2\text{C}_2\text{H}_4\text{OH}\}$ in $(\text{NH}_4)_6\text{Mo}_7\text{O}_{24} \cdot 4\text{H}_2\text{O}$ sharp breaks are observed on the curves of crystallization temperature and pH again formed solutions at content $0.92\% t_{\text{кр}} -4.0^\circ\text{C}$; pH 4.35; $d g/cm^3$ 1.22003; mm^2/s 2,44904. On the curves of density (3) and viscosity (4), the break is not so obvious due to the very small amount of additives. This is explained by the fact that within the studied ranges of component concentrations at breakpoints in the system there is a phase transition from ice to mixtures of salts of magnesium sulfate, monoethanolamine nitrate and ammonium molybdate.

Conclusion. Thus, the mutual influence of the components in the $\{99.7\%[30\%\text{MgSO}_4+70\%\text{H}_2\text{O}]+0.3\%\text{HNO}_3 \cdot \text{NH}_2\text{C}_2\text{H}_4\text{OH}\}-(\text{NH}_4)_6\text{Mo}_7\text{O}_{24}$ system was studied and the composition of a new liquid fertilizer based on monoethanolammonium nitrate and ammonium molybdate was recommended.

To select the optimal ratio of components in the fertilizer composition based on magnesium sulfate and monoethanolammonium nitrate, preliminary agrochemical tests of various compositions on cot-

ton were carried out. The results showed that the composition of the fertilizer, in which the ratio of the components $[30\%\text{MgSO}_4+70\%\text{H}_2\text{O}]$ and $\text{HNO}_3 \cdot \text{NH}_2\text{C}_2\text{H}_4\text{OH}$ equal to $1.0 : 0.006 \div 0.008$ has a high agrochemical activity, and also has a positive effect on accelerating the ripening and opening of cotton bolls.

The obtained research results serve as a scientific basis for the development of a technology for obtaining liquid fertilizers of complex action.

Acknowledgements

The authors acknowledge the immense help received from the scholars whose articles are cited and included in references to this manuscript. The authors are also grateful to the authors/ editors/publishers of all those articles, journals and books from where the literature for this article has been reviewed and discussed.

In addition, the authors express gratitude to the head of the Fergana Polytechnic Institute and the scientific community of the Department of Chemical Technology for their assistance in carrying out this research work.

The authors report no conflicts of interest.

The Source of funding is nil.

References:

1. Галынская Надежда. Роль кальция в жизни растений. URL: / 2018.– С. 9–10.
2. Тоғашаров А. С., Нарходжаев А. Х., Тухтаев С. Изучение растворимости и реологических свойств системы $\text{NaClO}_3 \cdot 3\text{CO}(\text{NH}_2)-\text{HN}_2\text{C}_2\text{H}_4\text{OH} \cdot \text{HNO}_3 - \text{H}_2\text{O}$ // Химический журнал Казахстана. – Алматы, 2009. – №2. – С. 59–66.
3. Саибова М. Т. Применение этаноламинов в сельском хозяйстве // Узбекский химический журнал.– № 1. 1983.– С. 58–64.

4. Трунин А. С. Петрова Д. Г. Визуально-политермический метод / Куйбышевский политехн. Инс-т.– Куйбышев. 1977.– 94 с.
5. Киргинцев А. Н., Трушников А. Н., Лаврентьева В. Г. Растворимость неорганических веществ в воде. Справочник. Изд-во «Химия», л. 1972.– С. 111–112.
6. Абдуллаева М. Т. Взаимодействие моноэтаноламина с уксусной кислотой. Узб. хим. журн. – № 3. 2008.– С. 50–54.
7. Фролов Ю. Г. Курс коллоидной химии // Поверхностное явление и дисперсные системы.– М.: 1982.– С. 117–124.
8. Здановский А. Б., Галлургия: – Л.: Химия. 1972.– 572 с.
9. Горбачев С. В. Практикум по физической химии –М.: Высшая школа. 1974.– 310 с.
10. Эргашев Д. А., Аскарлова М. К., Эшпулатова М. Б., Махаматова Г. Б., Омонбоева Г. Б. изучение взаимного влияния компонентов в системах, обосновывающих процесс получения жидкого удобрения // Евразийский союз ученых. 2019.– № . 9–1.– С. 33–37.
11. Эргашев Д. А., Аскарлова М. К., Исабаев З., Эшпулатова М. Б., Махаматова Г. Б., Исабаев Д. З. Исследование систем, обосновывающих процесс получения жидкого удобрения комплексного действия // Евразийский Союз Ученых.– № . 5–1 (62). 2019.– С. 25–30.
12. Эргашев Д. А., Аскарлова М. К., Эшпулатова М. Б., Исабаев З., Исабаев Д. З. Растворимость компонентов в системе $\text{Ca}(\text{NO}_3)_2\text{-HNO}_3 \cdot \text{NH}_2\text{C}_2\text{H}_4\text{OH-H}_2\text{O}$ // Universum: технические науки.– № 7. – (52). 2018.– С. 61–68.
13. Эргашев Д. А., Тураев Т. Т., Мирзаолимов А. Н., Аминбоев А. Ф., Хамдамова Ш. Ш. Физико-химическое обоснование процесса получения нового дефолианта // Universum: технические науки.– № . 2 (59). 2019.
14. Эргашев Д. А., Адиллов З. Х., Тожиев Р. Р., Хамдамова Ш. Ш. Получение хлоратсодержащих дефолиантов, обладающих инсектицидными свойствами олучение хлоратсодержащих дефолиантов, обладающих инсектицидными свойствами // Монография European Scientific Platform, – Фергана-Винница, 2021 г.
15. Изучение физико-химических свойств растворов в системе $\{[19,37\% \text{Ca}(\text{ClO}_3)_2 + 15,06\% \text{Mg}(\text{ClO}_3)_2 + 3,72\% \text{CaCl}_2 + 2,68\% \text{MgCl}_2 + 45,17\% \text{H}_2\text{O}]\} + 10,0\% \text{Co}(\text{NH}_2)_2 + 4,0\% \text{C}_2\text{H}_5\text{OH}\} - \text{CH}_3\text{COOH} \cdot \text{NH}_2\text{C}_2\text{H}_4\text{OH}$ // Universum: технические науки. 2018.– № 4. – (49).– С. 2–2.
16. Эргашев Д. А., Эшпулатова М. Б., Тураев Т. Т., Хамракулов З. А., Аскарлова М. К. Диаграмма растворимости системы $\text{Ca}(\text{ClO}_3)_2 - \text{CH}_3\text{COOH} \cdot \text{NH}_2\text{C}_2\text{H}_4\text{OH-H}_2\text{O}$ при 25 °С // Universum: технические науки.– №4. – (49). 2018.– С. 1–1.
17. Эргашев Д. А., Хамдамова Ш. Ш., Мирзаолимов А. Н., Мухаммедов С. Б. Получение хлоридов кальция и магния из доломита месторождения «Навбахор» // Universum: технические науки.– №11–2. – (68). 2019.– С. 69–74.
18. Кодирова Д. Т., Мирсалимова С. Р., Умаралиева М. Ж., Абидова М. А., Нурматова З. Н. Изучение процесса получения азотно-фосфорных удобрений разложением кзылкумских фосфоритов азотной кислотой // Universum: технические науки.– № 3–2. – (72). 2020.– С. 57–59.

<https://doi.org/10.29013/AJT-22-3.4-67-71>

*Butaev Khurshid,
researcher, Tashkent Chemical-Technological Institute*

*Ikramov Abduvakhob,
doctor of sciences, professor,
Tashkent Chemical-Technological Institute*

*Kadirov Khasan,
doctor of sciences, professor,
Tashkent Chemical-Technological Institute*

*Baltabaev Ulugbek Narbaevich,
associate professor, Tashkent Chemical-Technological institute,
Tashkent, Republic of Uzbekistan,*

COMPARATIVE CHARACTERISTICS OF OCTANE-ENHANCING ADDITIVES BASED ON O- AND N-CONTAINING RAW MATERIALS

Abstract. For the purpose of obtaining effective octane-increasing additives, the tart-product dissolved in spent hexane is separated in a vacuum distillation apparatus – by-products of JV–LLC “Uz-Kor Gas Chemical”. It was found that the obtained fraction with $C_{12} - C_{18}$, the basis of which is aromatic hydrocarbons, is the most important component of octane-boosting additives.

Keywords: octane-increasing additive, octane number, spent hexane, tar product.

Introduction

It is known that the bulk of the oil produced in Uzbekistan is characterized by a high content of asphaltenes and resinous compounds and a low content of aromatic hydrocarbons and hydrocarbons of the isometric structure. Gasoline obtained by direct distillation of a mixture of oil and gas condensate has an octane number of about 50 MON (motor octane number). In order to bring it to the SS requirement, there are two ways: chemical processing – reforming, platforming, destructive hydrogenation, etc., which requires huge capital costs. The second method is the use of octane-enhancing additives and dopants. The capacities of the FR reformers do not allow the production of gasoline with an octane rating of Ai-80 and higher. Therefore, at present, the Fergana refinery uses tetraethyl lead to increase the octane number of low-octane gasolines [1].

Currently in developed countries to increase the octane the number of gasoline instead of tetraethyl lead, aliphatic alcohols are used – methanol, ethanol, isopropanol; ethers – methyl tert-butyl ether (MTBE), ethyl tert-butyl ether (ETBE), amyl tert-butyl ether (ATBE), diisopropyl ether (DIPE) [2]; aromatic amines – monomethylaniline (MMA), ash-less highly effective additive – AHEA (70% MMA + 30% methanol) [3]; metallocenes – ferrocene, manganese organic compounds (Hitech-3000) [4], ADA, Ferrada, etc. [5].

It was determined that methyl tert-butyl ether (MTBE) has the best properties. In 1978, MTBE production facilities with a capacity of 100 thousand tons per year were put into operation in Italy [6–15]. The process is based on the use of methanol and isobutylene contained in the C_4 fraction from the vapor-phase pyrolysis of hydrocarbons as raw materials.

The purpose of this work is to compare the octane-increasing properties of new alcohols, ethers and esters, amines and amides.

Results and their discussions

In this regard, we have developed new octane-increasing additives based on aliphatic alcohols – methanol, ethanol, propyl alcohol, isobutyl alcohol, esters and ethers – methyl acetate, ethyl acetate, a mixture of acetates, methyl tert-butyl ether, amines – hexamethylenetetraamine, acetonitrile metals.

To increase the octane number of low-octane gasolines, oxygen-containing compounds – oxygenates – alcohols and ethers – are used instead of highly toxic tetraethyl lead. Esters are the most widely used: however, recently, due to the revealed cases of

groundwater pollution, in some countries the use of MTBE in gasoline is limited.

Alcohol additives are used to gasolines less than ethers, but now interest in them has increased.

We have modified methanol with the addition of methyl acetate, acetone and urotropine in the following composition; % mass, methanol – 70%; methyl acetate – 10; acetone – 13; acetonitrile – 5.0; urotropine – 2.0 and was added to gasoline A-72 in the amount of 8%.

The antiknock properties of A-72 containing 18% OPD-12 (octane-enhancing additive) are shown in (Table 1).

The antiknock resistance of the developed compositions was tested on the UIT-85 unit (Table 2).

Table 1. – Composition of octane-increasing additives

№ composition	Cocrab, % об.				
	Methanol	Methylacetate	Acetone	Acetonitrile	Urotropine
OID-12	70	10	13	5	2
OID-13	65	15	12	7	1
OID-14	60	20	15	5	–
OID-15	55	25	20	–	–
OID-16	50	20	15	13	2
OID-17	45	25	15	10	–
OID-18	80	10	10	5	–

Table 2. – Anti-knock resistance of compositions

Composition	Amount, %	Octane number, ON		Octane number increase
		Without additives	With additives	
OID-12	5.0	50	58	8.0
OID-12	8.0	69	76	7.0
OID-13	5.0	69	72.0	3.0
OID-13	10.0	69	76.0	7.0
OID-14	5.0	50	59.0	9.0
OID-14	10.0	72	77.0	5.0
OID-15	5.0	72	75.0	3.0
OID-15	10.0	69	75.0	6.0
OID-16	5.0	50	57.0	7.0
OID-16	10.0	69	77.0	8.0
OID-17	5.0	50	60.0	10.0
OID-17	5.0	69	73.0	4.0
OID-17	10.0	72	81.0	9.0

The effect of various additives, including methanol, on increasing the octane number of gasoline was investigated in the FR laboratory. At the same time, it was found that the addition of methanol in

the amount of 20% to the base gasoline A-76 leads to an increase in its octane number up to 79.0 RPM. And the addition of 50 mg/l hitech and 2% MMA to 75.6, i.e. 3.6 units.

Table 3. – Physicochemical and operational properties of A-72 gasoline containing 8% OID-12

The name of indicators	SS requirements 2084– –72 to gasoline A-72	Gazoline A-72 with 8% OID-12
Detonation resistance motor octane number	76.0	83.0
Research Octane Number	not normalized	89.0
Lead content 20 g/l	0.17	отс.
Fractional composition		
The start of gasoline distillation, °C, not less	35.0	35.0
10% not higher	55.0	44.0
50% not higher	100.0	92.0
90% not higher	160.0	145.0
The end of the boiling of gasoline, °C, not higher	185.0	170.0
Residue %	1.5	0.9
Loss%	4.0	3.0
Acidity, mg KOH per 100 sm ³ of gasoline	3.0	2.8
Concentration of actual tar, mg per 100 sm ³ of gasoline	10.0	6.5
Induction period min.	900	890
Mass fraction of sulfur, %	0.1	0.02
Copper strip test	withstands	withstands
Water-soluble acids and alkalis	missing	missing
Saturated vapor pressure, mm, Hg	500–700	620
Mechanical impurities and water	missing	missing
Density at 20 °C kg/m ³	not normalized	0.722
Cloud point, °C	not normalized	minus 45

In this regard, we have prepared various compositions based on methanol and tested their antiknock properties, some of them are shown in (Table 4).

The anti-knock properties of the synthesized compositions showed that the most active compo-

sition is OID-12 when it is involved in base gasoline in an amount of 10% volume leads to an increase in octane number by 6 units.

Table 4. – Composition of oxygen and nitrogen-containing compositions (% vol.)

Composition symbol	Methanol	Ethanol	Butanol	Methyl acetate	Ethyl acetate	Urotropine
1	2	3	4	5	6	7
OID-19	70.0	10.0	8.0	8.0	2.0	2.0
OID-20	72.0	8.0	10.0	6.0	4.0	–
OID-21	74.0	6.0	10.0	8.0	20.0	–

1	2	3	4	5	6	7
OID-22	70.0	–	20.0	8.0	–	2.0
OID-23	65.0	–	27.0	6.0	–	2.0
OID-24	75.0	–	17.0	6.0	2.0	–
OID-25	75.0	–	13.0	10	5.0	–
OID-26	60.0	5.0	–	20	15.0	–

The production of methanol and ethanol has been established in the republic well. In the production of ethanol by the biochemical method, a first running is formed, the so-called “ether-aldehyde fraction” (EAF), which contains up to 95% ethanol. On the basis of EAF,

acetic acid, and methanol, we synthesized methyl and ethyl acetate using a well-known method. The resulting methyl and ethyl acetate were tested as antiknock additives. The test was carried out in the laboratory of the FR. The test results are shown in (Table 5).

Table 5. – Results of tests of methyl – and ethyl acetate as octane-increasing additives (sample-1-methyl acetate: sample-2-ethyl acetate)

№	Catalyst base: straight petrol	ON	Additive concentration% vol.	ON	Octane number increase
1	50:50	71.4	8% sample № 1	72.0	0.6
2	50:50	71.4	10% sample № 1	72.8	1.4
3	50:50	71.4	10% sample № 2	73.4	2.0
4	50:50	71.4	10% sample № 2	75.6	4.2
5	40:60	71.8	8% sample № 2	72.1	0.3
6	40:60	71.8	10% sample № 2	72.0	0.2

As can be seen from these tables, ethyl acetate is the most effective. When introduced into base gasoline in an amount of up to 10% of the mass, the octane number of gasoline increases up to 4.2 units.

Conclusions:

Thus, systematic research has been carried out to develop new highly active, environmentally friendly, energy- and resource-saving octane-enhancing ad-

ditives in gasoline based on local raw materials. It was found that a composition consisting of methanol – 70%, methyl acetate – 10,0%, acetone – 13%, acetonitrile – 5,0%, urotropine – 2,0%, manganese acetate 50 mg/l is the most effective for increasing the octane number gasoline. Adding it in the amount of 5–8% by volume allows you to increase the octane number of gasoline up to 7 units.

References:

1. Kurbanov A. A., Ibragimov K. A., Dosumova E. Ya. and others. The problem of withdrawal of lead additives from the composition of gasolines of the Fergana refinery // Uzbek. Journal. Oil and gas.– No. 3. 2002.– 21 p.
2. Orekhova A. The use of additives and additives is the most economical way to improve the quality of gasoline // The Chemical Journal,– No. 12. 2002.– P. 42–44.
3. Danilov A. P. The use of additives in fuels for cars.– M.: Chemistry, 2000.– 229 p.
4. Kapustin V. M. Oil and alternative fuels with additives and additives / V. M. Kapustin.– M.: Kolos, 2008.– 332 p.
5. Rudyak K. B., Sotov S. V., Yasinenko V. A., Kankaeva I. N., Khaldin I. A. Efficiency of application and environmental properties of monomethylaniline in the production of high-octane gasolines. Oil refining and petrochemistry.– No. 6. 2013.– P. 56–59.

6. Emelyanov V.E. Shumovsky O. Yu., Polukhina I. P., Balashov R. D. Influence of the hydrocarbon composition of gasoline compositions on the effectiveness of methyl tert-butyl ether and monomethylaniline. The world of petroleum products. Bulletin of oil companies.– No. 12. 2012.– P. 6–8.
7. Sviridova E. V., Ivanchina E. D., Kirgina M. V. Study of the influence of additives and additives on the octane number of gasoline: Electronic resource. Resource-efficient technology – the energy and enthusiasm of the young.– Tomsk: TPU Publishing House, 2013.– P. 37–39.
8. Ershov M. A., Emelyanov V. E., Klimova T. A. Biobutanol versus other oxygenates. The world of petroleum products. Bulletin of oil companies.– No. 2. 2012.– P. 3–6.
9. URL: <http://www.gks.ru/dbscripts/cbsd/DBinet.cgi?pl=9400098/> (date accessed: 01.08.2016).
10. Danilenko T. V. Development of fuel compositions of gasoline with the addition of aliphatic alcohols / T. V. Danilenko.– M.: Kolos, 2005.– 185 p.
11. Kapustin V. M. New technologies for the production of high-octane gasoline / V. M. Kapustin, E. A. Chernysheva, R. V. Khakimov // Business journal Neftegaz. RU.– No. 4. 2015.– P. 24–28.
12. Bazarov B. I., Yusupov D., Erakhmedov D. A. Multifunctional ecological alternative fuels and fuel additives // Uzbek. Journal oil and gas,– No. 3. 2003.– P. 42–43.
13. Bazarov B. I., Yusupov D., Erakhmedov D. A., Dzhumabaev A. B. Alternative composite combustible mixtures and added components // Compos. Materials,– No. 2. 2003.– P. 31–33.
14. Karimov A. U., Yusupov D., Ergashev A. A., Bazarov B. I. Synthesis of esters and ethers, obtaining additives based on them // Uzbek. Journal of Oil and Gas,– No. 4. 2004.– P. 78–79.
15. Yusupov D., Karimov A. U., Bozorov B. I., Ergashev A. A. New oxygenated antiknock agents to increase the octane number of gasolines // DAN RUz,– No. 6. 2004.– P. 53–55.

<https://doi.org/10.29013/AJT-22-3.4-72-75>

Geldiev Y. A.,

*PhD student in the Department of Chemistry
Termez State University*

Turaev Kh. Kh.,

*doctor of chemical sciences, professor
Termez State University*

Umbarov I. A.,

*doctor of technical sciences, professor
Termez State University*

THERMAL ANALYSIS OF MODIFIED POLYSILICIC ACID WITH AMINO ALCOHOLS

Abstract. The study examined the thermal analysis of polysilicic acid gels modified with solutions of different concentrations of ethanolamine in absolute ethanol. The effect of temperature on the sorption properties of these compounds at 30 °C, 50 °C and 80 °C was also analyzed thermally.

Keywords: polysilicic acid, ethanolamine, thermal analysis, sorption, desorption, carbon dioxide.

Introduction. Inorganic compounds of silicon – silicates are very common in the earth's crust and are present in almost all minerals. Polysilicic acids are mainly modified by silanol groups. There are basically two different methods used. In the first method, the organic matter is introduced into the polymerization reaction together with the substances forming polysilicates. Although the sol-gel method, which uses organosilicon compounds, is more efficient, mainly valuable monomers are used [1; 2].

The second method modifies existing polysilicates or aluminosilicates by adding organic matter. This process takes place with low yields and only on surfaces. Therefore, it can be widely used to obtain compounds that are mainly used in surface-based processes [3; 4].

The thermo gravimetric method can be used to study the degree of modification of silicates with organic matter. It uses the decomposition of silicates at high temperatures. The added compounds are relatively easily broken down [5].

Silica gels have strong sorption properties and can be used for almost any substance. Various modi-

fications are used to increase their sorption selectivity. At the same time, thermogravimetric methods are widely used in the study of sorption properties of gases and liquids [6].

Research methods. Thermal analysis was performed on a DTG-60 device manufactured by Shimadzu in Japan. Thermal stability analyzes were studied in the 40–60 °C range. Sorption properties were studied at 30 °C, 50 °C at 80 °C at a CO₂ flow rate of 100 ml/min, and desorption at 110 °C at a flow rate of 100 ml/min argon gas.

Experimental part. Synthesis of sorbents. Gel of polysilicic acid was obtained by fine neutralization of sodium orthosilicate solution with 0.1 M solution of sulfuric acid. This gel is repeatedly washed in a solution of sulfuric acid with pH = 4 and then in distilled water and filtered. The precipitate is heated to 110 °C until a constant mass is obtained.

Technical ethanolamine was distilled at low pressure in an inert medium. A solution of ethanolamine in ethyl alcohol was prepared. Soak 10 ml of the solution in 5 g of polysilicic acid for 5 hours. It is then

heated to 80 °C until the mass remains unchanged. Excess ethanolamine was isolated by low pressure driving. The process was performed separately with 10, 20, 30% solutions.

The decomposition rate and thermal stability of the obtained sorbents were studied at temperatures up to 600 °C.

Analysis of the obtained results. The thermal analysis of the samples at high temperatures is almost the same, with temperatures above 200 °C decreas-

ing only due to the water released as a result of the decomposition of the water and silanol groups in the silica gel (Fig. 1).

The decomposition of the samples can logically be divided into 3 parts: up to 200 °C, 200–400 °C, and 400–600 °C. The decomposition rates of the samples at these stages are given in Table 1. The results are given in percentages as the starting materials are obtained in different masses during the experiments.

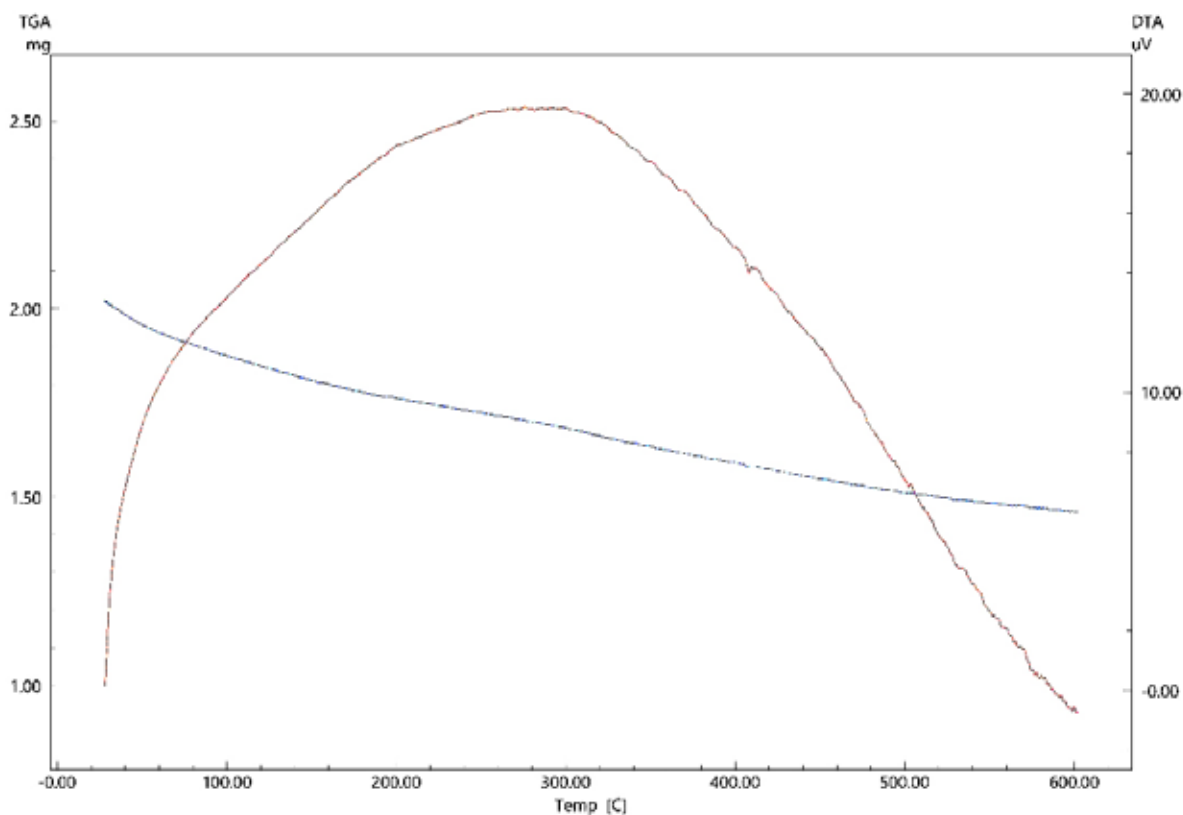


Figure 1. Thermogravimetric analysis of silica gel modified with 30% solution ethanolamine

Table 1. – The degree of decomposition of the obtained samples at different temperatures

№	Samples	Degradation rate, %			Toatl, %
		40–200 °C	200–400 °C	400–600 °C	
1	Modified with 10% solution	8.754%	8.612%	6.421%	23.787%
2	Modified with 20% solution	9.221%	8.584%	6.352%	24.157%
3	Modified with 30% solution	12.525%	8.663%	6.436%	27.624%
4	Unmodified	5.442%	8.278%	6.378%	20.098%

In the first decomposition stage, mainly the separation of sorption water and gases is observed. This is because non-organic modified polysilicic acid also

decomposes in this range. It can also be assumed that the bulk of the organic layer and the sorbed solvent are also separated.

In the second decomposition stage, the decomposition of the remaining organic part along with water in the form of crystal hydrate is also observed. It can be seen from the difference from the fragmentation of the unmodified sample that it is around 5% of the total fragmentation.

Since the third decomposition stage is mainly due to the decomposition of the silanol groups, it proceeds to almost the same extent in all samples.

Due to the fact that the decomposition is carried out in an inert medium, the modified samples are black due to the presence of carbon in the final products. In unmodified silica gels, the final product is white SiO_2 .

The table can be used to determine the degree of modification of polysilicic acid in solutions of different concentrations. In this case, the rate of increase in the mass of substances released during decomposition was used. According to him, 3.69% with 10% solution, 4.05% with 20% solution and 7.53% with 30% solution were found to contain modified organic compounds. This allows the samples to be used as sorbents due to the presence of nitrogen-containing functional groups in

the compounds. The absorption properties of these sorbents from carbon dioxide were also studied thermogravimetrically.

The sorption properties of CO_2 gas of the obtained samples were also analyzed by thermogravimetric method.

The change in the maximum sorption capacity during the sorption / desorption cycle of thermogravimetrically modified sorbents was studied. Maximum sorption capacities at 30 °C for sorption and 80 °C for desorption were used (Figure 2). During the cyclic operation of the sorbent in 2 temperature ranges, a decrease of 7–10% was observed after 5 cycles. Such a decrease can be explained by the partial release of amino groups at high temperatures. This is because the sorption capacity of the unmodified sample is virtually unchanged. The optimum conditions for the desorption process are around 80 °C, and at higher temperatures the desorption is faster and more complete, resulting in a significant reduction in the number of processing cycles. After desorption at 100 °C, after 5 cycles of the modified sample with 30% solution, the maximum sorption capacity decreases by more than 30%.

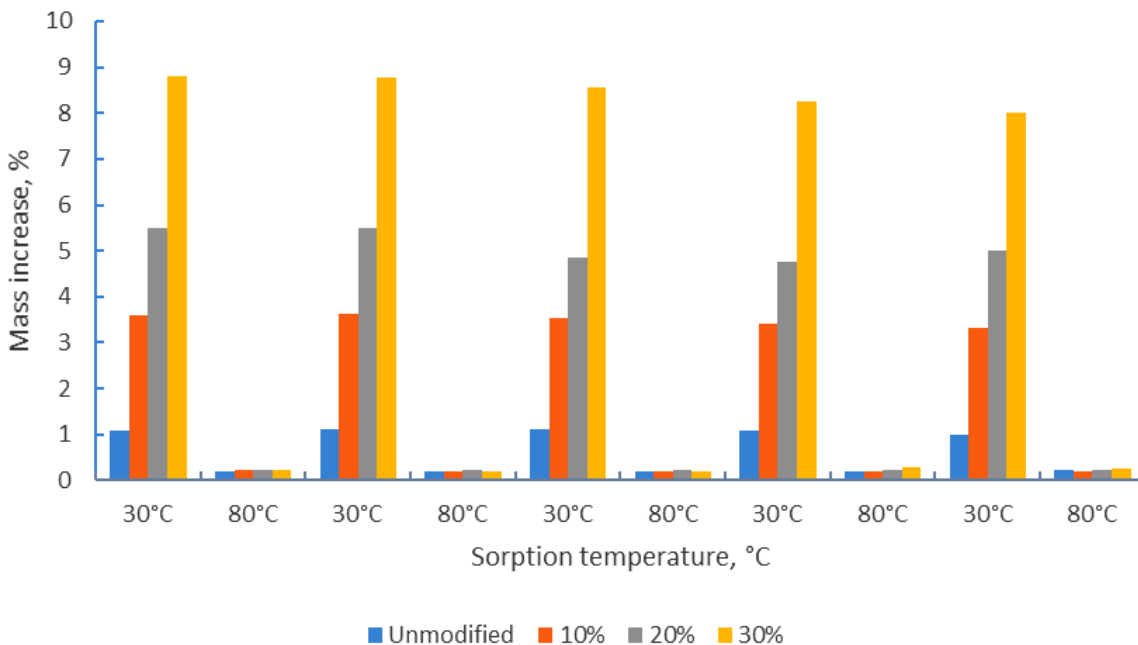


Figure 2. Cyclic performance of samples in the processes of sorption (30 °C) and desorption (80 °C) of carbon dioxide

Conclusion. The degree of modification of ethanolamine with solutions of different concentrations was determined thermally. The degree of modification was determined as the degree of fragmentation increased.

The ability of sorbents to absorb carbon dioxide also explains the importance of organic functional groups in sorption, since the increase is directly proportional to the increase in the organic content included.

References:

1. Эшмуродов Х. Э., Гелдиев Ю. А., Тураев Х. Х., Умбаров И. А., Джалилов А. Т. Б.Б.Э. Получение и исследование модифицированных глифталевых смол с кремнийорганическим соединением // *Universum: технические науки.* – Vol. 81. – № 12. 2020.
2. Эшмуродов Х. Э., Гелдиев Ю. А., Тураев Х. Х. Д. А. Т. Синтез и исследование олигомеров на основе эфиров кремниевой кислоты // *Universum химия и биология.* – Vol. 7. – № 70. 2020.
3. Zhang Y. et al. Adsorption Separation of CO₂/CH₄ from Landfill Gas by Ethanolamine-Modified Silica Gel // *Water, Air, Soil Pollut. Springer Science and Business Media Deutschland GmbH,* – Vol. 232. – № 2. 2021. – P. 1–11.
4. Fan Hongyu, Wu Zhanjun, Xu Qiaoqi, Sun T. Flexible, amine-modified silica aerogel with enhanced carbon dioxide capture performance // *J. Porous Mater.* – Vol. 23. – № 1. 2016. – P. 131–137.
5. Yang Y. et al. TEOS and Na₂SiO₃ as silica sources: study of synthesis and characterization of hollow silica nanospheres as nano thermal insulation materials // *Appl. Nanosci. Springer Science and Business Media Deutschland GmbH,* – Vol. 10. – № 6. 2020. – P. 1833–1844.
6. Staszczuk P., Nasuto R., Rudy S. Studies of Benzene Adsorption Layers on Silica Gels by Thermal Analysis and Mc Bain Balance Methods // *J. Therm. Anal. Calorim.* 2000. – 622. Springer, – Vol. 62. – № 2. 2000. – P. 461–468.

<https://doi.org/10.29013/AJT-22-3.4-76-81>

*Khamdamova Dilnoza,
Doctoral student of the department
“Pulp and Woodworking Technologies”
of the Tashkent Institute of Chemical Technology*

*Umarova Vasila,
Doctoral student of the department
“Pulp and Woodworking Technologies”
of the Tashkent Institute of Chemical Technology*

*Primkulov Mahmud,
Doctor of Technical Sciences Professor of the Department
of “Pulp and Woodworking Technologies”
of the Tashkent Chemical-Technological Institute*

OBTAINING CELLULOSE FROM THE MEDICINAL PLANT MILK THISTLE

Abstract. Cellulose was extracted from the stem of the medicinal plant- milk thistle. The fiber length, sorption properties, physical characteristics of width were studied by the method of IR-spectrum.

Keywords: cellulose, milk thistle, the degree of polymerization, IR-spectrum, the size of cellulose fibers, hydrolysis.

Introduction. It is known that the Institute of the Chemistry of Plant Substances named after V.I. acad. S. Yu. Yunusov AS RUz is concerned with the extraction of pharmaceutical substances. The institute has developed a number of methods for extracting a variety of medicinal preparations from the flora in Uzbekistan. In particular, from the medicinal plant Saint-Mary-thistle – then milk thistle (Latin *Silybum marianum*, in Uzbek *Ola o't*) [1]. Milk thistle is an annual or biennial herb. Stem is upright, massive, branched, glabrous, slightly branchy, 100–150 cm tall. Its ripe fruits and seeds are raw materials for the production of medicines. After the extraction of a number of compounds, meal remains that is not used [2–4].

At the beginning, the stems were crushed to 5–8 mm, then they were boiled in water to remove easily soluble substances. In this case, soluble substances are released from the stems, changing the op-

tical density of the liquid. As soluble substances are released into the solution, the optical density of the solution increases, the degree of light transmission decreases (Fig. 1). The kinetics of changes in optical density was determined using a **KFK-2** photoelectric colorimeter. After 40–45 minutes, the optical density of the liquid does not change, which means that there is no soluble part in the stems.

Objects and research methods. The objects of research are milk thistle stems, cellulose and fiber. To study the sorption properties of the samples, the methods of swelling in water and the test method for characterizing cellulose fibers were used. And also the method of IR-spectroscopy was used.

The aim of this work – extracting cellulose from milk thistle stems, studying the features of its structure, determining the size and fractional composition of cellulose fibers.

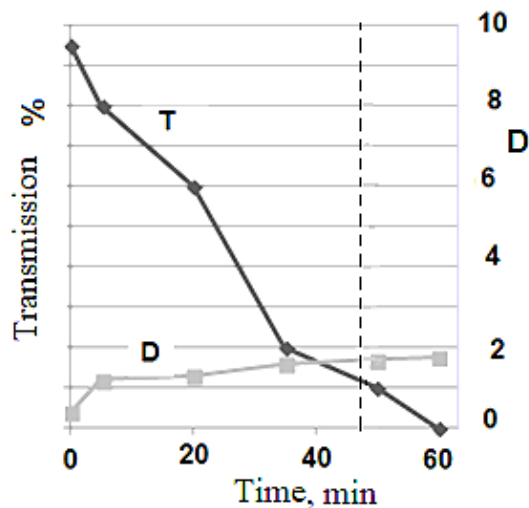


Figure 1. a) Kinetics of milk thistle stems extraction in water: T-light transmission; D-optical density of the liquid

After separating the soluble part into water, the remaining pulp containing cellulose was cooked. Isolation of cellulose from the mass was carried out by cooking in a 7% alkali solution for 4–5 hours.

Bleaching was carried out in 10% hydrogen peroxide solution for 2 hours. Structural-dimensional characteristics of cellulose from milk thistle, the determination of the size of fibers and the fractional composition in length and width were carried out by an automatic analyzer L&W Fiber Tester, developed by the company “Yuman” [5]. It is known that the length of the fibers has a great influence on the physical properties: strength and elastoplasticity. The instrument allows for advanced analysis of the properties of cellulose fibers.

The analyzer determines the following characteristics of fibers:

- average length of fibers in the sample, mm;
- average width of fibers in the sample, microns;
- average fiber shape factor in the sample;
- average bend angle;
- average number of all kinks per fiber;
- average length of one segment, mm;
- fraction of fines [6; 7].

The device was used to determine the average values of the length and width of the fibers, their frac-

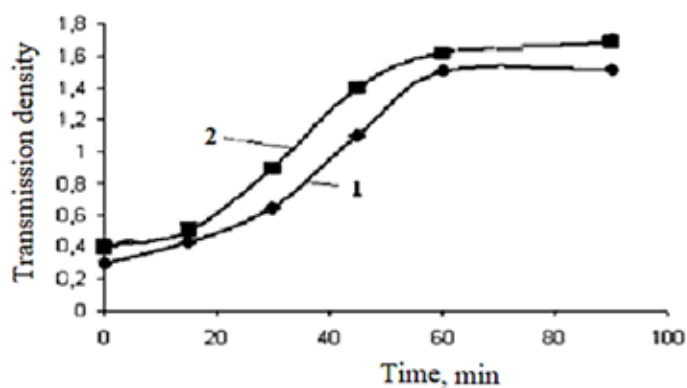


Figure 1. b) Kinetics of milk thistle stems extraction in alkali and peroxide: 1–7% NaOH; 2–10% H₂O₂

tional composition (distribution curves), as well as the shape factor (Fig. 2).



A



B

Figure 2. A – Automatic analyzer Fiber Tester; B – micrograph of milk thistle cellulose fibers

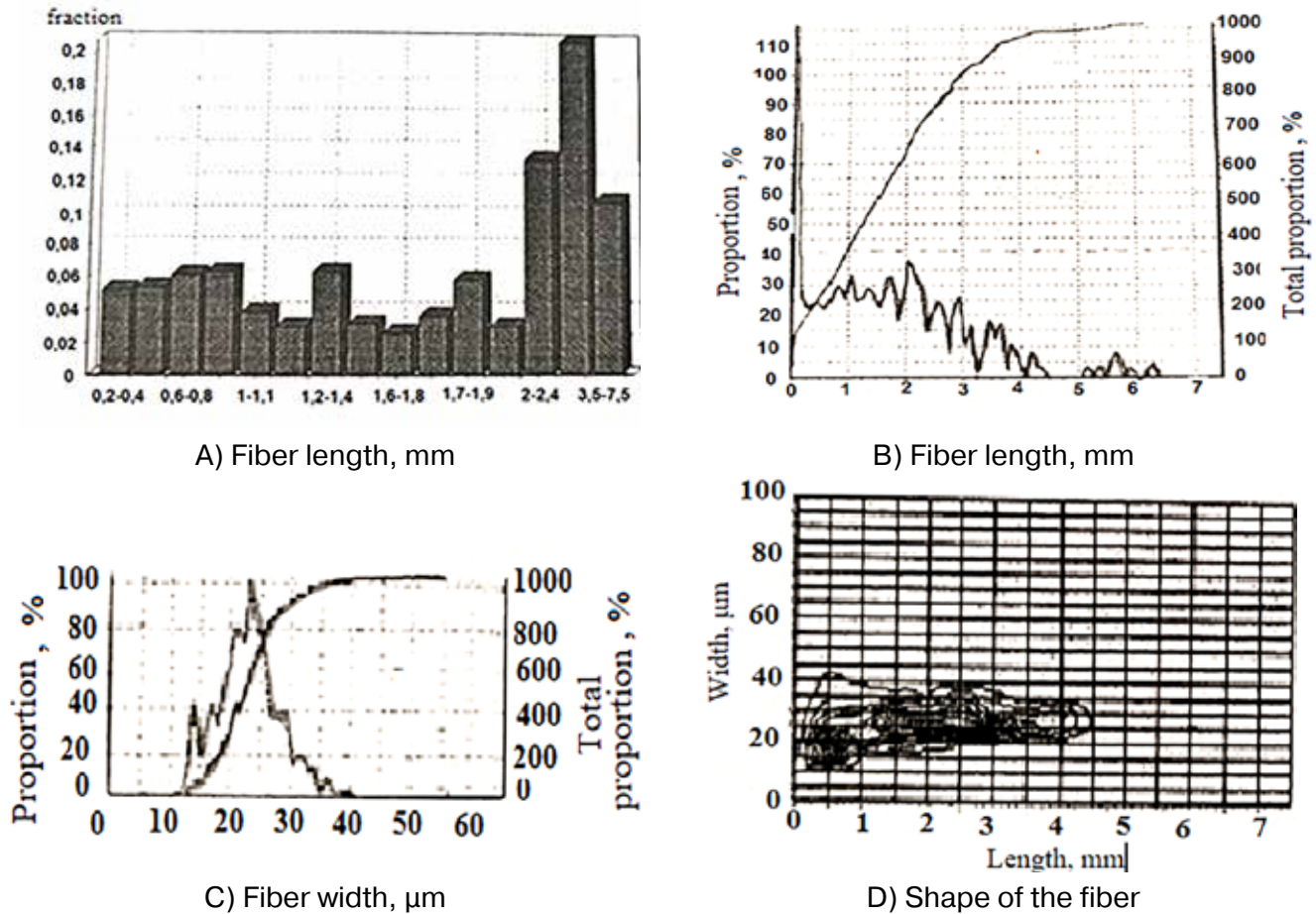


Figure 3. Fractional composition of milk thistle cellulose samples:
 a,b – fiber length; c – the width of the fibers; d – the shape of the fibers

Before determining the fiber length distribution curves in the pulp, using a microscope the type of fibers in samples was established. To do this, a fiber sample was diluted with water and applied on the glass surface, after water evaporation, the sizes and shapes of the fibers were photographed. They

are shown in the photo (Figure 2 b). The results of distribution curves averaged over the length of the fibers (integral curve 1) and percentage of the fraction (along the length of the differential curve; 2) are shown in (Figure 3). The results of determining the nature of the fibers are shown in (Table 1).

Table 1.– Structural-dimensional characteristics of cellulose

Variables	Weighted average value on the length	Weighted average value on the width
Average length	2.5 mm	1.038 mm
Average width	31.2 μm	22.2 μm
Shapes average factor	90.8%	80.6%

Cellulose fibers from milk thistle are characterized by a heterogeneous shape of various lengths (Fig. 3); the fraction of long fibers with a length of 3.5 to 7.5 mm reaches more than 0.2, when the

fraction of the rest does not exceed 0.08. The width of the fibers is in the range of 12–35 μm , then it is probably due to the fact that the stem consists of two different morphological parts – a flat flexible upper

layer (Fig. 4 a) and the middle of a loose white part (Fig. 4 b) in a ratio of approximately 90 : 10.

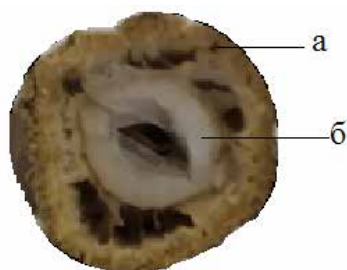


Figure 4. A cross section of the stem of a milk thistle

It is likely that small thin fibers are isolated from the middle part of the stem.

Sorption properties and IR-spectroscopy of milk thistle cellulose. After washing and drying, sorption properties of the resulting cellulose were determined, they are shown in (table 2).

From (table 2), it can be seen that the yield of cellulose is 26.0%, swelling in water is 187%, moisture sorption is about 11%, degree of polymerization is 870, ash content is 1.5% and whiteness is about 71%.

Study of IR-spectra of milk thistle cellulose. They are shown in (Figure 5). The spectra were obtained by pressing with KBr on an "IRAffinity-1" spectrophotometer [8–10].

Table 2 – Quality indicators of cellulose from milk thistle stems

yield of cellulose,%	Degree of swelling in water,%	* Moisture sorption,%	Degree of polymerization	Ash content,%	Whiteness,%
26.0	187	11.0	870	1.5	71.0

* Relative humidity – 65%

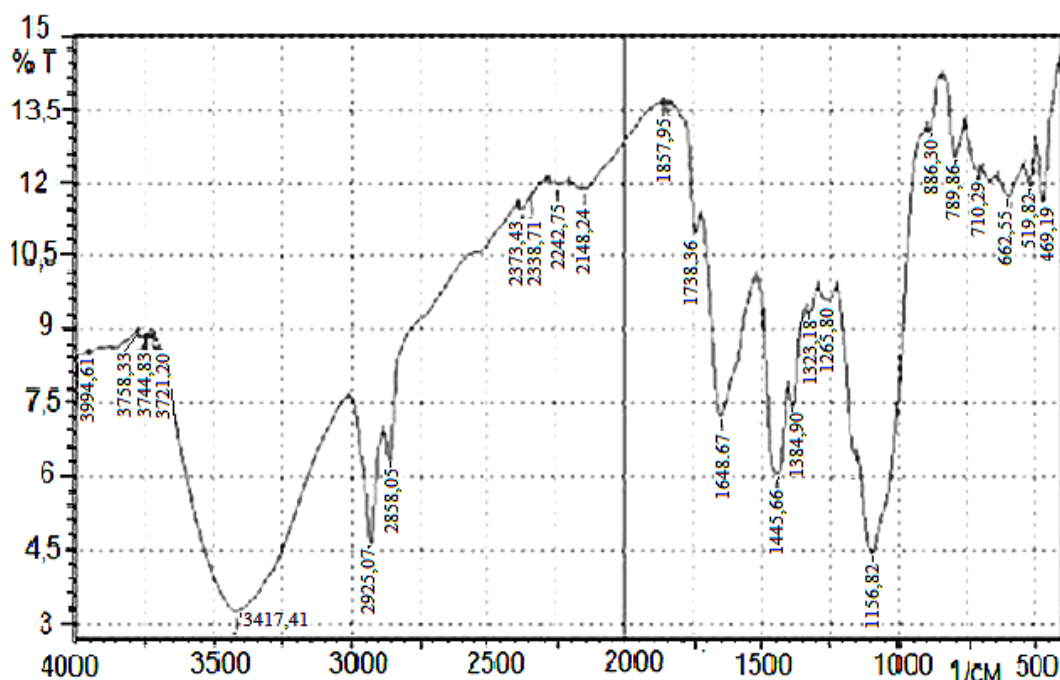


Figure 5. IR-spectra of milk thistle cellulose

Thus, the composition of milk thistle stems contains 26% cellulose with a degree of polymerization of 870, the average length and width of cellulose fibers is 2.5 mm and 22.2 μm , respectively. [11]

Analysis of the IR-spectra of cellulose shows that in the spectra in the range of 3250–3500 cm^{-1} , there is a broad blurry band with intense stretching vibrations caused by OH groups with a hydrogen bond.

Table 3.– Characteristic oscillations in the frequency of functional groups of milk thistle celluloses

Wave number, sm^{-1}	Group	Oscillation types	Intensity
3750	O-H (H bond is not formed)	Valence	Very high
3400	O-H (H bond is formed)	Valence	Broad and intensive
2900	- CH ₂	Valence	High
2260–2190	- C \equiv N	Valence	Average
1980	-C = C = C -	Asymm. valent	High
1465–1400	- CH ₂	Асимм. деформ.	
1400–1350	- CH ₃	Симм. деформ.	
1280–1100	- C-O-C-	Asymm. valent	Intensive
1075–1020	- C-O-C-	Asymm. valent	Intensive

Conclusion

A method has been developed for obtaining cellulose from the stems of medicinal plant – milk thistle. The optimal conditions, the average values of the length and width of the fibers, and their fractional

composition have been determined. Its sorption properties, degree of polymerization, ash content and other indicators have been studied. The chemical composition of the structures of the formed cellulose has been established by IR-spectroscopy.

References:

- Jahan S. M., Labooni A. P., Noori A., Quaiyyum M. A., Process For The Production Of Dissolving Pulp From Trema Orientalis (Nalita) By Prehydrolysis Kraft And Soda-Ethylenediamine (Eda) Process Jehat et al. (2008). "Dissoving pulp from Tremaorientalis" Bio Resources, – No. 3. 2008. – P. 816–828.
- Serkov A. T., Serkova L. A. Opredelenie nabuhaniya volokna v vode. [Determination of fiber swelling in water]. Him. volokna, – No. 5. 1974. – P. 70–71.
- GOST 12603–97. Bumaga I karton. Metod opredeleniya poverhnostnoy vpityivaemosti bumagi kapelnym sposobom. [Paper and cardboard. Method for determination of surface absorption of paper by drip method]. – Moscow, Standart inform Publ., 2005. – 8 p.
- Kocheva L. S., Brovarova O. V., Sekushin N. A., Karmanov A. P., Kuzmin D. V. Strukturno-himicheskaya harakteristika nedrevesnyih vidov tsellyulozyi. [Structural and chemical characteristics of non-wood pulp.]. Forest Journal, – No. 5. 2005. – P. 87–93.
- Konerinskiy N. N. Kompleksnaya himicheskaya pererabotka drevesinyi. [Complex chemical processing of wood]. Uchebnik dlya vuzov. Izdatelstvo AGTU, 2002. – 347 p.
- Autlov S. A., Bazarnova N. G., Kushnir E. Yu. Mikrokristallicheskaya tsellyuloza: struktura, svoystva, poluchenie i oblasti primeneniya. [Microcrystalline cellulose: structure, properties, production and applications]. Himiya rastitelnogo syirya, – No. 3. 2013. – P. 33–41.
- Zhbankov R. G. Infrakrasnyie spektryyi struktura uglevodov. [Infrared spectra and carbohydrate structure]. Science and technology, 1972. – 456 p.
- Moryiganov A. P. Perspektivnyie polimernyye materialyi dlya himiko-tekstilnogo proizvodstva [Promising polymeric materials for chemical and textile production]. Respublikanskiy him. Zhurnalob-va. im. D.I. Mendeleeva, – No. 1. 2002. – P. 58–66.
- Eshbo'taev A. G. IQ-practical application of the method spectroscopy. – Tashkent, 2014. – 34 p.

10. Jahan S. M., Rahman H., Rani S. P., Rahman M. Department of Chemistry, Eden Girls College, Dhaka. Ethylenediamine in alkaline cooking of jute stick for producing dissolving pulp Bangladesh. Res.,– No. 2. 2015.– P. 7–14.
11. Israel A. U., Obot I. B., Umoren S. A., Mkpennie Vand Asuquo J. E. Production of Cellulosic Polymers from Agricultural Wastes E-Journal of Chemistry,– Vol. 5.– No. 1. 2008.– P. 81–85.

<https://doi.org/10.29013/AJT-22-3.4-82-86>

*Kaypnazarov Turdibay Nzamatdinovich,
Junior Researcher S. Yu. Yunusov Institute,
of the Chemistry of plant Substances AS Uzbekistan*

*Uteniyazov Karimbay Kuanishbaevich,
Candidate of Chemical Sciences, Department
“Organic and inorganic chemistry”
Karakalpak State University,*

*Mirzaeva Makhira Risbaevna,
Candidate of Chemical Sciences, associate professor
of chemistry and chemical technology of Faculty
of Natural Science, Tourism and agricultural
technologies of Osh State University*

*Abdullayev Nasir Dzhalilovich,
S. Yu. Yunusov Institute of the Chemistry of Plant Substances
Candidate of Chemical Sciences, Academy of Sciences of Uzbekistan*

*Ramazonov Nurmurod Sheralievich,
S. Yu. Yunusov Institute of the Chemistry of Plant Substances
Doctor of Sciences, (in chemistry), Professor,
Head of the laboratory Chemistry of glycosides,
Academy of Sciences of Uzbekistan*

TRITERPENE GLYCOSIDES TRAGACANTHA STIPULOSA AND THEIR GENINS. STRUCTURE OF CYCLOSTIPULOSIDE D

Abstract. Three renowned compounds cycloartane series are highlighted from aboveground organs *Tragacantha stipulosa* Boriss– cyclosiversiosides E and F, cyclonifolioside B and a new glycoside – cyclostipuloside D that has structure 3-O- β -O – glucopyranoside, 6-O- β -D – xylopyranoside –20R, 24S – epoxycycloartan –3 β ,6 α , 16 β , 25 – tetraola. Structure of glycosides is determined based on NMR spectra ^1H and ^{13}C interpreted with 2M NMR – spectroscopy ^1H – ^1H COSY, ROESY, TOCSY, HSQC, HMBC.

Keywords: Cycloartans, cyclosiversiosides E and F, cyclonifolioside B, cyclostipuloside D.

Keeping research of cycloartan triterpenoids of *Tragacantha stipulosa* Boriss plant (сем. *Leguminosae*) [1; 2], renowned compounds of cyclosiversiosides E (1) и F (2) [3], cyclounifolioside B (3) [4] and new cycloartan glycoside cyclostipuloside D (4) had been extracted.

In IR spectrum compounds 4 has absorption band at 3035 cm^{-1} , cased CH_2 the cyclopropane ring group.

In the PMR spectrum (table) of cyclostipuloside D (4) as in specter of cyclostypuloside C [1] in strong field areas at 0.21 and 0.60 ppm we can see

that single – proton doublets splitted according to AB system ($^2J=3.5$ Hz) belonging to the protons of the methylene group of the cyclopropane ring.

Acid hydrolysis of compound **4** shows presence of glucose and xylose and cyclosiversigenin (**5**) In its composition as aglikon [3].

Except that as a result of hydrolysis we had connection **6** identical in its physico-chemical constants and spectral data with sievers and genin [5].

In NMR spectra 1H of siversigenina (**6**) there is single – proton signal at 5.25 ppm., applicable to olefin proton. There are not cyclopropane ring signals in NMR spectra 1H .

It is known that under the influence of acids 9,19-cyclopropane ring is disclosed with the formation of a double bond 9(11) [6].

In NMR spectra 1H compounds **4** at 4.85 (2H, d, $^3J=7.5$ Hz) and 4.92 (2H, d, $^3J=7.5$ Hz) we can see signals of two anomeric protons. Anomeric carbon atoms of two monosaccharide residues β -D- glucopyranoses and β -D- xylopyranoses resonates at 107.37 and 105.44 ppm. accordingly (table).

Signals of anomeric protons of monosaccharide residues in the PMR spectrum are revealed as doublets with $SSCC3J=7.5$ Hz, signifying β -configuration

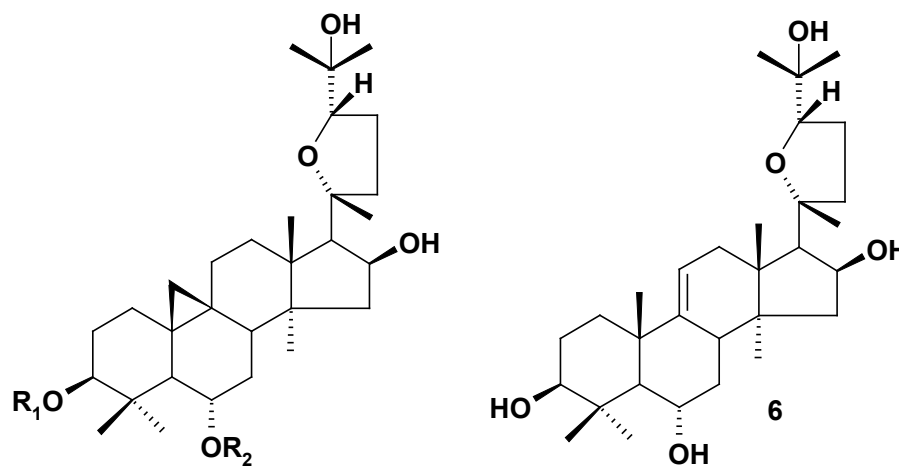
of glycoside bonds, C-1 conformation, and the pyranose form of both monosaccharide residues.

Based on results of comparative analysis of the values of chemical shifts of carbon atom signals in the ^{13}C NMR spectra of cyclostipuloside D (**4**) and cyclosiversigenin (**5**) found that the effect of glycosylation was subjected to hydroxyl groups at C-3 and C-6. Accordingly, it can be assumed that sugar residues are attached to genin via hydroxyl at C-3 and C-6.

Localization of carbohydrate residues was found by analyzing the spectra of COSY, TOCSY, HSQC and HMBC. The location of β -D-glucopyranose at C-3 aglycone is confirmed by the presence in the ROESY spectrum of correlation peaks of H-1 glucopyranose with H-3 and H-29 aglycone and in the spectrum of HMBC – correlation peak of H-1 glucopyranose and C-3 aglycone.

Based on the above data, it can be concluded that glucopyranose is attached to the hydroxyl group at C-3 and, consequently, xylopyranose is attached to the hydroxyl at C-6 of the aglycone.

Thus compound **4** us glycoside of cyclosiversigenin and has the structure of 3-O- β -D- glucopyranoside, 6-O- β -D- xylopyranoside –20R, 24S – epoxy-cycloartan – 3 β , 6 α , 16 β , 25 – tetraola.



1. $R_1=R_2=Xylp$;
2. $R_1=Xylp$, $R_2=Glcp$;
3. $R_1=Glcp(-2-Glcp)$, $R_2=H$;
4. $R_1=Glcp$, $R_2=Xylp$;
5. $R_1=R_2=H$.

Table 1. – Chemical shifts of signals in the NMR spectrum ^1H and ^{13}C of cyclosiversiosides E (1), F (2), cyclonifolioside B (3), cyclostipuloside D (4), cyclosiversigenine (5) and siversigenine (6) ($\text{C}_5\text{D}_5\text{N}$, O–TMC, δ , ppm.)

No	Compound						
	1[3]	2[3]	3 [4]	4		5[3]	6
	^{13}C	^{13}C	^{13}C	^1H	^{13}C	^{13}C	^{13}C
1	2	3	4	5	6	7	8
1	34.86	34.66	32.38	1.61; 1.26	31.97	35.16	33.24
2	26.68	29.03	30.62	2.37; 1.97	29.93	33.01	28.43
3	88.27	88.27	88.93	3.55	88.29	78.53	74.65
4	42.55	42.67	42.76	–	42.39	42.69	42.04
5	52.07	52.56	53.97	1.90	52.30	52.20	56.65
6	78.53	79.20	67.80	3.82	78.92	68.57	71.20
7	34.86	34.92	38.51	2.30; 1.87	34.38	39.08	39.94
8	44.11	46.24	46.81	1.96	45.49	47.50	47.58
9	21.15	21.13	21.02	–	20.83	21.19	142.13
10	28.38	28.89	29.42	–	28.63	30.11	45.18
11	26.24	26.49	26.28	1.83; 1.26	25.93	26.51	115.01
12	33.43	33.41	33.47	1.65; 1.57	33.15	33.65	36.97
13	45.15	45.08	45.10	–	44.82	45.28	45.18
14	46.13	46.24	46.19	–	46.00	46.41	42.04
15	45.18	45.75	46.66	2.36; 1.85	46.00	46.99	46.71
16	73.40	73.41	73.47	5.01	73.14	73.69	73.16
17	58.08	58.23	58.40	2.55	57.98	58.64	56.65
18	20.44	21.13	21.44	1.42	20.83	21.87	19.01
19	30.05	30.23	30.21	0.60; 0.21	28.77	31.70	23.64
20	87.27	87.27	87.28	–	87.00	87.48	86.98
21	27.10	28.60	28.59	1.30	28.63	27.38	27.86
22	31.89	32.24	34.96	3.12; 1.65	34.67	31.21	30.83
23	26.44	26.20	26.47	2.33; 2.06	26.20	26.69	26.83
24	81.60	81.69	81.75	3.90	81.44	81.93	81.43
25	71.23	71.29	71.28	–	71.00	71.48	72.48
26	28.13	28.21	28.21	1.58	27.92	28.44	29.10
27	28.57	28.60	27.15	1.30	26.81	28.81	29.75
28	28.38	27.10	20.16	0.96	19.60	29.67	32.04
29	16.64	16.65	28.87	2.02	28.34	16.38	17.90
30	20.44	19.87	16.59	1.37	16.37	20.47	19.81

Table 2.

1	2	3	4	5	6
	3-O- β -D-Xylp		3-O- β -D-Glcp(1 \rightarrow 2) Glcp	3-O- β -D-Glcp	
1	107.59	107.56	106.12	4.85	107.37
2	75.57	75.61	77.05	4.08	75.34
3	78.53	78.15	78.15	4.17	78.24
4	71.05	71.28	71.88	4.22	71.65

1	2	3	4	5	6
5	67.04	67.07	78.08	3.93	77.84
6			62.95	4.48;4.32	62.88
	6-O- β -D-Xylp	6-O- β -D-Glcp	\rightarrow 2) β -D-Glcp(1 \rightarrow 3) Agl	6-O- β -D-Xylp	
1	105.70	105.46	105.05	4.92	105.44
2	75.37	75.61	83.61	4.05	75.34
3	77.77	79.31	78.42	4.22	79.03
4	71.25	71.29	71.67	4.27	71.00
5	66.95	78.55	77.95	4.36;3.72	66.78
6		63.10	62.89		

EXPERIMENT

For general remarks and selection methods see [1].

Separation of the butanol fraction. When the column is eluted by the chloroform-methanol-water system (70:23:3) 27 mg of cyclosiversioside E had been isolated (**1**) (output 0,001%, here and further is given in terms of air-dry raw materials), 23 mg of cyclosiversioside F (**2**) (output 0,00092%), 17 mg of cyclonifolioside B (**3**) (output 0,00068%). With further elution by the same system we had 1.45 g of cyclostipuloside D (**4**) (output 0.058%).

Cyclosiversioside E (1). $C_{40}H_{66}O_{13}$, melt. temp. 257–258° C (from methanol).

PMR spectrum (C_5D_5N , m.d.): 0.15 and 0.60 (by 1H , d., $^3J=4.3$ Hz, 2H-19), 1.11, 1.31 ($2 \times CH_3$), 1.32, 1.40, 1.59, 1.94 (c., by 3H, tertiary methyl groups), 3.45 (1H, d.d., $J=11.7$ and 4.5 Hz, H-3), 3.80 (1H, d.d.d., $^3J=8.4$; 8.4 and 5.0 Hz, H-6), 2.52 (1H, d., $^3J=7.8$ Hz, H-17), 3.15 (2H, q, $^3J=11.0$ Hz, H-22), 3.90 (1H, d.d., $^3J=9.2$ и 5.2 Hz, H-24), 4.82 and 4.86 (by 1H, d., $^3J=7.3$ and 7.6 Hz accordingly H-1' и H-1'') [3].

Acid hydrolysis. 20 mg of cyclosiversioside E (**1**) 15 ml 0.5% methanol solution of sulfuric acid had been hydrolyzed at 70° C within 4 hours. Upon its cooling we fed 25 ml of water to reaction mix and methanol had been distilled. The precipitate had been filtered, flushed with water and, after drying, chromatographed on a column with silica gel. Eluting system chloroform-

methanol-water (70 : 23 : 3) we had 7 mg of cyclosiversigenin (**5**), $C_{30}H_{50}O_5$, melt. temp. 240–242° C (from methanol).

For NMR spectra ^{13}C refer to table.

Cyclosiversioside F (2). Provided 23 mg (0,00092%) of $C_{41}H_{68}O_{14}$, melt. temp. 260–261° C (from methanol).

PMR Spectrum: 0.21 and 0.60 (by 1H, d., $^3J=4.2$ and 4.1 Hz, 2H-19), 0.94, 1.30, 1.31, 1.39, 1.42, 1.60, 2.06 (s., by 3H, tertiary methyl groups), 2.53 (1H, d., $^3J=7.8$ Hz, H-17), 3.54 (1H, d.d., $^3J=11.7$ and 4.6 Hz, H-3), 3.81 (1H, d.d.d., $^3J=8.4$, 8.4 and 4.2 Hz, H-6), 3.15 (2H, q, $J=11.5$ Hz, H-22), 3.90 (1H, d.d., $^3J=9.1$ and 6.5 Hz, H-24), 5.05 (1H, q, $^3J=7.4$ Hz, H-16), 4.86 and 4.92 (by 1H, d., $^3J=7.4$ and 7.7 Hz accordingly H-1' и H-1'') [3].

Acid hydrolysis. 13 mg cyclosiversioside F (**2**) had been hydrolyzed according to above method and had 5 mg of cyclosiversigenin (**5**). In hydrolysate, paper chromatography comparison with authentic samples we revealed xylose and glucose.

For NMR spectra ^{13}C refer to table.

Cyclonifolioside B (3). Provided 17 mg (0,00068%) of $C_{42}H_{70}O_{15}$, melt. temp. 210–215° C (from methanol).

IR spectrum (KBr, ν , cm^{-1}): 2935 (cyclopropane group).

PMR spectrum (C_5D_5N , δ , ppm., J/ Hz): 1.51;1.11(H-1), 2.43;1.94(H-2), 3.58;(H-3), 1.66(H-5), 3.73(H-6), 1.82;1.64(H-7), .95(H-8), 1.90;1.21(H-11), 1.68;1.60(H-12), 2.13;1.77(H-15),

5.03;5.65(OH)(H-16), 2.54(H-17), 1.43(H-18), 0.56;0.22(H-19), 1.32(H-21), 3.10;1.68(H-22), 2.31;2.05(H-23), 3.89(H-24), 1.58(H-26), 1.30(H-27), 1.02(H-28), 1.96(H-29), 1.44(H-30), 5.42(H-1'-Glc(1→2) Glc), 4.13(H-2'), 4.24(H-3'), 4.30(H-4'), 3.95(H-5'), 4.50,4.44(H-6'), 4.99(H-1''-Glc(1→3) Agl), 4.30(H-2''), 4.33(H-3''), 4.18(H-4''), 3.88(H-5''), 4.53,4.37(H-6'') [3].

Acid hydrolysis. 5 mg of compound 3 had been hydrolyzed as its shown above. According to physical-chemical constants, and according to direct comparison with authentic samples, isolated compound 5 had been identified with cyclosiversigenin. In hydrolysate paper chromatography by comparison with authentic samples we had revealed xylose and glucose.

For NMR spectra ^{13}C refer to table.

Cyclostipuloside D (4). $\text{C}_{41}\text{H}_{68}\text{O}_{14}$, melt. temp. 252–254 °C (from methanol), $[\alpha]_D^{22} + 30.0 \pm 2^\circ$ (with 0.5; methanol).

IR spectrum (KBr, ν , cm^{-1}): 3391(OH), 3035 (cyclopropane group).

For NMR spectra ^1H and ^{13}C refer to table.

Acid hydrolysis. 30 mg of compound 4 had been hydrolyzed in 30 ml of 0.5% solution of methanol solution H_2SO_4 at 70 °C within 5 hours. Upon cooling we fed 30 ml of water, methanol had been

distilled, precipitates had been filtered, dried and chromatographed on silicagel, eluting with a chloroform-methanol system (15:1). Herewith we had 8 mg of compound 6, $\text{C}_{30}\text{H}_{50}\text{O}_5$, with melt. temp. 228–230 °C (ethyl acetate), IR spectrum (KBr, ν , cm^{-1}): :3420 (OH), 1648(C=C).

PMR spectrum of compound 6 (δ , ppm., $\text{C}_5\text{D}_5\text{N}$, TMS): 0.92, 1.06, 1.13, 1.30, 1.34, 1.53 ($6 \times \text{CH}_3$, s) и 1.46 ($2 \times \text{CH}_3$, s), 3.08 (2H, q, $^3\text{J}=11.9$ Hz, H-22), 2.49 (1H, d, $^3\text{J}=7.3$ Hz, H-17), 3.88 (1H, d, $^3\text{J}=8.9$ and 4.4 hz, H-24), 5.08 (1H, q, $\text{J}=6.6$ Hz, H-16), 5.25 (1H, 9(11)- double compound, s).

For NMR spectra ^{13}C refer to table.

Keeping elute the column with the same system, 12 mg of cyclosiversigenin has been isolated (5), $\text{C}_{30}\text{H}_{50}\text{O}_5$, with melt. temp. 239–240 °C (methanol), $[\alpha]_D^{22} + 49.0 \pm 2^\circ$ (from 1.37; methanol). IR spectrum (KBr, ν , cm^{-1}): 3396 (OH), 3035 (cyclopropane group).

Water solution has been heated within 3 hours, then neutralized with barium carbonate, residues had been removed, filtrate had been evaporated and chromatographed on paper in the butanol-pyridine-water system (6:4:3). Having compared with authentic samples we had revealed glucose and xylose.

References:

1. Кайпназаров Т. Н., Утениязов К. К., Качала В. В., Саатов З., Шашков А. С. Химия природ. соедин., 2002. – 228 с.
2. Кайпназаров Т. Н., Утениязов У. К. К., Саатов З. // Тритерпеновые гликозиды *Tragacantha stipulosa* и их генины. Структура циклостипулозида Е. // Химия природ. соедин. – (1). 2004. – С. 35–38.
3. Утениязов К. К., Саатов З., Абдуллаев Н. Д., Левкович М. Г. Химия природ.соедин., 1998. – 509 с.
4. Кучербаев К. Дж., Утениязов К. К., Качала В. В., Саатов З., Шашков А. С., Утениязов К. У., Халмуратов П. Химия природ. соедин., 2002. – 50 с.
5. Свечникова А. Н., Умарова Р. У., Горовиц М. Б., Сейтаниди К. Л., Рашкес Я. В., Ягудаев М. Р., Абубакиров Н. К. Химия природ.соедин., 1981. – 67 с.
6. Bentley H. R., Henry I. A., Irvine D. S., Spring F. S. J. Chem. Soc., 1953. – 3673 p.

<https://doi.org/10.29013/AJT-22-3.4-87-91>

Toshpulatov D. T.,

Mirzaev Sh.E.,

Nasimov A. M.,

Yakubov B. A.,

Samiev A. A.,

Tashpulatov Kh. Sh.,

Samarkand State University, Uzbekistan

SYNTHESIS OF [CO(BPY)(SCN)₄]²⁺ COMPLEX AND ITS PHOTOCHEMICAL PROPERTIES IN THE SOL-GEL MATRIX

Abstract. Synthesis of [Co(bpy)(SCN)₄]²⁺ complex carried and its photochemical properties studies explored in both organic solvent and tetraethoxysilane based sol-gel membrane. TEOS based sol-gel membrane shown suitable matrix and cobalt dye retain its photochemical properties inside the pores of membrane. Based on spectral changes in the sol-gel matrix, possible changes in molecular shape also discussed. Moreover, the sol-gel membrane confirm cobalt complex from photobleaching or degradation.

Keywords: complex, sol-gel matrix, TEOS, absorption, immobilization, MLCT band.

Introduction

Utilization of charge-transfer dye first commenced when Brian O'Regan and Michael Grätzel reported their revolutionary work in 1991 [1]. The general mechanisms for light-to-electrical power conversion in dye sensitizer solar cells as followed (i) light is absorbed by a sensitizer to form a molecular excited state; (ii) the excited state may inject an electron into the semiconductor thus causing charge separation; (iii) the oxidized sensitizer is "regenerated" by an external electron donor. Once the electron has performed useful work in the external circuit, it returns to a counter electrode where it reduces the oxidized electron donor. Hence the solar cell is termed "regenerative" as all oxidation chemistry at the dye-sensitized electrode is reversed at a dark counter electrode such that no net chemistry occurs.

It is known that Ru(II) polypyridines or Ru(II) complexes have been used as dye sensitizer widely because of remarkable advantages as: (i) ease of preparation; (ii) reversible electrochemical behav-

ior; (iii) light absorption in the visible spectral region; (iv) long-lived electronically excited states; (v) intense luminescence. These features made them perfect choice for such systems.

Despite such favored features, there are obstacles related to Ru which is "well-known" being high cost (32% cheaper than gold), low abundant (78th most abundant element!) and toxic. Hereof one could concern to other alternatives than Ru(II) polypyridines. Hereof one could concern to other alternatives than Ru(II) polypyridines. One of alternative is copper(I) complexes which were found a possible solution for that issue [2–6]. Being a tetrahedrally symmetric, copper(I) shown very promising results with both homoleptic and heteroleptic ligands. Other preferred complexes were found to be cobalt(II/III) complexes [7–12]. If one compare the structure of copper(I) and cobalt(II/III) complexes, the former have unique tetrahedral (sometimes distorted) shape while cobalt complexes possess octahedral shape (Figure 1).

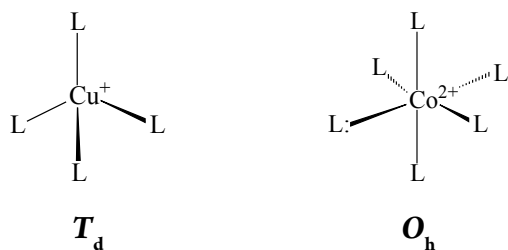


Figure 1. Different coordination geometry of Cu^+ and Co^{2+} complexes

In order to be practically useful, it is often required to immobilize molecule of interest in solid matrices. A number of papers dedicated to these issue ranging from composites to sol-gel membrane [13–16]. Immobilization not only maintains mechanical stability but also may shape of the photochemical properties of the dopant. Dye doped solid materials also found their application in catalysis and solar energy conversion systems [14–17]. The sol-gel technology possesses the following superiority: (i) the prepared nanoparticles have good uniformity (particle size distribution) and high purity, (ii) it is energy saving (because of temperature condition) and (iii) it can be used to prepare wide range of materials as coatings, fibers, and composite materials.

In this article we propose results of synthesis and immobilization of cobalt complex with unique photochemical properties. In order to find suitable environment for the synthesized dye, several matrices have been examined and the most favorable one is proposed.

Experimental

Materials and methods

Tetraethoxysilane (TEOS) was purchased from Haihang Industry Co., Ltd (PRC). All solvents: ethanol (EtOH), methanol (MetOH), acetonitrile (CAN), tetrahydrofurane (THF), dimethylformamide (DMF), hexane (C_6H_{14}), nitrobenzene (CH_3NO_2), acetone (CH_3COCH_3), benzene (C_6H_6), octane (C_8H_{18}), toluene (C_7H_8) were analytical grade and used without any further purification. Cobalt(II) chloride hexahydrate ($\text{CoCl}_2 \cdot 6\text{H}_2\text{O}$), 2,2-bipyridine ($\text{C}_{10}\text{H}_8\text{N}_2$), ammonium thiocyanate (NH_4SCN), hy-

drochloric acid (HCl) and nitric acid (HNO_3) were chemical pure and used as received. All buffers and solutions prepared using chemical pure grade reactants and doubly distilled water used as solvent.

Synthesis of $[\text{Co}(\text{bpy})(\text{SCN})_4]^{2+}$

In order to obtain desired complex, 1 eqn. of $\text{CoCl}_2 \cdot 6\text{H}_2\text{O}$, 1 eqn. of bipyridine and 4 eqn. of NH_4SCN weighted. Namely, tuzidan 2,38 grams of $\text{CoCl}_2 \cdot 6\text{H}_2\text{O}$, 1,56 grams bipyridine, 3,05 grams of NH_4SCN mixed in 96% ethanol and completely dissolved. The reaction mixture was refluxed at 70°C and stirred at 600 RPM for 3 hours. The temperature was increased gradually from the room temperature to 70°C . After 3 hours, the solution was cooled 12 hours down to the room temperature and precipitation occurred. The precipitation was vacuum filtered and decanted with 96% ethanol for several times until to obtain pure compound. The purified precipitate was kept overnight at 80°C in the drying oven (Memmert, Germany).

Immobilization of cobalt dye in sol-gel membrane

After several experiments on the condition of an optimal sol-gel cocktail content, the following ratio of components was chosen: TEOS, H_2O , $\text{C}_2\text{H}_5\text{OH}$: HCl 1: 4: 4: 0,15 respectively in order to complete the hydrolysis reaction, the sol mixture was stirred for 30 minutes at the room temperature. Consequently cobalt complex solution in DMF was added dropwise and vigorously stirred another 3 hours. Solution of sol then remained for 24 hours in the ambient temperature for aging. Microscope slides were taken and cut into 0.6×4 cm pieces. All glasses were activated in the aqueous solution of nitric acid for 1 hour and rinsed with ethanol and copious amount of water before dip coating process. Coated slides were kept another 24 hours in the ambient temperature and dried at 70°C overnight.

Spectroscopic studies of prepared membranes

The surface of the films was investigated using the light microscope Optika (Germany). UV-vis spec-

trophotometer EMC-30PC-UV (EMC Labs, Germany) was used to record the absorption spectra of the films. Elemental analysis was carried out on ED X-ray fluorescence spectrometer NEXDE (Rigaku, United States).

Results and discussion

Figure 2 presents electronic absorption spectra of $[\text{Co}(\text{bpy})(\text{SCN})_4]^{2+}$ in DMF. The absorption maximum is seen at 479 nm and the complex appears lilac. The spectrum considerably different from the spectrum of aqua complex of Co^{2+} where the absorption maximum is located around 550 nm. As cobalt(II) has d^7 configuration, the expected num-

ber of absorption bands should be three. Although both $d-d$ transitions are forbidden in centrosymmetric complexes (e.g. $[\text{Co}(\text{H}_2\text{O})_6]^{2+}$) because of the Laporte and the parity rules, such complexes possess low molar extinction coefficient meaning that less utilize the visual light (from the sun). Altering the molecular symmetry from centrosymmetric (molecule possessing center of inversion) to non-centrosymmetric leaves only the Laporte rule effective (Fig. 4). Moreover, planar and linear ligands as bpy and SCN respectively leads to form more rigid molecule and may cause to the violation of spin-forbidden rules.

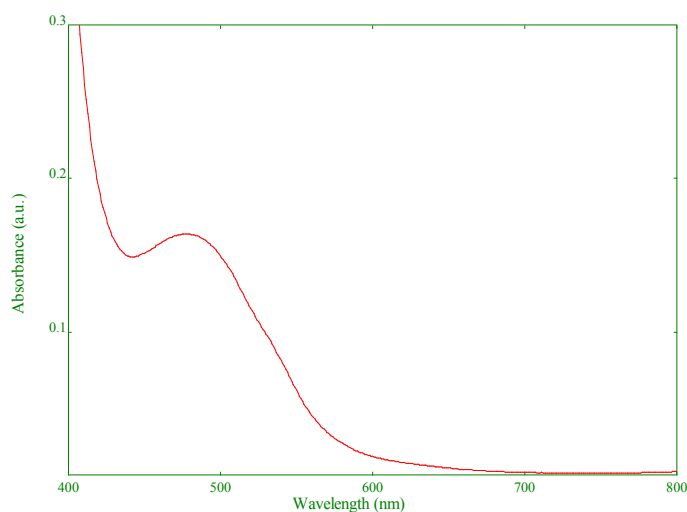


Figure 2. Absorption spectrum of $[\text{Co}(\text{bpy})(\text{SCN})_4]^{2+}$ in DMF

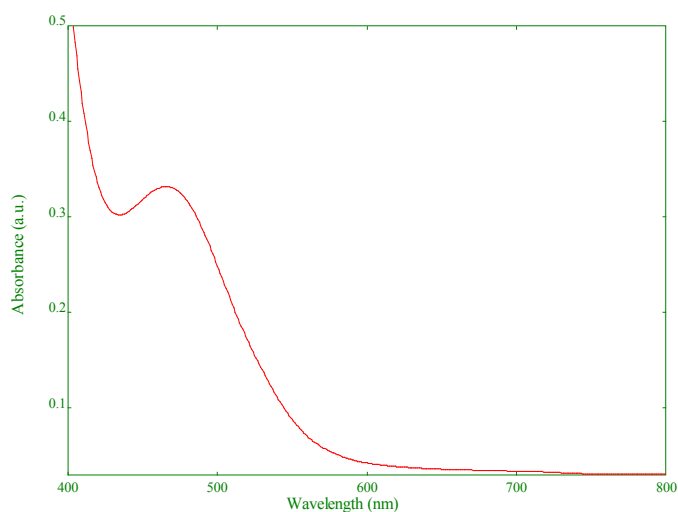


Figure 3. Absorption spectrum of $[\text{Co}(\text{bpy})(\text{SCN})_4]^{2+}$ in the sol-gel matrix

Figure 3 shows the absorption spectrum of $[\text{Co}(\text{bpy})(\text{SCN})_4]^{2+}$ in TEOS based sol-gel matrix. It can be seen the intense band at 479 nm blue-shifts by 14 nm upon the complex immobilization. This behavior was also observed elsewhere for Ru complexes in sol-gel matrix. Changing the molecular environment from less viscous media to the phase where free rotation is limited also initiate not only the chromic shifts in absorption spectra, but also in emission spectra. Hereof, we concluded that transferring the complex from the solution to the rigid membrane pores substantially improves molar absorptivity.

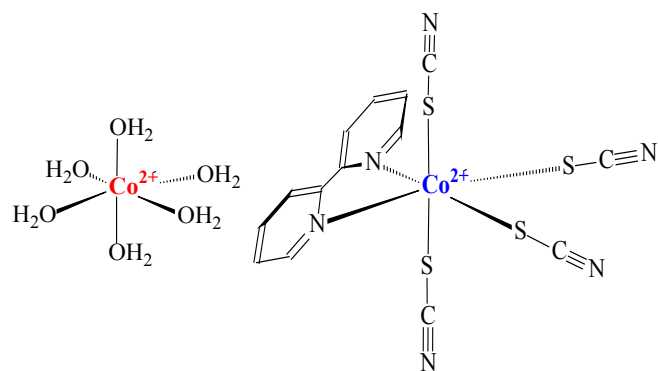


Figure 4. Centrosymmetric $[\text{Co}(\text{H}_2\text{O})_6]^{2+}$ and non-centrosymmetric $[\text{Co}(\text{bpy})(\text{SCN})_4]^{2+}$ molecules

Results of EDXRF analysis is shown in Fig. 5a and 5b. analysis shown that the dye doped matrix is consisted 99.8% (mass) SiO_2 and 0.156% (mass) Co. converting the elemental cobalt to $[\text{Co}(\text{bpy})(\text{SCN})_4]^{2+}$ gave a good consistency between the

initial and final composition of the immobilization process. Experiments on leaching the dye from the matrix also shown satisfying results and they confirmed that the sol-gel matrix is an excellent choice for further application.

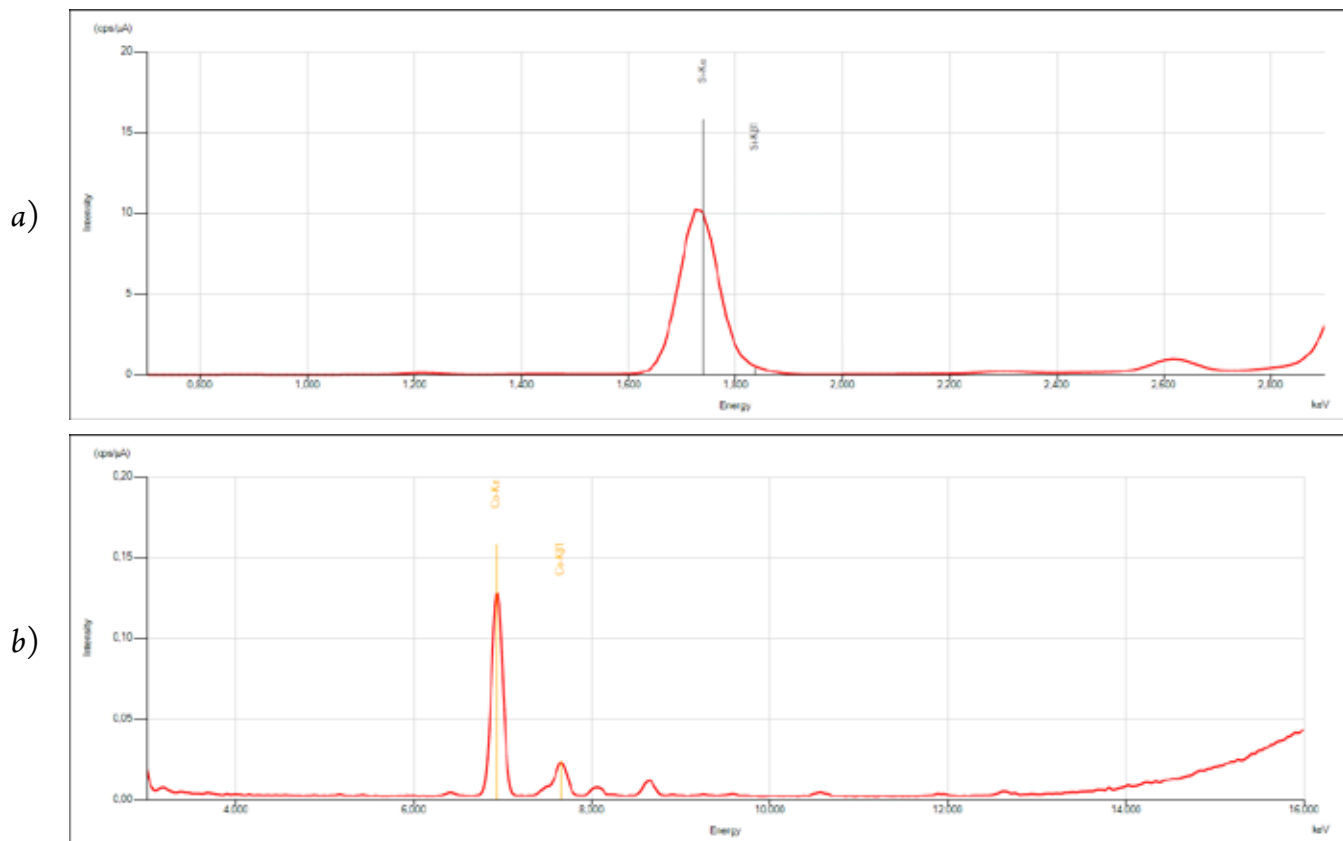


Figure 5. a) EDXRF spectrum of low Z-region; b) mid Z-region of the $[\text{Co}(\text{bpy})(\text{SCN})_4]^{2+}$ in TEOS based sol-gel matrix

Conclusions

$[\text{Co}(\text{bpy})(\text{SCN})_4]^{2+}$ complex has been synthesized and its photochemical properties were studied. The synthesized complex was entrapped in silicate xerogels produced by the sol-gel route.

Spectral evaluation of complex both in DMF and solid sol-gel matrix was discussed. Studies shown that the sol-gel matrix is suitable environment for the complex and the dopant retains its photochemical properties.

References:

1. Oregan B. and Gratzel M. A low-cost, high-efficiency solar-cell based on dye-sensitized colloidal TiO_2 films. *Nature* – 353. 1991.– P. 737–740.
2. Vorontsov I. I., et al. Capturing and analyzing the excited-state structure of a Cu(I) phenanthroline complex by time-resolved diffraction and theoretical calculations. *Journal of the American Chemical Society* – 131(18). 2009.– P. 6566–6573.
3. Iwamura M., et al. Coherent nuclear dynamics in ultrafast photoinduced structural change of bis(diimine) copper(I) complex. *Journal of the American Chemical Society*,– 133(20). 2011.– P. 7728–7736.

4. Siddique Z. A. et al. Structure-dependent photophysical properties of singlet and triplet metal-to-ligand charge transfer states in copper(I) bis(diimine) compounds. *Inorganic Chemistry*.– 42(20). 2003.– P. 6366–6378.
5. Lazorski M. S., Gest R. H., and Elliott C. M. Photoinduced multistep charge separation in a heteroleptic Cu(I) Bis(phenanthroline)-Based Donor-Chromophore-acceptor triad. *Journal of the American Chemical Society* – 134(42). 2012.– P. 17466–17469.
6. Lavie-Cambot A., et al. Improving the photophysical properties of copper(I) bis(phenanthroline) complexes. *Coordination Chemistry Reviews*,– 252(23–24). 2008.– P. 2572–2584.
7. Jiajia Gaoa, Govind Kumar Prajapatia, Yan Haoa, Lars Klooa. Exploring Lewis-base effects to improve the efficiency of [Co(bpy)₃]^{2+/3+}-mediated dye-sensitized solar cells. *ACS Appl. Energy Mater.*– 3, 6. 2020.– P. 5705–5711.
8. Yan Li, Hong Wang, Quanyou Feng, Gang Zhou and Zhong-Sheng Wang. Reduced graphene oxide–TaON composite as a high-performance counter electrode for Co(bpy)₃^{3+/2+}-mediated dye-sensitized solar cells. *ACS Appl. Mater. Interfaces* – 5, 16. 2013.– P. 8217–8224.
9. Jung-Min Ji, Haoran Zhou, Yu Kyung Eom, Chul Hoon Kim, Hwan Kyu Kim. 14.2% Efficiency dye-sensitized solar cells by co-sensitizing novel thieno[3,2-b] indole-based organic dyes with a promising porphyrin sensitizer. *Advanced Energy Materials*. 2020.– 124 p.
10. Hui-Seon Kim. A Soo-Byung Ko, a In-Hyuk Janga and Nam-Gyu Park. Improvement of mass transport of the [Co(bpy)₃]^{II/III} redox couple by controlling nanostructure of TiO₂ films in dye-sensitized solar cells. *Chem. Commun.*,– 47. 2011.– P. 12637–12639.
11. Thomas W. Hamann. The end of iodide? Cobalt complex redox shuttles in DSSCs. *Dalton Transactions* – 41. 2011.– P. 3111–3115.
12. Sun-Min Jung, In Taek Choi, Kimin Lim, Jaejung Ko, Jae Cheon Kim, Jae-Joon Lee, Myung Jong Ju, Hwan Kyu Kim, and Jong-Beom Baek. B-doped graphene as an electrochemically superior metal-free cathode material as compared to Pt over a Co(II)/Co(III) electrolyte for dye-sensitized solar cell. *Chemistry of Materials* – 26, 11.– P. 3586–3591.
13. Xuping Sun, Yan Du, Shaojun Dong, and Erkang Wang. Method for effective immobilization of Ru(bpy)₃²⁺ on an electrode surface for solid-state electrochemiluminescence detection. *Analytical Chemistry* – 77, 24. 2005.– P. 8166–8169.
14. Yali Li, Xiurong Yangb, Fan Yangb, Yingping Wangc, Peihua Zhengc, Xiaoxu Liuc Effective immobilization of Ru(bpy)₃²⁺ by functional composite phosphomolybdic acid anion on an electrode surface for solid-state electrochemiluminescence to sensitive determination of NADH. *Electrochimica Acta* – 66.– P. 188–192.
15. Yan Xiong, Jing Xu, Jian-Wei Wang and Ya-Feng Guan. A fiber-optic evanescent wave sensor for dissolved oxygen detection based on novel hybrid fluorinated xerogels immobilized with [Ru(bpy)₃]²⁺. *Analytical and Bioanalytical Chemistry* – 394. 2009.– P. 919–923.
16. Krzysztof Maruszewski, Marek Jasiorski, Małgorzata Salamon, Wiesław Stre. Physicochemical properties of Ru(bpy)₃²⁺ entrapped in silicate bulks and fiber thin films prepared by the sol-gel method. *Chemical Physics Letters* – 314. 1999.– P. 83–90.
17. Senthilkumaara S., Porkodia K., Vidyalakshmi R. Photodegradation of a textile dye catalyzed by sol-gel derived nanocrystalline TiO₂ via ultrasonic irradiation. *Journal of Photochemistry and Photobiology A: Chemistry* – 170.– P. 225–23.

<https://doi.org/10.29013/AJT-22-3.4-92-99>

Fayzullayev Normurot I.,
DSc, Professor, Department of Polymer Chemistry
and Chemical Technology, Samarkand State University,
University Samarkand, Uzbekistan
Kholmirezayeva Khilola N.,
Doctoral student Ph.D., Department of Physical
and Colloid Chemistry, Samarkand State University,
University Samarkand, Uzbekistan

DEVELOPMENT OF TECHNOLOGY FOR MAKING NANO SORBENT FROM WOOD PROCESSING WASTE

Abstract. 100–120 g of the test drug is placed on a smooth, clean white surface and examined by gently stirring in natural light. 20–30 g of the test drug is poured into a clean porcelain container and the odor is determined organoleptically. If it is necessary to enhance the odor, the porcelain dish is covered with a bottle, along with the medicine inside, and is placed in a water bath heated to boiling and heated for 5–7 minutes, after which the odor of the drug under test was detected again. **SEM** of **Phenom G2 pro** model was used to study the surface structure of the objects studied in the study, this allows images up to 25 nm in magnification in the range of 80 x to 45000 x. Grinding rate and granule size were evaluated and controlled using **ANALYSETTE22 MicroTec plus** laser diffraction particle size analyzer. This analyzer allows the determination of granulometric (mechanical) content in the range from 80 nm to 2000 μm . A **SARTORIUS MA 150** moisture meter was used to determine the moisture content of the samples studied in the study. The samples were dried to a constant mass at a temperature of $103 \pm 2^\circ\text{C}$.

Keywords: hydrolytic lignin, porosity, analyzer, filtrate, centrifuge, mycotoxin.

Introduction

To date, machinery and technology, including pharmaceuticals, petroleum, cosmetology, oil and gas refining industries, as well as high selectivity in various sectors of the economy, the demand for effective environmentally safe adsorbents is increasing [1–5]. Preparation of adsorbents that meet such requirements, the study of colloidal chemical properties of adsorbents. The study of the mechanism of adsorption processes in them poses new challenges to new scientific approaches, as well as to scientists and researchers in the field.

The influence of various factors on the synthesis of nanocarbon from the walnut peel, apricot kernel,

methane, natural gas, and propane-butane fractions was studied and the texture and sorption characteristics of the obtained nanocarbon were examined. In addition, the effect of various factors on the rate of formation of nanocarbon obtained from methane, natural gas, and propane-butane fractions was studied and optimal conditions for the process were proposed [6–10].

Currently, activated charcoal is used in the food industry, medicine, and other fields for the treatment of gases and effluents, and other water [11–12]. The use of charcoal, for example, to purify water, allows drinking water to meet basic requirements [13–16], and the use of them as electrodes of supercapaci-

tors allows the creation of inexpensive rechargeable electrochemical devices with high power and energy properties [17–19]. Therefore, the study of the raw material base for obtaining activated charcoal and improving its physical and technical characteristics is of particular interest [20]. Its black ash, obtained by burning walnut shells in the absence of oxygen, has sorption activity [21].

Experimental part

100–120 g of the test drug is placed on a smooth, clean white surface and examined by gently stirring in natural light. 20–30 g of the test drug is poured into a clean porcelain container and the odor is determined organoleptically. If it is necessary to enhance the odor, the porcelain dish is covered with a bottle, along with the medicine inside, and is placed in a water bath heated to boiling and heated for 5–7 minutes, after which the odor of the drug under test was detected again. **SEM of Phenom G2 pro** model was used to study the surface structure of the objects studied in the study, this allows images up to 25 nm in magnification in the range of 80x to 45000x.

Methods for determining the granulometric content. Grinding rate and granule size were evaluated and controlled using **ANALYSETTE 22 MicroTec plus** laser diffraction particle size analyzer.



Figure 1. ANALYSETTE 22 MicroTec plus: a unit for determining the unit of measurement for dry and wet samples using a laser

This analyzer allows the determination of granulometric (mechanical) content in the range from 80 nm to 2000 μm . A dispersion block in a liquid medium is used to prepare a sample of hydrolytic

lignin for analysis. In determining the granulometric composition of the finished product form of a complex nano sorbent (micro granules), the preparation of the sample is carried out in a dry dispersion block.

A **SARTORIUS MA 150** moisture meter was used to determine the moisture content of the samples studied in the study.



Figure 2. SARTORIUS MA 150: Moisture measuring device

Robust design, along with low space requirements and convenient operation, is key features of these analyzers. Fully automatic drying of the sample until a constant weight is achieved eliminates the need to program the endpoint removal parameter. It is possible to weigh from 1 mg to 150 g of product. The operating temperature is in the range of 40 $^{\circ}\text{C}$ to 220 $^{\circ}\text{C}$ at a temperature acceptable. The samples were dried to a constant mass at a temperature of $103 \pm 2^{\circ}\text{C}$.

Method for determining the ash content of raw materials. The porcelain crucible is fired in a muffle furnace to a constant mass, cooled in a desiccator, and weighed.

A portion of lignin weighing 2–3 g is weighed, the result of weighing is written with the accuracy of the third fraction in grams, and is placed in the crucible. The sample crucible is placed in a hood over an electric stove, burned without a flame, then baked in a muffle furnace at a temperature of 800–850 $^{\circ}\text{C}$ for 2–3 hours. After roasting, the crucible is cooled in the air for 5 minutes, then cooled in a desiccator, after which

it is pulled. Bake for another 30 minutes until the mass is less than 0.001 g. The mass fraction of ash (X_1) as a percentage is calculated according to formula 1:

$$X_1 = \frac{m_1}{m_1 \cdot \left(1 - \frac{W}{100}\right)} \cdot 100 \quad (1)$$

where, m is the mass before drying, g,

m_1 – mass after drying, g,

W – humidity of the sample under study, %.

The result of the analysis is taken as the arithmetic mean of two parallel determinations, the allowable differences between them should not exceed 0.01%. A test sample of 20 g of hydrolytic lignin is placed in a beaker with a capacity of 600 cm³ and weighed to the second fraction. Add 100 cm³ of hot distilled water, mix well with a glass rod and leave for 5–10 minutes. The precipitated solution is filtered under a vacuum in a porcelain funnel through a paper filter.

Another 100 cm³ of hot distilled water is added to the sediment of the sample being tested in the beaker, mixed, and filtered under vacuum. This wash is repeated 3–4 times (according to the methyl orange indicator) until the water is neutral. The volume of washing water is transferred to a measuring tube with a volume of 500 cm³, the volume is adjusted to the mark with distilled water and mixed. 25 cm³ of the resulting solution is titrated with 0.1M sodium hydroxide solution in the presence of methyl orange indicator.

The mass fraction of acids (in terms of sulfuric acid) is calculated as a percentage according to formula 2.

$$X_2 = \frac{V \cdot K \cdot T \cdot V_2}{V_1 \cdot m \cdot \left(1 - \frac{W}{100}\right)} \cdot 100 \quad (2)$$

Here, V is the volume of 0.1M NaOH solution used for titration, cm³

K – correction factor for the titer of 0.1 M NaOH solution

0.0049 – a mass of sulfuric acid per 1 cm³ of solution with a net concentration of 0.1 mol/dm³, g

V_1 – the volume of washing water obtained for titration, cm³

V_2 – total volume of washing water, cm³

m – the mass of sample, g

W – humidity of the detected sample, %

The result of the analysis is taken as the arithmetic mean of two parallel determinations, the allowable differences between them should not exceed 0.01%.

Approximately 10 g of the analyzed lignin sample is weighed (by absolute dry matter) (the result of weighing in grams is written to the second decimal place), into a flask, add 100 cm³ of water, and boil for 3 minutes. Stop the flask with the return current capacitor. The substances in the tube are then quickly filtered under vacuum through a paper filter, and the first parts of the filtrate are discarded. The filtrate is cooled and its pH is determined. A **pH-150 MI** millivoltmeter was used to determine the pH. The result of the analysis is taken as the arithmetic mean of the results of two parallel determinations, the absolute discrepancy between them does not exceed the allowable difference of 0.2.

A portion of the air-dry lignin (approximately 2 g) is poured into a 250 ml conical flask and filled with 100 ml of distilled water. A return flow condenser is attached to the flask and placed in a boiling water bath and the water level in the bath should be slightly higher than the water level in the tube. Extraction is carried out for 3 hours. The lignin suspension is then filtered by vacuum in a porous glass filter dried to a constant mass and washes the lignin from the tube to the filter with hot water. The lignin filter is dried and weighed to a constant mass in an oven at $103 \pm 2^\circ\text{C}$ at a constant weight. The mass fraction of water-soluble substances ($\mathcal{E}_{p.s.}$) and the fraction of absolute dry lignin are calculated according to formula 3.

$$\mathcal{E}_{p.s.} = \frac{m_2 - (m - m_1)}{m_2} \cdot 100 \quad (3)$$

Here, m is the filter mass with lignin residue, g

m_1 – empty filter mass, g

m_2 – absolute dry lignin sample mass, g.

The result of the analysis is taken as the arithmetic mean of two parallel determinations, the allowable differences between them should not exceed 0.02%.

A portion (2–3 g) of air-drying lignin is poured into a liner wrapped in filter paper. A lignin sleeve is placed in the nozzle for removal and the level of lignin in the sleeve should be 1 ... 1.5 cm below the level of the siphon pipe. Pour 200 ml of solvent (alcohol: benzene mixture in a 1 : 2 ratio) into the flask. The instrument for extraction is collected and placed in a water bath. The bath temperature is set at 5–10 °C above the boiling point of the solvent. Water is fed to the refrigerator at a rate that ensures complete condensation of the solvent vapors.

Extraction is continued for 4–5 hours, after which the apparatus is removed from the bath, and the nozzle is separated from the tube and the refrigerator. The extract is poured into a dried flask to a constant mass (pour into a flask dried to constant weight) and the solvent is distilled in a water bath. The tube with cubic residues is dried in an oven at 103 ± 2 °C to a constant mass and weighed.

The mass fraction of soluble substances in organic solvents ($\vartheta_{o.p.}$) is the proportion of absolutely dry lignin calculated by formula 4.

$$\vartheta_{o.p.} = \frac{m - m_1}{m_2} \cdot 100 \quad (4)$$

Where m is the mass of the flask together with the extract substance, g

m_1 – the mass of empty tube, g;

m_2 – the mass of absolutely dry lignin, g.

The result of the analysis is taken as the arithmetic mean of two parallel determinations, the allowable differences between them should not exceed 0.2%.

The device is assembled for testing, the general view of which is shown in Figure 13.

When a vacuum network is available, pump 1 is removed and the rest of the system is connected to the vacuum line. Clamp 3 serves to introduce air into the evacuation system and uses a front vacuum pump. It also serves to regulate the vacuum measured with a pressure gauge 4. When operating with a water flow pump, the vacuum is regulated by changing the water flow rate with a water tap. Tube 2 acts as a buffer tank. Valve 5 is used to shut off tube 7.

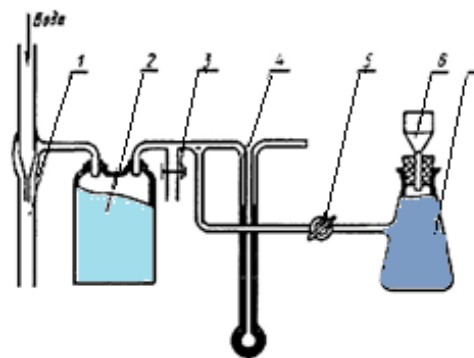


Figure 3. Device diagram for detecting open porosity: 1 – water flow pump, 2 – double-necked tube, 3 – clamp, 4 – pressure gauge, 5 – connecting tap, 6 – funnel, 7 – suction tube

The test sample is averaged and reduced to a volume of about 25 cm³, is dried in a layer of not more than 5 mm for 1 h (105 ± 2) °C. 10 ± 0.1 cm³ of the dried sample is poured into the measuring cylinder with a slight shaking, transferred to a pre-weighed weighing bottle, closed with a lid and weighed with an error of not more than 0.01 g. The sample is poured through a funnel into a conical flask, 100 cm³ of water is poured into it and its level is recorded.

The contents of the flask are boiled for (15 ± 1) minutes, after which cold distilled water is added to the initial volume and the outer surface of the tube is cooled to room temperature with tap water. A paper filter is placed on the bottom of funnel 6 and moistened with water. When valve 5 is closed, a vacuum (60 ± 5) mm of mercury is generated in the system, then a vacuum is created in the tube by turning the tap 5, after which the tube is turned off again. During assimilation of the filter, care must be taken to insure that it is firmly attached to the bottom of the funnel and that the connecting hoses are not twisted. The contents of the conical flask are poured into the suction funnel without loss and the sample is flattened with a spatula on the filter surface. Turn the tap to (60 ± 5) mmHg (mercury column) maintaining the vacuum, and assimilation begins. The stopwatch was started at the same time. After 3 minutes, the test sample is transferred to a weighing bottle before weighing. The rest of the sample

in the filter is removed with a spatula, transferred to the vial without loss, and closed with a lid. The wet sample weighing bottle is weighed with an error of not more than 0.01 g no later than 3 minutes after the end of suction. The tap is turned off, the filter is removed from the funnel, water is poured from the tube and the device is prepared for the next test. V_{Σ} – the total volume of pores (cm^3/g) is calculated using formula 5.

$$V_{\Sigma} = \frac{m_1 - m}{m \cdot \rho} \cdot 100 \quad (5)$$

Here, m is the dry mass, g,

m_1 – wet mass, g;

ρ – water density, g/cm^3 .

The density of water is calculated as $1 \text{ g}/\text{cm}^3$ for any room temperature up to 35°C . The test result is taken as the arithmetic mean of two parallel determinations, the allowable differences between them should not exceed 4% of the smaller value.

The method of sorption-desorption of molecular nitrogen allows the dead analysis of micro- and meso cytes, their size distribution, and determination of surface area.



Figure 4. ASAP 2020 Micromeritics: a device for studying the nano-porous structure of hydrolytic lignin

To study the nano-porous structure of hydrolytic lignin, we analyzed the surface area using physical sorption methods **ASAP 2020 Micromeritics** (USA) and we used an automated system for to study of the porous structure of materials. This system allows to determination of the surface area, as well as a complete analysis of micro- and meso cytes, distributing their volume. Hole diameter measurements range from 0.35 to 100 nm.

Build a calibration graph. Comparative solutions are prepared to construct the calibration curve. To do this, 0.5 is added to 10 measuring tubes, each with a capacity of 50 cm^3 ; 1,0; 1,5; 2,0; 3,0; 4,0; 5,0; 6,0; 7,0; 8,0 cm^3 of indicator solution ($1500 \text{ mg}/\text{dm}^3$) is then

added to the volumes with water at the specified temperature ($20 \pm 2^\circ\text{C}$). The resulting solutions contain 1 dm^3 , the density of the indicator is 15, respectively; to equal 30; 45; 60; 90; 120; 150; 180; 210; 240 mg/dm^3 . The optical density of the reference solutions is measured on a blue light filter photo electro calorimeter with a wavelength (λ) of 400 nm in cuvettes with a light-absorbing layer thickness of 10 mm. Distilled water is used as the element. Based on the obtained data, a calibration graph is constructed because the optical density of the solutions depends on the mass concentration of the reference solutions. **Analysis.** Approximately 0.1 g of the test drug, previously dried to a constant mass, is weighed (the weighing result is recorded

to the nearest third decimal place). The weighed part of the drug is poured into a 50 cm³ conical flask, 25 cm³ of indicator solution is added, is closed with a stopper, and shaken in a device to shake the liquid in the container for 20 minutes. After shaking, the suspension is transferred to centrifuge tubes and centrifuged for 15 minutes, 5 cm from the clarified solution is carefully pipetted and its optical density is determined. If the optical density of the clarified solution exceeds 0.8 optical units, it is transferred to measuring tubes of 25 or 50 cm³, depending on the optical density of 5 cm³ of the solution. The solution in the flask was diluted with distilled water to the specified mark. After dilution, the optical density of the solution should be 0.1 to 0.8 optical units. In this case, the dilution coefficient is 5 or 10.

Based on the obtained value of the optical density, the residual mass concentration of the indicator in the detected solution is determined using the calibration curve. **Processing of results.** The adsorption activity on the indicator (X_3) is calculated using formula 6 in milligrams per 1 g of product.

$$X_3 = \frac{(C_1 - C_2 \cdot K) \cdot 0.025}{m} \quad (6)$$

Here, C_1 – mass concentration of initial indicator solution, mg / dm³;

C_2 – mass concentration of the solution after contact with the test sample, mg/dm³.

K – the dilution coefficient of the solution obtained for analysis after contact with the sample;

m – the weight of test sample, g;

0.025 – the volume of indicator solution obtained for determination, dm³

The result of the analysis is taken as the arithmetic mean of the results of two parallel determinations, the absolute discrepancy between them shall not exceed a difference of 10 mg per 1 g of the permissible test sample.

Preparation of a standard solution of mycotoxin at a concentration of 1000 µg/cm³. The standard 5.0 mcg dry mycotoxin by net weight should be dissolved in 5 ml of methanol.

Preparation of a working solution of mycotoxin. Approximately 10 ml of 0.1 M phosphate buffer solution pH = 6.5 is required to prepare the working solution of mycotoxin and a 50 µl standard solution of the selected toxin in methanol should be added at the adjusted concentration. A 50 cm³ volumetric flask is labeled with 0.1 M phosphate buffer solution pH = 6.5 to calculate that the toxin concentration in the working solution is 1000 µg / dm³, and mix well.

Analysis. 0.001 g of the weighed sample (clearly weighed) is poured into an Eppendorf-type solution with a volume of 2 cm³. To the same solution is added 1 cm³ of the working solution of the toxin. The sorption process is carried out for one hour at a temperature of 37 °C in a thermos shaker at a speed of 1400 rpm. The resulting suspension is centrifuged for 5 minutes at a speed of 10.000 rpm. The obtained supernatant and starting solution used “RIDAS-CREEN” test systems for in vitro analysis according to the method proposed by the manufacturer of the solution (R-Biopharm AG, Germany) case is analyzed for the number of mycotoxins in it by the method of competitive immuno enzyme analysis. For 1 mg of sorbent, the sorption capacity of the sorbent substance is calculated according to formula 7:

$$\text{Sorption ability} = \frac{C_{\text{initial}} - C_r}{m_s} \quad (7)$$

Here, C_{initial} – the composition of the toxin in the working solution, mkg;

C_r – the content of residual toxin in the working solution after the sorption process, mkg.

m_s – mass of sorbent sample, g

Сорбция фoизи 8-формула билан ҳисобланади:

$$\text{Sorption \%} = \frac{C_{\text{initial}} - C_r}{C_{\text{initial}}} \cdot 100\% \quad (8)$$

Here, C_{initial} – the value of the toxin concentration in the working solution, mkg/cm³.

C_r – the value of the residual toxin concentration in the working solution after the sorption process, µg/cm³

The results of the analysis are the arithmetic mean of the three parallel determinations.

Preliminary studies of mechanic activation in wood processing wastes such as wood shaving, Cellulose lignin, and hydrolytic lignin have been conducted. Based on several characteristics obtained, hydrolytic lignin was selected as the main research object. Pre-ground and dried hydrolytic lignin is a free-flowing sawdust-like mass of brown color with a small addition of partially hydrolyzed sawdust.

The chemical analysis showed that "Seasoned" hydrolytic lignin does not contain free sulfuric acid, because of the high content of ash components (28.9%) and it is washed away for many years by atmospheric precipitation during storage in the open air.

Microphotographs clearly show the structural properties of hydrolytic lignin, which partially retains the anatomical structure of the original wood. An evolved system of capillary cavities of various sizes is observed, from the internal cavities of the cells to the pores in the walls, to the micro-cavities of the layered structure. A closer examination reveals the structure of the strongly lignified primary wall and the true median lamina protruding from it. Numerous layers of the secondary cell wall with highly developed interfibrillar porosity are also clearly distinguishable.

Conclusion

1. The use of mechanically activated hydrolytic lignin as the basis of a complex nano sorbent is most preferable.

2. Mechanical activation of hydrolytic lignin is purposefully carried out in one cycle, at a rotation speed of 5000 rpm.

3. All studied specimens are characterized by the absence of micropores, the significant size of mesocyttes, and the significant outer surface.

4. Mechanically activated lignin can be the basis of a nanoporous sorbent and a carrier of other sorption systems.

5. Polysaccharide components of yeast biomass and natural aluminosilicates and others can be used as such sorption systems.

6. For various purposes, such complex sorbents can be used as entero sorbents for the purification of drinking and wastewater, the separation of heavy metal ions from multi-component solutions, and the removal of toxins from the bodies of animals and humans.

7. For each specific sorption system, the complex nano sorbent composition must be optimized to achieve maximum efficiency.

References:

1. Bobomurodova S. Y., Fayzullaev N. I., Usmanova K. A. Catalytic aromatization of oil satellite gases // *International Journal of Advanced Science and Technology*, – 29(5). 2020. – P. 3031–3039.
2. Fayzullaev N. I., Bobomurodova S. Y., Avalboev G. A. Catalytic change of C₁-C₄-alkanes // *International Journal of Control and Automation*, – 13(2). 2020. – P. 827–835.
3. Mamadoliev I. I., Fayzullaev N. I., Khalikov K. M. Synthesis of high silicon zeolites and their sorption properties // *International Journal of Control and Automation*, – 13(2). 2020. – P. 703–709.
4. Mamadoliev I. I., Fayzullaev N. I. Optimization of the activation conditions of high silicon zeolite // *International Journal of Advanced Science and Technology*, – 29(3). 2020. – P. 6807–6813.
5. Omanov B. S., Fayzullaev N. I., Musulmonov N. K., Xatamova M. S., Asrorov D. A. Optimization of vinyl acetate synthesis process // *International Journal of Control and Automation*, – 13(1). 2020. – P. 231–238.
6. Hilola N. Xolmirzayeva¹, Normurot I. Fayzullayev² Obtaining Nanocarbon from Local Raw Materials and Studying Its Textural and Sorption Properties // *IJETI*, – 70(2). 2022. – P. 163–171.
7. Fayzullaev N. I., Bobomurodova S. Y., Xolmuminova D. A. // Physico-chemical and texture characteristics of Zn-Zr/VKTS catalyst. *Journal of Critical Reviews*, – 7(7). 2020. – P. 917–920.
8. Mamadoliev I. I., Fayzullaev N. I. Optimization of the activation conditions of high silicon zeolite // *International Journal of Advanced Science and Technology*, – 29(3). 2020. – P. 6807–6813.

9. Fayzullaev N. I., Kholmiraeva H. N. Synthesis and Study of High – Silicon Zeolites from Natural Bentonite // *Solid State Technology*, – 63(6). 2020. – P. 3448–3459.
10. Hilola N. Xolmirzayeva Characteristics of the $\text{Fe}_2(\text{MoO}_4)_3 \cdot \text{MoO}_3$ catalyst used in the synthesis of nanocarbons from methane // *ACADEMICIA: An International Multidisciplinary Research Journal*, 2021. – P. 598–605.
11. Fayzullaev N. I., Bobomurodova S. Y., Xolmuminova D. A. // Physico-chemical and texture characteristics of Zn-Zr/VKTS catalyst. *Journal of Critical Reviews*, – 7(7). 2020. – С. 917–920.
12. Камбарова Г.Б. Состав и свойства активных углей, полученных из отходов орехового дерева // *Наука и новые технологии*. – № 4. 2011. – С. 159–161.
13. Оболенская А. В., Ельницкая З. П., Леонович А. А. Лабораторные работы по химии древесины и целлюлозы. – М.: Экология, 1991. – 320 с.
14. Богаев А. Н., Горелова О. М., Курочкин Э. С. Изучение закономерностей процесса пролиза скорлупы кедрового ореха и получение на ее основе активированного угля с заданными свойствами // *Ползуновский вестник*. – № 3. 2014. – С. 217–220.
15. Оффан К. Б., Петров В. С., Ефремов А. А. Закономерности пиролиза скорлупы кедровых орехов с образованием древесного угля в интервале температур 200–500 °С // *Химия растительного сырья*. – № 2. 1999. – С. 61–64.
16. Оффан К. Б. Превращения скорлупы кедровых орехов при термическом и химическом воздействии: дисс. ... канд.хим.наук. – Красноярск, 2001. – 110 с.
17. Ефремов А. А., Оффан К. Б., Киселев В. П. Исследование состава жидких и газообразных продуктов пиролиза скорлупы кедровых орехов // *Химия растительного сырья*. – № 3. 2002. – 47 с.
18. Камбарова Г.Б., Сарымсаков Ш. Получение активированного угля из скорлупы грецкого ореха // *Химия твердого топлива*. – № 3. 2008. – С. 42–46.
19. URL: <https://doi.org/10.3103/S0.361521908030129>
20. Wang W., Qi J., Sui Y., He Y., Meng Q., Wei F., Jun Y. An Asymmetric Supercapacitor Based on Activated Porous Carbon Derived from Walnut Shells and NiCo_2O_4 Nanoneedle Arrays Electrodes // *American Scientific Publishers*. – V. 18. – No. 8. 2018. – P. 5600–5608(9).
21. URL: <https://doi.org/10.1166/lnn.2018.15410>
22. Фарберова Е. А., Тиньгаева Е. А., Чучалина А. Д., Кобелова А. Р., Максимов А. С. Получение гранулированного активного угля из отходов растительного сырья // *Изв.вузов. Химия и хим.технология*. – Т. 61. – No. 3. 2018. – С. 51–57.
23. URL: <https://doi.org/10.1166/lnn.2018.15410>
24. Тумурханов Б. А., Султыгова З. Х., Арчакова Р. Д., Медова З.С.-А. Синтез высокоэффективных сорбентов из скорлупы грецкого ореха // *Сорбционные и хроматографические процессы*. – Т. 12. – No. 6. 2012. – С. 1025–1032.

<https://doi.org/10.29013/AJT-22-3.4-100-109>

*Kholikulov B. N.,
Tashkent Chemical-Technological Institute Tashkent Uzbekistan*

*Makhsumov A. G.,
Tashkent Chemical-Technological Institute Tashkent Uzbekistan*

*Umrzokov A. T.,
Department of Chemical Technology,
Navoi State Mining Institute, Uzbekistan*

*Ziyadullayev A.E
Tashkent Chemical-Technological Institute Tashkent Uzbekistan*

SYNTHESES AND TECHNOLOGY OF 2-BROMO-SUBSTITUTED BIS-CARBAMATE DERIVATIVES, PROPERTIES AND THEIR APPLICATION.

Abstract. The article studied the synthesis of N, N'-hexamethylenebis[(2-bromophenoxy)-carbamate], The products of N, N'-dichloro substitution, N, N'-dinitroso substitution, N, N'-disodium substitution and N, N'-dibenzyl substitution were studied N, N'-hexamethylenebis[(2-bromophenoxy-carbamate)] formed during the synthesis. Reaction centers and the reaction mechanism involved in the synthesis of these substances have also been proposed. proved by IR spectroscopy. The process used organic solvents and catalysts. The reaction yield was from 90.6% to 93.3%. The biological activity of the obtained substances was studied and compared with the Roslin preparation.

Keywords: 2-bromo-substituted bis-carbamates, N, N'-hexamethylenebis[(2-bromophenoxy)-carbamate], N, N'-dichloride, N, N'-dinitroso, N, N'-disodium, N, N'-dibenzyl.

Introduction. Today, the modern search for the chemistry and properties of bis-carbamate compounds that are currently intensively developing are attracting the attention of many researchers, both in Uzbekistan and abroad [1–4]. This is connected, on the one hand, with the rich possibilities of phenyl, carbamate, halogen, polyhydrocarbon groups in the molecules of organic compounds, and, on the other hand, with the properties of the most organic compounds, valuable for practical use, bromophenyl groups, as well as bis-carbamate bonds. Many examples are written when the introduction of halogen- and phenyl-carbamate bonds leads to the appearance of various kinds of gamma – possessing biological, pharmacological activity, the ability to inhibit the corrosion of metals, coatings, stabilizers for halogen-containing polymers, impregnations,

and also, as anti-aging of vulcanization of rubbers, the creation of a solvation theory intensification of the processes of dyeing and printing fabrics from natural and chemical fibers in liquid ammonia and organic solvents [5–8]. In addition, the study of the regularities of solid-phase fixation of dyes from textile materials, the creation of the theoretical foundations for the use of bio-catalytic systems for the processes of enrichment of tequistyle materials, the plasma-chemical activation of fibers that form polymers, the use of high-frequency fields and microwave radiation in chemical-and-chemical production is of great importance [9–12].

This is explained by the high reactivity of the highly diverse functional group to complex formation. It was necessary to determine high-precision unique optimal methods for the introduction of bis-

carbamate groups into the indicated types of compounds and to study the dependence of the reactions used due to the mobile proton at N-H substituting functional groups. As a result, a new, previously poorly studied and represented by only the simplest examples, a region of derivatives of two bromophenyl-containing bis-carbamates appeared [13–17].

Methods and materials. 1. Synthesis of N, N'-hexamethylene bis [(2-bromophenoxy)-carbamate]. Into a three-necked flask, equipped with a reverse actuator with a calcium chloride tube, mechanical stirrer, thermometer and dropping funnel, placed 17.3 g (0.1 mol) of 2-bromophenol in 50 ml of DMF, 25 ml triethylamine, and while stirring, 8.5 ml (0.05 mol) of HMDI was added dropwise from a dropping funnel. The reaction continued for 4–5 hours at a temperature of 28–49 °C. The precipitate was filtered off, washed with distilled water 2–3 times, and dried at room temperature. Appearance white-grayish powdery product. Yield 23.83g (92.4% of theoretical): T.melt. =107–108°C; R_f =0.75; M_m =513.8. The individuality of the obtained product was checked by TLC on a fixed layer (Al₂O₃) II degree of purity in the system: (C₆H₆: CH₃COOC₂H₅: 4); Found,%: C 46,59; H 4,17; N5,41; Br 30,88 Calculated for C₂₀H₂₂Br₂N₂O₄,% C46,71; H 4,28; N5,45; Br 31,10:

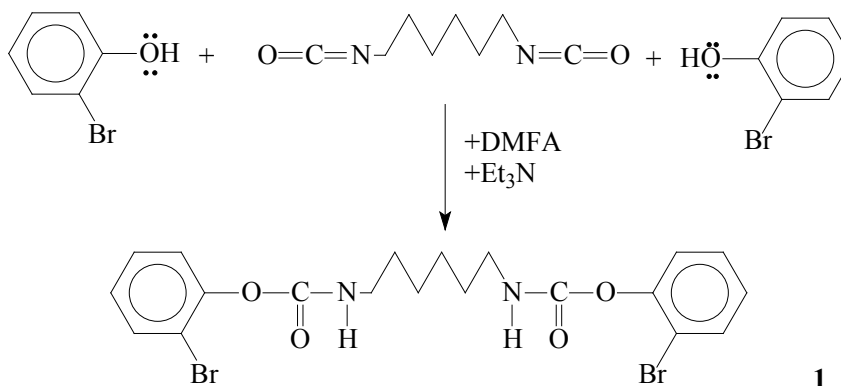
2. Preparation of N, N'-dichloro-N, N'-hexamethylene bis [(2-bromophenoxy)-carbamate]. Into a three-necked flask, equipped with a reverse actuator with a chlorine tube, automixer and thermometer, 5.14 g (0.01 mol) of N, N'-hexamethylene bis [(2-bromophenoxy)-carbamate], 60 ml carbon tetrachloride, 27.0 g of wet alumina and 4.8 g of calcium hypochlorite was added dropwise at 37 °C for 4 hours. Then the reaction mass was left for 33 hours. The precipitate that formed was filtered off and washed with ether. Received 5.28 g (90.6% of theoretical); T.melt.=89–90°C; R_f=0.73; M_m =582.8; Found,%: C 41.04; H 3.33; N4.79; Cl 12.07; Br 27.14 Calculated for C₂₀H₂₀Br₂Cl₂N₂O₄,%: C41.18; H 3.43; N4.80; Cl 12.18; Br 27.26

3. Obtaining N, N'-dinitroso-N, N'-hexamethylene bis [(2-bromophenoxy) -carbamate]. To a suspension of the composition 5.14 g (0.01 mol) of N, N'-hexamethylene bis [(2-bromophenoxy)-carbamate], 70 ml of 98% formic acid with stirring and cooling to 0–5 °C in portions over 1 hour was added 0.13 mol of NaNO₂, then stirring at the same temperature, the reaction was continued for 1 hour. TLC analysis of the reaction mixture every 6–10 minutes. The formed precipitate was filtered off, washed with 50 ml of ice water, and dried in air at room temperature. For methods (A-D), the filtrate was extracted with ethyl acetate (2 × 50 ml), washed with ice water and 5% aqueous soda solution, dried with magnesium sulfate and evaporated to dryness. For all methods (A-D), precipitates and residues after evaporation of the extracts were combined. The obtained N, N'-dinitroso compounds-N, N'-hexamethylene bis [(2-bromophenoxy)-carbamate] were determined by R_f, washed off with acetone sorbent. The solvent was evaporated to dryness at room temperature in a desiccator vacuum. The N, N'-dinitroso derivative of N, N'-hexamethylene bis [(2-bromophenoxy)-carbamate] was recrystallized from hexane and ethyl acetate. Product (3) yield –5.32 g (93.3% of theoretical); R_f=0.71; M_m =571.8; T.melt.=330 °C (decomposition). Found,%: C 41.82; H 3.36; N9.66; Br 27.97; Calculated for C₂₀H₂₀N₄Br₂O₆,%: C41.97; H 3.49; N9.79; Br 27.94.

4. N, N'-dibenzyl-N, N'-hexamethylene bis [(2-bromophenoxy) -carbamate]. In a three-necked flask equipped with a return flow with a calcium chloride tube, with an auto mixer and a thermometer, 5.38 g (0.01 mol) of N, N'-disodium-N, N'-hexamethylene bis [(2-bromophenoxy)-carbamate], 40 ml dry benzene. 2.4 ma (0.02 mol) of benzyl iodide was added dropwise while changing slowly. The mixture was then stirred for 13 hours while heating in a boiling water bath. After cooling, 25 ml of water was added, the precipitate was separated and recrystallized with 50% alcohol. Product yield (5) – 6.33 r (91.4% from theoretical); T.melt.=168–169 °C;

$R_f=0.76$; $M_M=693.8$; Found, %: C 58.69; H 4.83; N 3.89; Br 22.89; Calculated for $C_{34}H_{34}Br_2N_2O_4$, %: C 58.80; H 4.90; N 4.03; Br 23.03.

N, N'-diisopropyl-N, N'-hexamethylene bis [(2-bromophenoxy)-carbamate] Obtained similarly by the above-described method. Interactive compounds (IV) $(CH_3)_2CHJ$ and CH_3J connections received (6) and (7) with outputs 90,2% and 87.3;



The reaction is carried out in a medium of dimethylformamide and triethylamine at room temperature for 4 hours. It should be noted that derivatives of N, N-

Results and discussion: New derivatives of N, N'-hexamethylene bis [(2-bromophenoxy)-carbamates] were obtained by the interaction of ortho-bromophenol with hexamethylene diisocyanate. Selective, energy-saving, waste-free technological synthesis was carried out according to the scheme:

hexamethylene bis [(2-bromophenoxy)-carbamates] were obtained in a rather high yield. Physicochemical parameters of compounds (1) are given in (table 1).

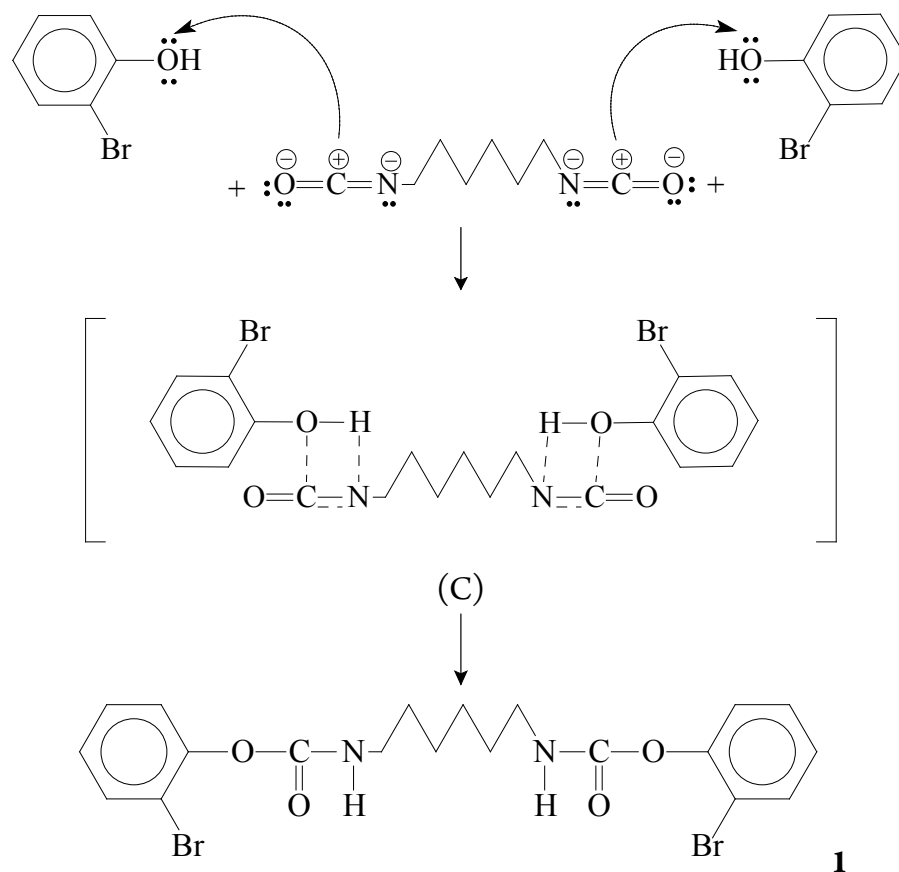
Table 1. – Physicochemical parameters of compounds (1)

Names	Structural formula	Out-put, %	T.melt., °C	R_f	Grossformula	Element. Analysis, %				M_M
						Calcul.		Find.		
						N	Br	N	Br	
		92.4	107–108	0.75	$C_{20}H_{22}Br_2N_2O_4$	5.45	31.1	5.41	30.88	513.8

High density, selectivity and easy mobility of the electron cloud group $-N = \overset{\oplus}{C} = O$ cause its high reactivity. The product yield was 92.4%. As expected, the products were obtained with good yields by the mechanism of the AN reaction. The physicochemical characteristics of bis-carbamate derivatives are apparently due to the high density and easy mobility of the electron cloud conjugated $(-N = \overset{\oplus}{C} = O)$ group, which leads to an increase in the positive charge on the carbon atom of the isocyanate group, facilitating the attack of this atom by the nucleophilic agent, this is the answer to the question of whether this occurs

by increasing the positive charge on the carbon atom or by stabilizing the transition state. However, in our case, $-\ddot{O}H$ hydroxyl group, having a free pair, attacks the electrophilic center in the isocyanate molecule with the formation of an intermediate product (C), which then rearranges into the final reaction product.

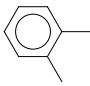

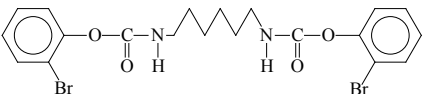
On the basis of our proposals and literature data, the probable mechanism of the interaction of 2-bromophenol with hexamethylene diisocyanate can be represented by the following scheme:



One of the starting reagents was purified using preparative thin-layer chromatography on Al_2O_3 in the system ($\text{HCOOH}:\text{CH}_3\text{COCH}_3:\text{CHCl}_3=0.5:$

4.5: 1.0). To prove the structure of N, N'-polymethylene bis-[(2-bromophenoxy)-carbamate], the method of IR spectroscopy was used (Table 2).

Table 2.- IR – spectra of compounds (1)

Structural formula	IR- spectra, ν , cm^{-1}						
	—N—H		—N—C—O— H O	—C—O O		$\text{—CH}_2\text{—}$	N—CH_2
	3394	771–726	1284	1690	721–767	2938–2942	3.35

To study the reactivity with respect to N-H reaction centers, N, N'-hexamethylene-bis-[(2-bromophenoxy)-carbamate], we carried out rare reactions: N, N'-dinitrosation, N, N'-dichlorination, N, N'-dimetallization and N, N'-dialkylation.

Chemical transformations of N, N'-polymethylene bis[(2-bromophenoxy)-carbamate]. Obtaining N, N'-dichlorinated compounds (1). Derivatives of N, N'-polymethylene-bis[(2-bromophenoxy)-carbamate] (1) are the most valu-

able raw material for the further synthesis of various biologically active compounds used in engineering, agriculture, and also have a high reaction center of the N-H group for carrying out reactions of nucleophilic and electrophilic substitutions. We have developed an efficient, affordable, cheap, stable and environmentally friendly method for carrying out the N, N'-dichlorination of a bis-carbamate derivative with calcium hypochlorite on wet alumina.

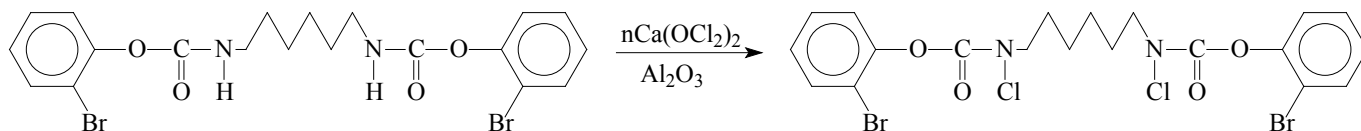
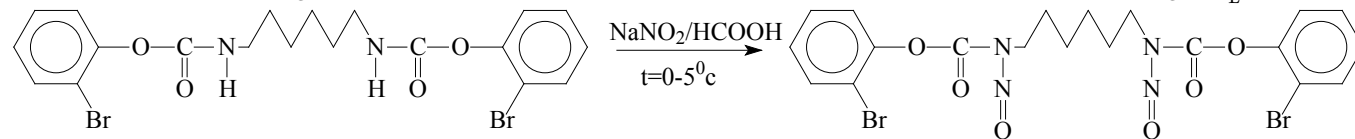


Table 3. – Physicochemical characteristics of compounds (2)

Structural formula	Compound 2 Out put,%	T.melt °C	R_f	Gross formula	Element. Analy- sis,%				M_m
					Calcul.		Find.		
					N	Cl	N	Cl	
	90.6	89–90	0.75	$C_{20}H_{20}Br_2Cl_2N_2O_4$	4.8	12.1	4.7	12.07	582.8

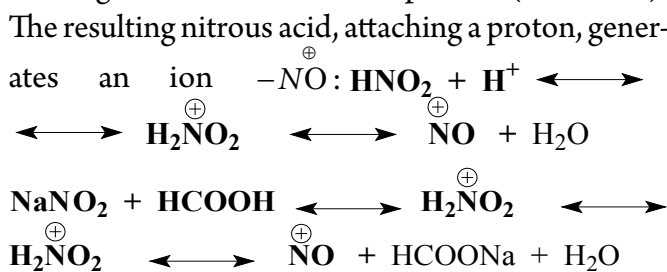
Outlet connections (2) – 90.6%. T.melt = 89–90°C; Physicochemical parameters are given on the table 3.

Preparation of N, N'-dinitroso derivatives of compounds (1): The reactions of N, N'-dinitrosidation of compounds (1) are comparatively little studied in the world literature. According to the literature and our own research, nitrogen atoms associated with the



3

The attacking agent is nitrosonium ion $-N^{\oplus}$. Since nitrous acid, which is the most common nitrosating agent, which exists in free form, sodium nitrite and a strong acid were used for the process (HCOOH). The resulting nitrous acid, attaching a proton, generates an ion



polymethylene $-(CH_2)_n$ -chain react with nitrosos. As a result of the reaction of N, N'-dinitrosidation, N, N'-hexamethylene-bis[(2-bromophenoxy)-carbamate] (1) with $NaNO_2$ (in excess) in 98% HCOOH at a temperature of 0–5°C, N, N'-dinitroso-substituted (3) with a yield 93.3%. N, N'-dinitrosidation proceeds by the mechanism of electrophilic damage (S_E).

N, N'-dinitrosation is carried out while cooling the reaction mixture: an increase in temperature is undesirable, since this reduces the yield of the target product, and sometimes affects the direction.

N, N'-dinitroso compounds are identified by absorption bands $N-N=O$ group.

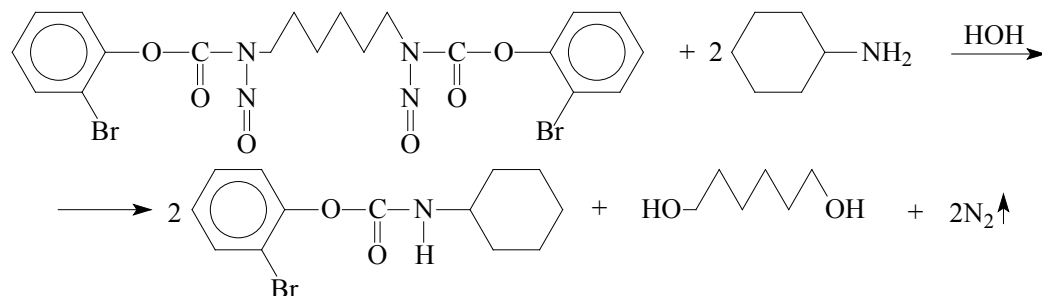
A stripe in the area $1500-1420\text{ cm}^{-1}$ for $N-N=O$ group (table 4).

Table 4. – IR – spectra of compounds (3)

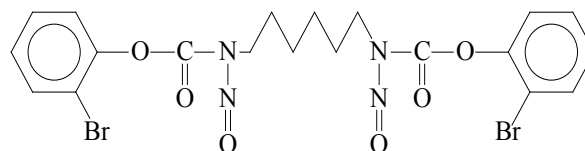
Connection name	IR – spectra, v, cm^{-1}						
	$-CH_2-$	$N-C=O$		$N-N=O$	C-Br	$C=O$	
	2920	1621	771–736	1500–1420	654	1690	768–732

In addition to spectral data, the structure of N, N'-dinitroso compounds was additionally confirmed by a chemical method, i.e. by reaction of N, N'-dinitrosoation products with amines. The reac-

tion of N, N'-dinitroso-N, N'-hexamethylene bis [(2-bromophenoxy)-carbamate] with aqueous solutions of ammonia with cyclohexylamine gave mono- and 1,3-disubstituted carbamates [26–27].



Thus, the resulting compounds once again prove that the nitrogen atoms bound to the polymethylene chain are subjected to nitrosation at N, N'-dinitrosidation of -N, N'-hexamethylene-bis [(2-bromophenoxy)-carbamate].



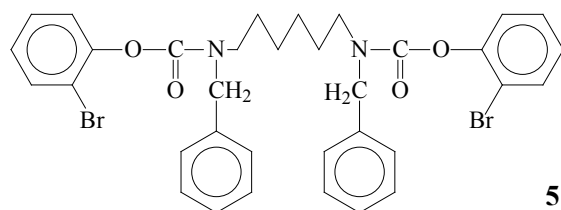
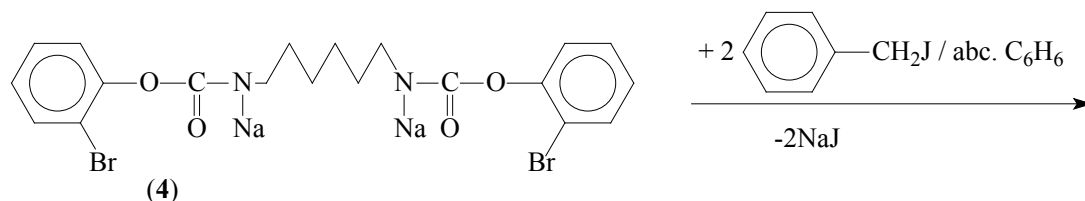
These conclusions are in good agreement with the literature data [26–27]. Physicochemical parameters of the compound (1) on table 5.

Table 5. – Physicochemical characteristics of compounds (3)

Structural formula	Out-put%	T.melt °C	R _f	Gross formula	Element analysis, %		M _m
					Calcul.	Find	
					N	N	
	93.3	330	0.71	C ₂₀ H ₂₀ N ₄ Br ₂ O ₆	9.79	9.66	571.8

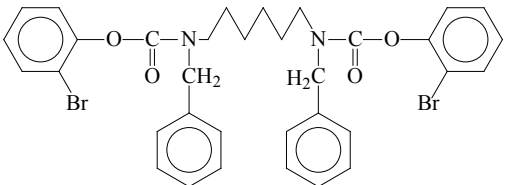
Preparation of N, N'-dibenzoyl-substituted bromo-carbamate derivatives of compounds (1). Dibenylation at N-H groups in bis-carbamates (1) with benzyl iodides is of undoubted interest for establishing the reactivity of compounds (1). Ben-

zylation reactions were carried out, the interaction of N, N'-disodium derivatives of N, N'-hexamethylene with benzyl iodide in anhydrous benzene at a temperature of 35–48 °C and benzyl iodide was added dropwise with stirring for 4.5 hours.



The occurrence of the benzylation reaction exclusively at the N, N'-nitrogen atom is explained, apparently, by the relatively easy dissociation of sodium from this atom after the presence of neighboring carbonyl groups. The connection (5) yield was ~91.4%.

Table 6. – Physicochemical characteristics of compounds (5)

Structural formula	Out-put%	T.melt °C	R _f	Gross formula	Element. analysis, %		M _m
					Calcul	Find	
					N	N	
	91.4	168–169	0.76	C ₃₄ H ₃₄ Br ₂ N ₂ O ₄	4.03	3.89	693.8

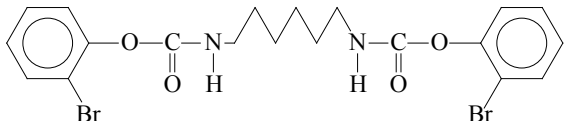
Physicochemical characteristics of the drug (5), given on the table 6.

Similarly, according to the method described above: N, N'-diisopropyl- N, N'-hexamethylene bis [(2-bromophenoxy) -carbamate] in 90.2% yield, T.melt.=111–112 °C and N, N'-dimethyl- N, N'-hexamethylene bis [(2-bromophenoxy) -carbamate] was obtained using the above-described method with a yield of 87.7%; T.melt.=97–98 °C.

Regulating activity of compounds: For the growth of the stimulating medium of compounds N, N'-hexamethyl bis [(2-bromophenoxy) -carbamate], tests in the laboratory of plant chemistry of the Academy of Sciences of the Republic of Uzbekistan in laboratory conditions, biot cultural services served vegetable and cotton seeds. In the experiments, cucumbers of the “Uzbekistan-740” variety, tomatoes of the “Temp” variety and medium-staple cotton of the “6524” variety were used. The preparations were dissolved in DMF and the method of

pre-sowing seed soaking was used for 18–20 hours; 0.01; 0.001; 0.0001 and 0.00001%. Repetition of experiments 4th fold. Accounting for measuring the length of the stem and root in 10-day-old cotton seedlings. It was accepted that all drugs tend to stimulate muscle growth, both in vegetables and cotton. Primary screening was carried out according to the method of Yu. V. Rakitin. This method allows you to quickly determine the degree of physiological activity of new chemical compounds, which reveals the stimulation or inhibition of the germination of plant seeds, as well as by changing the length of the roots and the length of the stem part. The preparations were tested for seed locks in solutions of different concentrations, followed by germination in Petri dishes. Control seeds were soaked in distilled water. Each series of experiments is accompanied by control. The control variants and the culture medium of the experiments are fixed 3.5, 7 and 10 days after inoculation (table 7).

Table 7. – Effect of preparation 1 on seed germination and growth cotton seedlings “S-6524”

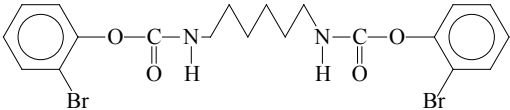
Drug	Experiments	Concentration, %	Germination, °C	Cotton	
				Root growth, %	Stem growth, %
	Control-water	b/0	100.0	100.0	100.0
		0.1	100.0	114.3	106.3
		0.01	87.0	93	92
		0.001	91.0	109	96
		0.0001	97.4	156.3	139.6
		0.00001	95.1	117.6	121.5
	Roslyn – (famous)	0.75–1.0	96	103.3	102.7

The study of the studied drug on the growth-stimulating activity of cotton shows, that the drug contributed to the germination of seeds and the development of the seedling system. Thus, the preparation of (1) N, N'-hexamethylene bis [(2-bromophenoxy)-carbamate] -when using 0.0001% and 0.00001% accelerated the growth of the root and stem of seeds above the control (table 7).

It was found that when soaking tomato seeds, the compounds (1) in total: N, N'-hexamethylene bis

[(2-bromophenoxy)-carbamate]:0,1;0,01;0,001% (7,500 times dilution) helped to increase their germination, most efficient germination improved environment improved by drug study (1), outstripping control by 56%. The best effect of stimulation of the roots of roots and stems of tomato seedlings was obtained by us when the seeds were soaked in a solution with the preparation (1), the stimulation of root growth was 77%, and the stem part 49% compared to control (table 8).

Table 8. – Effect of preparation 1 on seed germination and growth of tomato seedlings “TEMP”

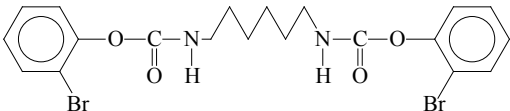
Drug (1)	Experiments	Concentration, %	Germination, seed 2,3,5 day, %	Tomato	
				Root growth, %	Stem growth, %
	Control-H ₂ O	b/0	55.0	100.0	100.0
	0.1	60.0	129.2	136.3	
	0.01	57.0	148.6	139.7	
	0.001	59.0	153.4	144.5	
	0.0001	60.0	177	149.2	
	0.00001	57.0	138.7	125.6	
	Roslyn – (famous)	0.75–1.0	56.0	107.4	104.5

Study of the drug (1) for growth stimulation of activity on cucumber seeds of minor effects. The growth impulse is mainly observed in the stem of the seedlings. The drug (1) N, N'-hexamethylene bis [(2-bromophenoxy)-carbamate] – at a concen-

tration of 41.4% increased control, and also, respectively, compared with the control (table 9).

The effect of preparation 1 on seed germination and growth of seedlings of cucumbers variety “Uzbekistan-740”.

Table 9.

Drug (1)	Experiments	Concentration, %	Germination across 5 days, %	Cucumbers	
				Seed growth, %	Stem growth, %
	Control-H ₂ O	b/0	85.0	100.0	100.0
	0.1	88.0	117.0	109.3	
	0.01	90.0	118.0	117.5	
	0.001	90.0	136.4	139.6	
	0.0001	88.0	139.7	141.7	
	0.00001	85.0	118.6	114.3	
	Roslyn – (famous)	0.75–1.0	85.0	103.4	102.7

Thus, the drug(1) at a concentration of: (0.1; 0.01; 0.001%) is the most effective growth-stimulating drug for vegetables and cotton in laboratory

conditions and further more in-depth study in the field is recommended.

Conclusion: When studying the synthesis, properties and use of bromo-substituted bis-carbamate

derivatives, the reaction was carried out at room temperature for 4 hours in the presence of dimethylformamide and triethylamine. In the process, it was observed that derivatives of the starting material, N, N'-hexamethylene-bis[(2-bromophenoxy-carbamates)], were formed in much higher yields. In this case, the high density, selectivity and easy mobility of the group electron cloud were based on its high reactivity. To study the reactivity with N-H

reactive centers, N, N'-hexamethylene-bis-[(2-bromophenoxy-carbamate)], N, N'-dinitation, N, N'-dichlorination, N, N'-dimetallization, N, N' Reactions – dialkylations were carried out and analyzed, and the yield was 92.4%. The biological activity of the obtained compounds was studied, the drug at a concentration (0.1; 0.01; 0.001%) was tested in the laboratory and recommended as the most effective drug for the growth of vegetable and cotton crops.

References:

1. Makhsumov A. G., Atakhodzhaeva M. A. Synthesis and antimicrobial activity of bromine-PE pyrazolyl-M-methylcarbamate // *Chemical Pharmaceutical Journal*, – Moscow, – No. 4. 1988. – P. 431–433.
2. Sutoris V., Sunak J., Cipinova H. Preparation of ethinyl esters and carbamates and the study of their pesticidal action // *Chem. J. Vesti*, – 23. – No. 11. 1969. – P. 47–48.
3. Melnikov N. N., Baskanov Yu. A. Synthesis and physiological activity on plants of isopropyl ethers of some arylcarbamic acids // *J. General Chemistry*, – No. 24. 1954. – P. 376–379.
4. Karmanova L. P., Kuchin A. V., Koroleva A. A. Chemistry, technology of bioregulators // 17th Mendeleev Congress on General and Applied Chemistry, Kazan, Russian Federation, 2003. – P. 243. Moszynski Wieslaw. The pesticidal activity of aryl esters of N-arylcarbamic acid // *Organga. Ponaik. Ingot. Organ.* 1980. – P. 53–58.
5. Makhsumov A. G., Samadov S. Zh., Nazirov Z. Sh. The production technology of the bis derivative – [(ortho-aminoacetylphenoxy) – carbamate] and its properties // *Chemical Journal of Kazakhstan*, – Almaty, – No. 2. 2008. – P. 163–170.
6. Makhsumov A. G., Atakhodzhaeva M. A., Talipova M. A., Djuraev A. D. Synthesis and study of PYA pyrazolyl N-methylcarbamates // *Chemical- Pharmaceutical Journal*. – Moscow, – No. 4. 1988. – P. 431–433.
7. Makhsumov A. G., Zakirov U. B., Atakhodzhaeva M. A. Study of the pharmacological properties of propargylcarbamate derivatives // *J. Physiol, active substances*, – Kiev, Ukraine, – Vol. 13. 1981. – P. 50–52.
8. Patent 7074782 United States / Carbamate in case of caspase and their application // Beblington David, Knegtel Ronald, Mortimore Michael // *IPS⁷*, from 07 D213/8; it is declared on August 21, 2003; Published on; – July 11. 2006.
9. Khatamova M. S., Makhsumov A. G. Modern achievements in the synthesis of bis (alkyl) -carbamate derivatives and their properties // *Semical Journal of Kazakhstan, Special issue – Almaty*, 2007. – P. 120–124.
10. Siddikova Kh. H. Makhsumov A. G., Isaev A. N. “*Nauchny Vestnik*”, And. State University, – No. 4. 2017. – P. 22–25.
11. Makhsumov A. G., Nabiev V. A., Valeeva N. G. Development of synthesis, properties of derivative 1-amino-antraquinon and its bio-simulating activity // *Monthly International scientific Journal “Austria-science”*. I part, – No. 16. 2018. – P. 65–70.
12. Barkan Ya. G. Organic chemistry // – Moscow, “Higher School”, 1973. – P. 471. Barkan Ya. G. Organic chemistry // – Moscow, “Higher School”, 1973. – 471 p.
13. Makhsumov A. G., Ismatov D. N., Valeeva N. G. Synthesis, properties and biological activity N, N'-hexamethylene bis-[(1-naphthoxy)-carbamate]. *International journal of Engineering sciences and research technology*, – 7(8). 2018. – P. 194–200.

14. Makhsumov A. G., Absalyamova Q. M., Ismailov B. M., Mashayev E. E. Synthesis and properties of the derivative-N, N1-hexamethylene bis – [(ortho- aminoacetylphenoxy)] – carbamate and its application // “Universim: chemistry and biology”.– Moscow. 2019.– No. 3.– P. 65–71.
15. Makhsumov A. G., Samadov S. J., Valeeva N. G. Synthesis and properties of the derivative-N. N-tetra-methylene bis- (h-ferrocenylphenoxy) – carbamate and its application // International Journal of Engineering and Scientific Research, (Indiya). – Vol. 7.– Issue 2. Month,2019.– P. 1–7.
16. Makhsumov A. G. Synthesis, properties and biological activity of L-borneola carbamate derivative // International Journal of Engineering and Scientific Research, (Indiya).– Vol. 7.– Issue 1. January, 2019.– P. 1–8.
17. Makhsumov A. G., Ismatov D. N., Valeeva N. G., Asadova R. D., Ruzmatov b. Modern advances in the synthesis of new derivatives of acetylene dithiocarbamate and their biological activity // International Journal of Engineering and Scientific Research, (Indiya).– Vol. 7.– Issue 3.– March, 2019.– P. 1–9.

Contents

Section 1. Mathematics	3
<i>Javadov Khaladdin</i>	
DISTRIBUTION OF PRIME NUMBERS. INVOLUTE NATURE OF PRIME NUMBERS. RIEMANN HYPOTHESIS	3
Section 2. Medical science	11
<i>Shermatova G. D., Eshbakova K. A., Narbutaeva D. A., Karakulova A. M.</i>	
ANTIOXIDANT AND ANTIHYPOXIC ACTIVITY OF EMODIN AND CHRYSOPHANOL.....	11
Section 3. Mechanics	14
<i>Kalmova Maria</i>	
THE SCOPE OF APPLICATION OF DEVICES WHOSE OPERATION IS BASED ON TAKING INTO ACCOUNT THE CONNECTIVITY OF THERMOELECTROELASTIC FIELDS.....	14
Section 4. Food processing industry	17
<i>Rakhmonov Kakhramon Sanokulovich, Khudaikulov Anvar Shavkatovich, Atamuratova Tamara Ivanovna</i>	
TECHNOLOGICAL ASPECTS OF THE PRODUCTION OF WHEAT BREAD VARIETIES USING SPONTANEOUS FERMENTATION STARTERS	17
<i>Yulchiev Aslbek, Serkayev Qamar, Mirzaev Abdugappor, Asqarov Ibrokhim</i>	
TECHNOLOGICAL SCHEME OF REFINING OF COTTONSEED OIL PURIFIED FROM GOSSYPOL	23
Section 5. Technical sciences	30
<i>Akhmedov Ulug Karimovich, Kurambaev Sherzod Raimberganovich, Bakhtiyarov Sardorbek Bakhtiyarovich</i>	
OBTAINING COTTONSEED OIL THAT MEETS THE REQUIREMENTS OF FOOD SAFETY OF THE POPULATION	30
<i>Soliev L., Jumaev M. T., Nizomov I. M., Makhmadov Kh.R., Olimdzonova N. V., Muzafarova D. V.</i>	
FORMATION OF INVARIANTE QUILIBRIA IN MULTICOMPONENT SYSTEMS AND DETERMINATION OF SOLID PHASE CRYSTALLIZATION PATHWAY.....	35
<i>Nurov Kurbonali Bozorovich, Dzhuraev Tukhtasun Dzhuraevich, Jafarov Amirsho Sayobidovich</i>	
INVESTIGATION OF THE REGION OF EXAMINATION OF MELTS IN SYSTEMS In – B ^{VI} (B ^{VI} – S, Se, Te) BY THE ACOUSTIC METHOD	44
<i>Radkevich Maria Viktorovna, Shipilova Kamila Bakhtiyarova, Abdukodyrova Malokhat Noridzhonovna</i>	
A REVIEW OF METHODS FOR ASSESSING THE EVAPORATION OF LIQUID DROPS UNDER VARIOUS CONDITIONS.....	52
Section 6. Chemistry	59
<i>Ergashev Dilmurod Adiljonovich, Khamdamova Shokhida Sherzodovna, Mirzaolimov Akmal Nabiyevich, Eshpulatova Matluba Boymuradovna</i>	
THE SOLUBILITY OF COMPONENTS IN THE SYSTEM {99.7[30MgSO ₄ +70% H ₂ O]+0.3%HNO ₃ ·NH ₂ C ₂ H ₄ OH-(NH ₄) ₆ Mo ₇ O ₂₄ ·4H ₂ O.....	59
<i>Butaev Khurshid, Ikramov Abduvakhob, Kadirov Khasan, Baltabaev Ulugbek Narbaevich</i>	
COMPARATIVE CHARACTERISTICS OF OCTANE-ENHANCING ADDITIVES BASED ON O- AND N-CONTAINING RAW MATERIALS	67

<i>Geldiev Y. A., Turaev Kh. Kh., Umbarov I. A.</i> THERMAL ANALYSIS OF MODIFIED POLYSILICIC ACID WITH AMINO ALCOHOLS	72
<i>Khamdamova Dilnoza, Umarova Vasila, Primkulov Mahmud</i> OBTAINING CELLULOSE FROM THE MEDICINAL PLANT MILK THISTLE	76
<i>Kaypnazarov Turdibay Nzamatdinovich, Uteniyazov Karimbay Kuanishbaevich, Mirzaeva Makhira Risbaevna, Abdullayev Nasir Dzhililovich, Ramazonov Nurmurod Sheralievich</i> TRITERPENE GLYCOSIDES TRAGACANTHA STIPULOSA AND THEIR GENINS. STRUCTURE OF CYCLOSTIPULOSIDE D	82
<i>Toshpulatov D. T., Mirzaev Sh.E., Nasimov A.M., Yakubov B. A., Samiev A. A., Tashpulatov Kh. Sh.</i> SYNTHESIS OF $[\text{CO}(\text{BPY})(\text{SCN})_4]^{2+}$ COMPLEX AND ITS PHOTOCHEMICAL PROPERTIES IN THE SOL-GEL MATRIX	87
<i>Fayzullayev Normurot I., Kholmirezayeva Khilola N.</i> DEVELOPMENT OF TECHNOLOGY FOR MAKING NANO SORBENT FROM WOOD PROCESSING WASTE.....	92
<i>Kholikulov B.N., Makhsumov A. G., Umrzokov A. T., Ziyadullayev A.E.</i> SYNTHESES AND TECHNOLOGY OF 2-BROMO-SUBSTITUTED BIS-CARBAMATE DERIVATIVES, PROPERTIES AND THEIR APPLICATION.....	100
